

HARVARD UNIVERSITY  
Graduate School of Arts and Sciences



DISSERTATION ACCEPTANCE CERTIFICATE

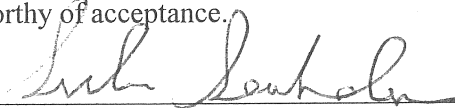
The undersigned, appointed by the  
Department of Physics  
have examined a dissertation entitled

Explorations in Dirac Fermions and Spin Liquids


presented by

Rudro Rana Biswas

candidate for the degree of Doctor of Philosophy and hereby  
certify that it is worthy of acceptance.

Signature 

Typed name: Professor Subir Sachdev, Chair

Signature 

Typed name: Professor Bertrand Halperin

Signature 

Typed name: Professor Amir Yacoby

Date: April 14, 2011

# Explorations in Dirac Fermions and Spin Liquids

A dissertation presented

by

Rudro Rana Biswas

to

The Department of Physics

in partial fulfillment of the requirements

for the degree of

Doctor of Philosophy

in the subject of

Physics

Harvard University

Cambridge, Massachusetts

May 2011

©2011 - Rudro Rana Biswas

All rights reserved.

Thesis advisor  
**Subir Sachdev**

Author  
**Rudro Rana Biswas**

## **Explorations in Dirac Fermions and Spin Liquids**

### **Abstract**

A significant portion of this dissertation is devoted to the study of the effects of impurities in substances whose low energy modes can be described by fermions obeying the gapless Dirac equation in 2+1 dimensions.

First, we examine the case of a spin vacancy in the staggered flux spin liquid whose excitations are Dirac fermions coupled to a  $U(1)$  gauge field. This vacancy leads to an anomalous Curie susceptibility and does not induce any local orders. Next, a Coulomb charge impurity placed on clean graphene is considered. We find that the Dirac quasiparticles in graphene do not screen the impurity charge, to all orders in perturbation theory. However, electronic correlations are found to induce a cloud of charge having the *same* sign as the impurity charge. We also analyze the case of a local impurity in graphene in the presence of a magnetic field and derive the spatial fourier transform of tunneling spectroscopy data obtained on an almost-clean graphene sheet in a magnetic field.

We then move on to Strong Topological Insulators (STI) whose surfaces are inhabited by an odd number of Dirac fermion species. Local impurities on the STI surface are found to induce resonance(s) in the local density of states (LDOS) in their vicinity.

---

In the case of magnetic impurities that may be approximated by classical spins, we show the existence of RKKY interactions that favor ferromagnetic aligning of randomly placed impurity spins *perpendicular* to the STI surface when the doping is insignificant. Finally we also consider the effects of a step edge on the STI surface and calculate the spatial decay of LDOS perturbations away from it.

The last chapter of this dissertation contains the theory for a new kind of spin liquid in a system of spin halves arranged in a triangular lattice, whose excitations are spin one Majorana fermions. This gapless spin liquid is found to possess certain properties that are exhibited by the recently discovered spin liquid state in the organic charge transfer salt  $\text{EtMe}_3\text{Sb}(\text{Pd}(\text{dmit})_2)_2$ .

# Contents

Title Page . . . . .	i
Abstract . . . . .	iii
Table of Contents . . . . .	v
Citations to Previously Published Work . . . . .	viii
Acknowledgments . . . . .	ix
Dedication . . . . .	xiii
<b>1 Introduction</b>	<b>1</b>
1.1 Dirac Fermions . . . . .	1
1.1.1 Graphene . . . . .	3
1.1.2 Strong Topological Insulators . . . . .	8
1.2 Spin Liquids . . . . .	16
1.2.1 The staggered flux spin liquid . . . . .	17
1.2.2 The Majorana Spin Liquid on the triangular lattice . . . . .	20
<b>2 Theory of quantum impurities in the staggered flux spin liquid</b>	<b>24</b>
2.1 Synopsis . . . . .	24
2.2 Introduction . . . . .	25
2.3 Theory and Results . . . . .	32
2.3.1 Bulk theory . . . . .	33
2.3.2 Relationship to earlier work . . . . .	34
2.3.3 Impurity exponents . . . . .	37
2.3.4 Linear response to a uniform applied field . . . . .	39
2.4 Conclusions . . . . .	45
<b>3 Coulomb impurity in graphene</b>	<b>48</b>
3.1 Synopsis . . . . .	48
3.2 Introduction . . . . .	49
3.3 Non-interacting electrons . . . . .	52
3.4 Interacting electrons . . . . .	56
3.5 Conclusions . . . . .	62

---

<b>4</b>	<b>Quasiparticle Interference and Landau Level Spectroscopy in Graphene in the presence of a Strong Magnetic Field</b>	<b>63</b>
4.1	Synopsis . . . . .	63
4.2	Introduction . . . . .	64
4.3	Theory . . . . .	65
4.4	Results . . . . .	68
4.5	Conclusion . . . . .	72
<b>5</b>	<b>Impurity-induced states on the surface of 3D topological insulators</b>	<b>75</b>
5.1	Synopsis . . . . .	75
5.2	Introduction . . . . .	76
5.3	Theory . . . . .	78
5.4	Results . . . . .	81
5.5	Conclusion . . . . .	85
<b>6</b>	<b>Scattering from Surface Step Edges in Strong Topological Insulators</b>	<b>87</b>
6.1	Synopsis . . . . .	87
6.2	Introduction . . . . .	88
6.3	Theory . . . . .	91
6.4	Results . . . . .	95
	6.4.1 The perfect reflector . . . . .	95
	6.4.2 Discussion of recent experiments . . . . .	96
	6.4.3 Generic step edges . . . . .	98
6.5	Conclusion . . . . .	99
<b>7</b>	<b>SU(2)-invariant spin liquids on the triangular lattice with spinful Majorana excitations</b>	<b>100</b>
7.1	Synopsis . . . . .	100
7.2	Introduction . . . . .	101
	7.2.1 Low energy theory . . . . .	103
7.3	The mean field Majorana Hamiltonian on a triangular lattice . . . . .	107
	7.3.1 Majorana mean field theory from a spin Hamiltonian: an example	107
	7.3.2 The general low energy effective theory on the lattice . . . . .	110
	7.3.3 The low energy effective theory in the presence of a perpendicular magnetic field . . . . .	112
	7.3.4 The spectrum in the presence of the Zeeman coupling . . . . .	114
7.4	Properties of the clean Majorana spin liquid . . . . .	114
	7.4.1 The low energy density of states (DOS) . . . . .	115
	7.4.2 Specific Heat . . . . .	116
	7.4.3 Magnetic susceptibility . . . . .	116
	7.4.4 The Wilson ratio – comparison with a 2DEG . . . . .	117
	7.4.5 Static Structure Factor . . . . .	118

---

7.4.6	Effect of a perpendicular magnetic field . . . . .	119
7.5	Effects of weak disorder . . . . .	121
7.5.1	The bond impurity potential . . . . .	121
7.5.2	The disorder-averaged self energy in the Born approximation .	121
7.5.3	The disorder-averaged self energy in the self-consistent Born approximation (SCBA) . . . . .	123
7.5.4	The disorder-averaged single particle density of states . . . . .	124
7.5.5	The specific heat in the presence of impurities . . . . .	125
7.5.6	The spin susceptibility in the presence of impurities . . . . .	126
7.5.7	The Wilson ratio in the presence of impurities – comparison with a 2DEG . . . . .	127
7.5.8	The thermal conductivity . . . . .	128
7.6	Conclusions . . . . .	130
	<b>Bibliography</b>	<b>132</b>
	<b>A The relation between the Majorana and spin 1/2 Hilbert spaces</b>	<b>148</b>



# Citations to Previously Published Work

Chapter 2 appears in its entirety in the paper:

“Theory of quantum impurities in spin liquids”, A. Kolezhuk, S. Sachdev, R. R. Biswas and P. Chen, Phys. Rev. B, **74**, 165114 (2006)

Chapter 3 appears in its entirety in the paper:

“Coulomb impurity in graphene”, R. R. Biswas, S. Sachdev and D. T. Son, Phys. Rev. B, **76**, 205122 (2007)

Chapter 4 appears in its entirety in the paper:

“Quasiparticle interference and Landau level spectroscopy in graphene in the presence of a strong magnetic field”, R. R. Biswas and A. Balatsky, Phys. Rev. B, **80**, 081412(R) (2009)

Chapter 5 appears in its entirety in the paper:

“Impurity-induced states on the surface of three-dimensional topological insulators”, R. R. Biswas and A. Balatsky, Phys. Rev. B, **81**, 233405 (2010)

Chapter 6 appears in its entirety in the paper:

“Scattering from surface step edges in strong topological insulators”, R. R. Biswas and A. Balatsky, Phys. Rev. B, **83**, 075439 (2011)

Chapter 7 as well as Appendix A appear in their entirety in the 2011 preprint:

“SU(2)-invariant spin liquids on the triangular lattice with spinful Majorana excitations”, R. R. Biswas, L. Fu, C. R. Laumann and S. Sachdev, arXiv:1102.3690.

Electronic preprints (shown in `typewriter font`) are available on the Internet at the following URL:

`http://arXiv.org`

# Acknowledgments

It seems like yesterday that I walked past a snow filled Harvard Yard and into Jefferson Laboratory for the first time. As I look back at this journey from my vantage point that is now, I realize that a large part of what I was able to accomplish during this period is due to the interactions that I was able to have with some truly remarkable people. I am happy to use this opportunity to thank some of these incredible people.

I thank my advisor, Prof. Subir Sachdev, for his guidance through my graduate years, for letting me work on new materials and problems that excited me, even if that meant that he would have to invest in helping me chart a course that is different from the usual. Time and again, I have had the privilege of learning from watching Subir make symmetry and scaling arguments whose extraordinary elegance was matched only by how inevitably *predictive* they were, completely unlike the hand-waving, uncertain and jaded arguments elsewhere. I also thank him for relentlessly inspiring me with his work ethic – I continue to be humbled and inspired by how much he accomplishes in any given day.

Much of my mindset as a physicist has been influenced by my many discussions with Bert Halperin, an incredible physicist and my hero. I thank Bert for co-advising me at every step and for every physics discussion we have had over these years. Everything that I have done right as a physicist during my years at Harvard, I owe in large part to him. I thank him especially for reinforcing my belief that good Physics is lucid and crisp, that the non-trivial need not be obscure. I also thank him for nurturing me, for humoring me, for challenging me, for encouraging me and above all, for always being there for me when I knocked on his door.

I thank the many distinguished experimentalists at Harvard who educated me and helped me have my feet more firmly planted in ground reality, being as I was, a theorist. Specifically, I wish to thank Profs. Amir Yacobi, Jenny Hoffman, Charlie Markus, Misha Lukin, Markus Greiner as well as Dr. Joe Peidle. I would also like to thank Yang Qi, Liang Fu, Lars Fritz, Cenke Xu, Chris Laumann, Jimmy Williams as well as all my co-graduate students for the many enriching conversations.

Thank you Sheila, for making the department such a warm and welcoming place for people from all corners of the globe. I take this opportunity to thank all the administrative staff, especially Bill Walker, Heidi Kaye, Dayle Maynard and Marina Werbeloff, for putting their hearts and minds into making our lives better and for making sure that we were not plagued by worries of a non-academic nature.

During my year as a visiting graduate student at Los Alamos National Lab, I had the good fortune of making acquaintance with Sasha Balatsky, who has since been not just my collaborator and mentor, but also a great friend and source of encouragement. Thank you Sasha, for taking me under your wings and for your unflinching support. I also thank him for introducing me to many wonderful physicists with whom I got to collaborate and interact including Profs. Shoucheng Zhang, Aharon Kapitulnik, Hari Manoharan, Ivan Schuller, Dan Arovas, Naoto Nagaosa, Misha Fogler, Mike Crommie and their students and postdocs.

I thank Dr. Pabitra Sen, with whom I worked at the Schlumberger-Doll Research labs over one summer, on Bert's suggestion. Not only did we end up solving an exciting problem in classical 'soft' statistical mechanics, but Pabitra has continued to

be interested in and supportive of my career over these years.

The flip side of having a spouse in a different academic institution is that I had the good fortune to meet and interact with some great physicists in her department. I wish to thank Profs. David Stroud, John Wilkins, Duncan Haldane, David Huse, Zahid Hasan, Ali Yazdani and N. Ong for welcoming me and treating me as one of their own, whenever I stopped by their offices.

I thank the folks at the Tata Institute of Fundamental Research, Mumbai, especially my string theory co-conspirators – Profs. Shiraz Minwalla, Gautam Mandal and Avinash Dhar, who not just taught me some of the best physics courses I have ever attended, but helped me set off on the path to becoming a physicist in the very best way possible. I also thank Profs. Kedar Damle and Deepak Dhar for insightful discussions and for their support.

No person has a greater hand in my becoming a physicist than Partha Pratim Roy, my high school physics teacher. He taught me to understand everything from first principles, to never be afraid to challenge a well established dogma with a well posed ‘why’ and that I needed to derive it to believe it. When I decided to follow the traditional wisdom of going to IIT-Kanpur for an undergraduate degree and go to Presidency College, Calcutta, for Physics Honors instead, I was fortunate to have met Prof. Dipanjan Rai Chaudhuri, who helped me develop a perspective on what Physics problems are important and worth pondering over. I would also like to acknowledge the wonderful times I had at Presidency, especially in the company of Shamik and Samriddhi.

I thank Arnab Sen, my partner in crime from the Tata Institute, my collaborator and my dear friend, who has been an excellent sounding board for ideas both in and outside of Physics. It is a wonderful fortuitous turn of events that reunited us in Cambridge during the last year of my PhD and what a memorable year this has been!

I thank my grandmother, who took it upon herself to bring me up, and to never allow me to feel anything but utterly loved. She provided the initial spark for my love for mathematics and playfully got me thinking about geometry while I gobbled up the delicacies that she made especially for me. She also inculcated in me my love for books and allowed me to indiscriminately help myself to her endless shelves of books. She carefully wove in references to my great grandfather, Prof. Meghnad Saha, with just the right mixture of awe and irreverence and constantly pointed out that academic performance was not to be equated with intellectual curiosity. Thank you too, Bulki Mashri and Mike, for giving me a taste of how wonderful having a family can be like.

I wish to end by thanking my wife, Srividya, who is not just an incredibly sharp physicist with an uncanny knack for spotting the most interesting and relevant points in any discussion, but has also been an indefatigable force of nature in supporting me through thick and thin. It is not a stretch to say that this dissertation is as much our labor of love as it is mine. She has imagined me more perfect than I believed true and has then made me work harder than I imagined possible to prove her right. At the end of this journey is yet another new beginning for us and I cannot wait to travel down this path with her.

*To my lovely wife,  
Srividya.*

# Chapter 1

## Introduction

### 1.1 Dirac Fermions

#### The Dirac Equation

In 1926, Erwin Schrödinger wrote down a wave equation[125] which described the time evolution of the quantum mechanical wave function of a non-relativistic particle:

$$i\hbar\frac{\partial}{\partial t}\psi(x,t) = \left(-\frac{\hbar^2\nabla^2}{2m} + V(x)\right)\psi(x,t) \quad (1.1)$$

Using the correspondence  $E \rightarrow i\hbar\partial/\partial t$  and  $p \rightarrow -i\hbar\nabla$ , this is equivalent to the non-relativistic equation for the energy  $E = p^2/(2m) + V$ . The discovery of this equation led to the question of whether a similar equation could be written to describe the motion of a relativistic particle, whose energy and momentum are treated on the

same footing according the following equation from special relativity:

$$E^2 = p^2 c^2 + m^2 c^4 \quad (1.2)$$

Here  $c$  is the speed of light and  $m$  is the rest mass of the particle. This question was answered in 1928 by Paul Dirac[29]. He discovered that one could write down a relativistic wave equation which was linear both in energy and momentum, and which squared to Eq. (1.2). However, this was possible only if the wave function was assumed to be a multicomponent object with at least 4 components. Thus came to be the Dirac equation for the electron, in which the concept of spin arose naturally from the aforementioned multiple components of the wave function. It is reproduced below in modern notation:

$$(-i\hbar\gamma^\mu\partial_\mu + mc)\psi(x) = 0 \quad (1.3)$$

where the ‘gamma matrices’ are required to obey the relation:

$$\{\gamma^\mu, \gamma^\nu\} = 2g^{\mu\nu} \quad (1.4)$$

Here,  $g^{\mu\nu}$  is a constant (Minkowski) metric and  $\{A, B\} = AB + BA$  is the *anti*-commutator. This construction of the gamma matrices and the Dirac equation can be generalized to any number of dimensions. In particular, for (2+1) dimensions, we can construct the  $2 \times 2$  gamma matrices<sup>a</sup>

$$\gamma^0 = \sigma^z, \quad \gamma^x = i\sigma^y, \quad \gamma^y = -i\sigma^x \quad (1.5)$$

---

<sup>a</sup>This convention is one of many related by unitary transformations.



in terms of the Pauli sigma matrices  $\sigma^{x,y,z}$ . These lead to the following Hamiltonian<sup>b</sup>

$$\mathcal{H}_D = c \boldsymbol{\sigma} \cdot \hat{\mathbf{p}} + \Delta \sigma^z, \quad \Delta = mc^2 \quad (1.6)$$

There are two kinds of particles described by this Hamiltonian, with dispersions  $E_{\pm}(\mathbf{p}) = \pm \sqrt{p^2 c^2 + \Delta^2}$ . The spectrum has a gap of size  $2|\Delta|$  around zero energy. In the sections below we will deal with the special case of  $\Delta = 0$ , when the dispersions become photon-like  $E_{\pm}(\mathbf{p}) = \pm pc$ , i.e, vary linearly with the momentum (see Figure 1.1).  $c$  is now identified with the propagation speed of these gapless excitations.

### 1.1.1 Graphene

In 1947, Wallace made a remarkable discovery[151] while calculating the band structure of graphite. Graphite is composed of layers of carbon atoms, with the interlayer bonds being much weaker than the intralayer bonds. Each layer is composed of carbon atoms arranged in a hexagonal lattice. Wallace found that a nearest neighbor tight-binding model on a hexagonal lattice of carbon atoms yields a semi-metallic dispersion, with the valence and conduction bands well-separated at all points of momentum space except at the high symmetry  $K$  and  $K'$  points of the planar Brillouin zone, as shown in Figure 1.1. Since there is only one free mobile electron on each carbon atom, the chemical potential in a clean monoatomic sheet of these carbon atoms, called ‘graphene’, should lie exactly at the  $K$  and  $K'$  points where the conduction and valence bands touch. Wallace further showed that the band structure near these

---

<sup>b</sup>In deriving the Hamiltonian Eq. (1.6) from Eq. (1.3), one needs to recall that  $x^0 \equiv ct$ . Also, note that in Eq. (1.6),  $\hat{\mathbf{p}} = (\hat{p}_x, \hat{p}_y)$ .

points is the same as that obtained for the Dirac equation in 2+1 dimensions (i.e, Eq. (1.6)).

Half a century later, Wallace's calculation was tested directly by an experiment when Andre Geim's group at the University of Manchester was able to isolate single-atom-thick sheets of graphene[99]. For this remarkable discovery, Andre Geim and Konstantin Novoselov were awarded the Nobel prize in Physics in 2010. After this discovery, many experiments have been performed on this material and it is clear that graphene indeed hosts four species of Dirac fermions – the multiplicity coming from the two spin states in combination with the location of the Dirac point (at the  $K$  or  $K'$  point of the Brillouin zone).

Some of the first experiments to be performed on graphene were studies of its transport properties as a function of doping. Since the density of states at the Dirac point is very low (vanishing linearly as the energy shift from the Dirac point), it is very easy to tune the chemical potential through the Dirac point by modulating a back gate. It was found that near the Dirac point, the conductance became saturated at some low but nonzero value[180, 98]. Many theories explaining this behavior have been written down and there is a consensus that this phenomenon is controlled by scattering from charged impurities in the vicinity of the graphene sheet, possibly embedded in the substrate[3]. Understanding the effects of charged impurities in graphene near the neutrality point is thus a very important step towards understanding its transport properties in the lightly-doped regime.

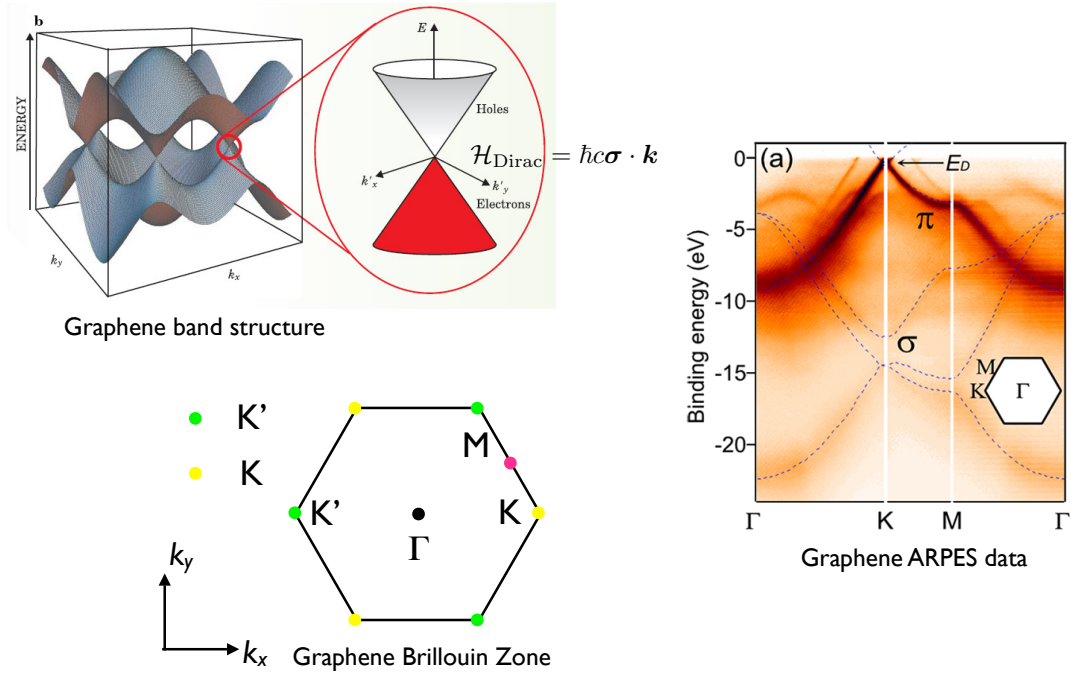


Figure 1.1: The band structure of graphene – there are two species of Dirac particles at the  $K$  and  $K'$  points. Due to the method of construction of the highly symmetric hexagonal Brillouin zone (the Wigner-Seitz cell), each of these points appears thrice on the boundary, contributing one-third of the Dirac quasiparticles in each case. The ARPES data on the right showing the measured Dirac dispersion at the  $K$  point is reproduced from [102], while the three-dimensional band structure is reproduced from the review [163].

### Coulomb Impurity

To understand the response to charged impurities in metals, one takes into account two main aspects of the response of the electron gas. First, since the bare Coulomb field is long-ranged, a screening cloud supplied by the metal's copious charge carriers shields the impurity. This effect can be treated semiclassically using the Thomas-Fermi approximation [61], yielding an exponential screening of the bare Coulomb field. The strength of this screening is given by the inverse Debye screening length  $\lambda_D^{-1}$  and

is proportional to the density of states at the Fermi surface. The second effect arises due to the wave nature of the electrons and leads to an oscillatory component of the response. This phenomenon was discovered by and is named after Friedel [37]. These oscillations occur at the Fermi wave vector  $k_F$ .

In graphene, at the neutrality point, both  $k_F$  and the density of states at the Fermi level  $\propto \lambda_D^{-1}$  are zero. As a result, there is no conventional screening of a Coulomb charge in graphene. However, the peculiar structure of particle-hole excitations of the Dirac gas encourages us to look more closely at this scenario.

From the purely dimensional point of view, any long-wavelength response of the induced charge density in graphene around a Coulomb impurity charge  $Q$  at  $\mathbf{r} = 0$  should have the form

$$\delta\rho(\mathbf{r}) = F(Q)\delta(\mathbf{r}) + \frac{G(Q)}{r^2} \quad (1.7)$$

Since the Dirac equation Eq. (1.6) with  $\Delta = 0$  gives only one physical scale – the velocity  $c$  – we cannot form any natural length scale for use in the function above. In 1984, DiVincenzo and Mele[30] concluded that there is a finite value for  $G(Q)$ . In Chapter 3 it is shown that if exchange corrections coming from electronic interactions are neglected,  $G(Q) = 0$  to all orders in perturbation theory. In other words, for small enough values of  $Q$ , an impurity Coulomb charge induces only some local charge  $F(Q)$ , which turns out to be of the physically reasonable *opposite* sign. However, inclusion of exchange contributions leads us to conclude that  $G(Q)$  is nonzero and has the *same* sign as  $Q$  – a remarkably peculiar effect. A schematic explaining the full scenario is shown in Figure 1.2.

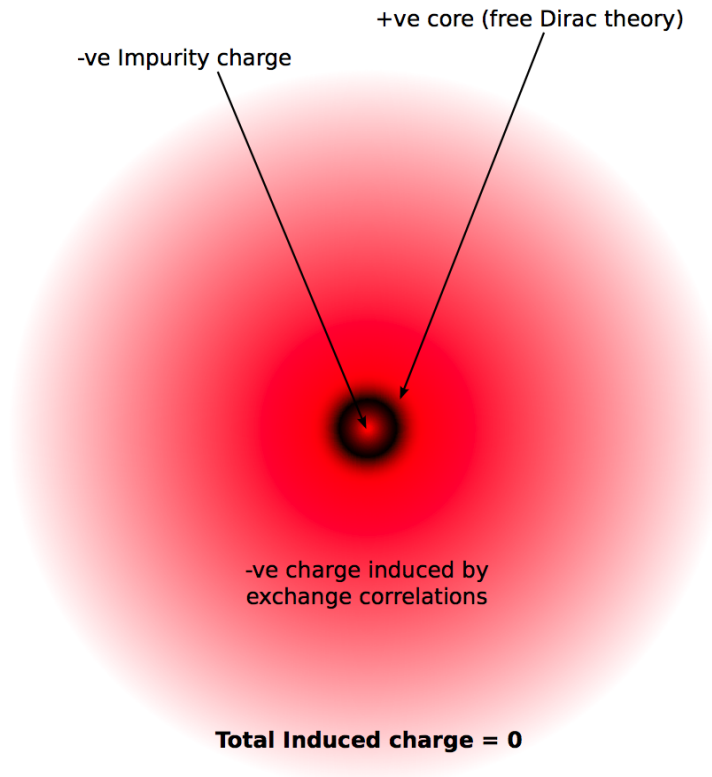


Figure 1.2: Graphene's response to a negative Coulomb charge placed on it: red/black = -/+ve charge . The intrinsic response of the Dirac quasiparticles is to create a local shell of positive charge around the impurity. Further electronic correlations create a distributed sheet of *negative* charge surrounding the impurity. The total amount of charge induced is found to be zero.

### Impurity in a magnetic field

Nearly a decade after Wallace's discovery of the Dirac quasiparticles in graphene, in 1956 McClure pointed out[86] a remarkable feature of the Dirac spectrum when the orbital effect of a magnetic field perpendicular to the graphene sheet is considered. In such a scenario, the energy spectrum of electrons with quadratic dispersions gets quantized into evenly spaced discrete Landau levels with the inter-level gap being proportional to the magnetic field. However, the Landau levels for the Dirac quasi-

particles in graphene are *not* evenly spaced. The energy difference  $E_n$  between the  $n^{\text{th}}$  Landau level from the zeroth Landau level at the Dirac point is found to be proportional to  $E_n \propto \sqrt{|nB|}$ . This Landau level structure has been verified in many experiments[79]. It will also be interesting to study the unconventional structure of the Landau level wavefunctions Eq. (4.3). One way to probe these wavefunctions is to find their response to local impurities. It is now possible to analyze large areas<sup>c</sup> of almost clean graphene using scanning tunneling microscopes[88]. The only impurities present are local defects in the graphene lattice that may be modeled as local potential impurities. In Chapter 4 an analysis is presented where the spatial Fourier transform of the scanning tunneling spectra (FT-STs) is calculated for such a scenario. The expected result is summarized in Figure 4.2.

### 1.1.2 Strong Topological Insulators

Over the last decade (2000-2010), a remarkable sequence of developments have occurred in our understanding of a particular aspect of the topology of electronic bands in materials with strong spin-orbit interaction. These developments relied on an interesting property of electronic states – the Kramers degeneracy[72] in the presence of time reversal symmetry (TRS). Since an electron has spin half, the time reversal operator  $\Theta$  satisfies the special property

$$\Theta^2 = -1 \tag{1.8}$$

---

<sup>c</sup>Comparable to the magnetic length under typical experimental conditions  $\sim 50\text{\AA}$

The consequence of this is that if the Hamiltonian possesses TRS, then the time-reversed partner of any eigenstate is another *orthogonal* state with the same energy – hence the forcing of a *degeneracy*. This remarkable fact can be proved by calculating the overlap between an eigenstate  $|\psi\rangle$  and its time-reversed partner  $|\tilde{\psi}\rangle = \Theta|\psi\rangle$ . Using the anti-unitary property[160] of  $\Theta$  which tells us that  $\langle\alpha|\beta\rangle = \langle\tilde{\beta}|\tilde{\alpha}\rangle$ , along with the property Eq. (1.8), we find that

$$\langle\tilde{\psi}|\psi\rangle = \langle\tilde{\psi}|\tilde{\tilde{\psi}}\rangle = \langle\tilde{\psi}|\Theta^2|\psi\rangle = -\langle\tilde{\psi}|\psi\rangle = 0 \quad (1.9)$$

which is the statement of Kramers degeneracy mentioned above. In materials without spin-orbit interaction this devolves into a simpler statement that the two spin states for any orbital eigenstate have to be degenerate. For materials with spin-orbit coupling, however, there are richer possibilities.

Much of the work that will be described here was initially motivated by attempts to find materials which are useful for spintronics – that allowed control and transport of the electron spin. For this reason, materials were sought which contained extended electronic states that are forced to be spin-polarized because of spin-orbit coupling. One such possibility was shown in 2005 by Kane and Mele[63] – they argued that there existed a nontrivial phase in graphene with strong enough spin-orbit coupling where extended edge modes had to exist that were spin-polarized. For the edge states to exist, graphene had to become gapped in the bulk. Inside this energy gap, peculiar edge modes had to exist in the nontrivial phase. In this phase, at a given edge and energy, there was only one pair of eigenstates that were also Kramers degenerate. These states had opposite momenta (because they were time-reversed partners) but any back-scattering was forbidden by TRS-preserving disorder! This

is easily seen by showing that the action of a TRS-preserving unitary time evolution operator  $U(t) = \Theta U(t)^\dagger \Theta^{-1}$  can *never* convert  $|\psi\rangle$  to  $|\tilde{\psi}\rangle$ :

$$\langle \tilde{\psi} | U(t) | \psi \rangle = \langle \tilde{\psi} | \Theta U(t)^\dagger \Theta^{-1} | \tilde{\psi} \rangle = \langle \tilde{\psi} | U(t) \Theta^2 | \psi \rangle = - \langle \tilde{\psi} | U(t) | \psi \rangle = 0 \quad (1.10)$$

As a result, these states circumvent the mandatory localization transition in one dimension[2] for the spin-orbit-free case and need not get localized due to weak potential disorder – making them ideal for carrying some form of spin-polarized current. In 2006, Bernevig and Zhang [14] predicted that CdTe/HgTe/CdTe quantum wells would also exhibit such a nontrivial phase with extended (spin-polarized) edge modes if the well depth was tuned above a critical value. This prediction was realized just a year later by Konig and others [70].

In a later paper [64], Kane and Mele gave the first argument that the special phase of graphene discussed above is one of two ‘topologically-classified’ states that are possible for an electronic band-structure – the ‘normal’ insulator and a ‘topological’ insulator, the latter possessing an extended set of edge modes. The mathematical definition of the associated  $Z_2$  topological invariant is involved, but the core physics is as follows. Let us consider a semi-infinite sheet of a two dimensional insulator with spin-orbit interaction. Suppose that the edge is along the  $x$ -direction and so the momentum  $k_x$  is a good quantum number because of translational invariance along the edge. Let us plot the spectrum as a function of  $k_x$  as shown in Figure 1.3. Inside the bulk energy gap, there may exist states that are confined to the edge of the material. We shall show that there are two ‘topological’ ways to classify these edge states, using Kramers degeneracy. For this, we need to introduce the concept of time-reversal-invariant-momenta (TRIM): these are points  $\mathbf{k}$  on the Brillouin zone



such that they are same as their time-reversed partner  $-\mathbf{k}$ . Along the  $k_x$  axis, there are two such points  $k_x = 0$  (call it  $\Lambda_1$ ) and  $k_x = \pi$  (call it  $\Lambda_2$ ). Because of Kramers degeneracy, each surface band has a degenerate pair related by time reversal (the ‘Kramers pair’) and these bands need to cross each other at the TRIM. As we follow a surface band from one TRIM  $\Lambda_1$  to the other,  $\Lambda_2$ , it can either be degenerate with the same other band at both points or may ‘switch’ its Kramers partner – the two scenarios being sketched in Figure 1.3. Now, it is clear that no analytic perturbation to the Hamiltonian (which does not ‘tear’ the bands) can transform one case to the other, without closing the bulk gap. This is thus the basis of defining the two classes of ‘normal’ and ‘topological spin hall’ insulators.

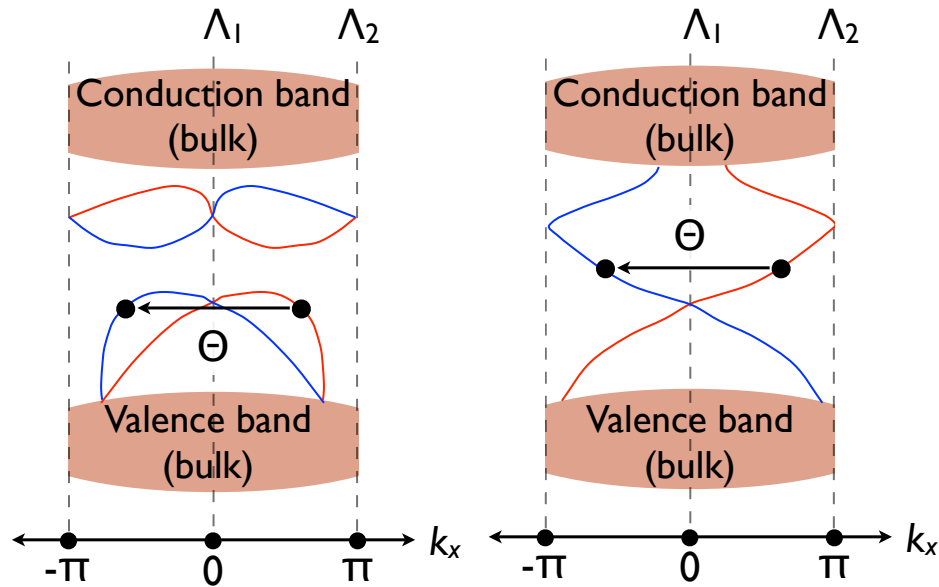


Figure 1.3: The two possibilities for the topology of edge states in two dimensional band insulators that preserve time reversal symmetry. The red and blue bands form the Kramers pair – applying the time reversal operator  $\Theta$  on one state with momentum  $k_x$  will produce a state in the Kramers partner with momentum  $-k_x$ . The TRIM  $\Lambda_{1,2}$  are  $k_x = 0, \pi$  because reversing them brings one back to the same point in the (periodic) Brillouin zone.

In three dimensional band insulators an analogous classification exists[42, 40, 89, 116] which is similar in spirit in that it relies upon the concepts of Kramers degeneracy and the switching/retaining of Kramers pairs as one moves between the four TRIM<sup>d</sup> of the surface Brillouin zone. We shall not explore this classification in detail here because it is far outside the main focus of this dissertation. Suffice it to say that it can be shown that a class of three dimensional band insulators exists such that their surfaces host gapless surface bands with an *odd* number of gapless Dirac points located at some of the four TRIM points. These are known as ‘strong’ topological insulators, since in the presence of TRS-preserving perturbations and disorder their surface states are predicted to remain gapless (and extended[117]). In 2007, Fu and Kane[42, 40] predicted a number of materials that are strong topological insulators, aided in part by a very simple prescription that they discovered for finding topological insulators in materials with inversion symmetry[40]. Following that, numerous materials have been experimentally discovered both preceding (like Bi<sub>2</sub>Se<sub>3</sub>[166]) and following (like Bi-Sb alloys[53] and Bi<sub>2</sub>Te<sub>3</sub>[21]) their theoretical prediction.

The surfaces of Bi<sub>2</sub>Se<sub>3</sub> and Bi<sub>2</sub>Te<sub>3</sub> host single Dirac cones at the Brillouin zone center ( $\mathbf{k} = 0$ , the  $\Gamma$  point). The equation for the effective Hamiltonian near those Dirac points can be written down as

$$\mathcal{H}_D = c \boldsymbol{\sigma} \times \hat{\mathbf{p}} \quad (1.11)$$

where the Pauli matrices  $\boldsymbol{\sigma} = (\sigma_x, \sigma_y)$  are proportional to the surface projection of the actual electron spin operator  $S_i = (\hbar/2)\sigma_i$ . This can be shown to be equivalent to

---

<sup>d</sup>The four TRIM are given by the four combinations for  $(k_x, k_y)$  with values  $k_{x,y} = 0, \pi$ .

the  $\Delta = 0$  case of the standard form Eq. (1.6) of the 2+1 dimensional Dirac equation by applying a unitary transformation on the spin states which rotates the  $x$  and  $y$  spin axes by 90 degrees. In any case, the equation describes electronic states whose spins lie in the plane of motion and are locked to a set orientation with respect to the direction of their momentum, and whose energies vary linearly with their momenta.

### Effects of local impurities

From the preceding discussion it is clear that the surface states on strong topological insulators (STI) are remarkable because of their predicted resilience to disorder. It is thus a very useful exercise to investigate the possible effects of impurities on these states. Using the T matrix formulation, we have provided a non-perturbative evaluation of the effects on these states due to isolated short-ranged potential or (classical) magnetic impurities in Chapter 5. We find that such impurities create resonances or enhancements in the density of states close to the Dirac point<sup>e</sup>, which decay slowly as the inverse square of the distance from the impurity as shown in Figure 5.2. These resonances sharpen and move closer to the Dirac point as the impurity strength becomes large. Spin textures are induced near a magnetic impurity due to the strong spin-orbit coupling. These in turn mediate nontrivial RKKY interactions between magnetic impurities

$$U_{\text{RKKY}} = a_1 \mathbf{S}_1 \cdot \mathbf{S}_2 + a_2 \hat{\mathbf{r}}_{21} \cdot (\mathbf{S}_1 \times \mathbf{S}_2) + a_3 (\mathbf{S}_1 \cdot \hat{\mathbf{r}}_{21})(\mathbf{S}_2 \cdot \hat{\mathbf{r}}_{21}) \quad (1.12)$$

---

<sup>e</sup>Such features have already been observed, as seen in unpublished data from the talk D2.00002 on “STM and STS studies of electronic states near macroscopic defects in topological insulators” given by Z. Alpichshev at the APS March Meeting, 2011.

composed respectively of the Heisenberg, Dzyaloshinskii-Moriya and dipole-dipole terms<sup>f</sup>. A simplification occurs when the chemical potential is close to the Dirac point (the undoped case) – only the Heisenberg and dipolar interactions remain and because the Fermi wavelength is zero, these interactions do not oscillate in space and the interaction energy decays as the cube of the distance between the impurity spins.

A consequence of the form of this interaction is that two spins prefer to align parallel to each other but perpendicular to the line joining them, as shown in Figure 1.4. As a result, if magnetic impurities are randomly placed on an undoped STI surface, all impurity interactions are simultaneously satisfied only if they ferromagnetically align perpendicular to the surface. We thus predict a transition to this phase at low temperatures (see Figure 1.4). Such a transition has an important consequence – the value of  $\Delta$ , the gap parameter in Eq. (1.6), is proportional to the collective magnetic moment perpendicular to the STI surface and so this transition will also open a gap in the surface state spectrum. Such a process has recently been observed when the  $\text{Bi}_2\text{Se}_3$  surface is doped with iron atoms[164] and currently there exists no alternate explanation for this phenomenon. Such a gap opening may be utilized to observe phenomena related to the quantization of the magnetoelectric effect in these materials, which is a direct consequence of the  $Z_2$  classification[77].

---

<sup>f</sup>In Eq. (1.12),  $\mathbf{r}_{21}$  is the vector joining the two impurity spins  $\mathbf{S}_{1,2}$  while  $a_{1-3}$  are functions of  $r_{21}$  and the impurity-2DEG interaction strengths.

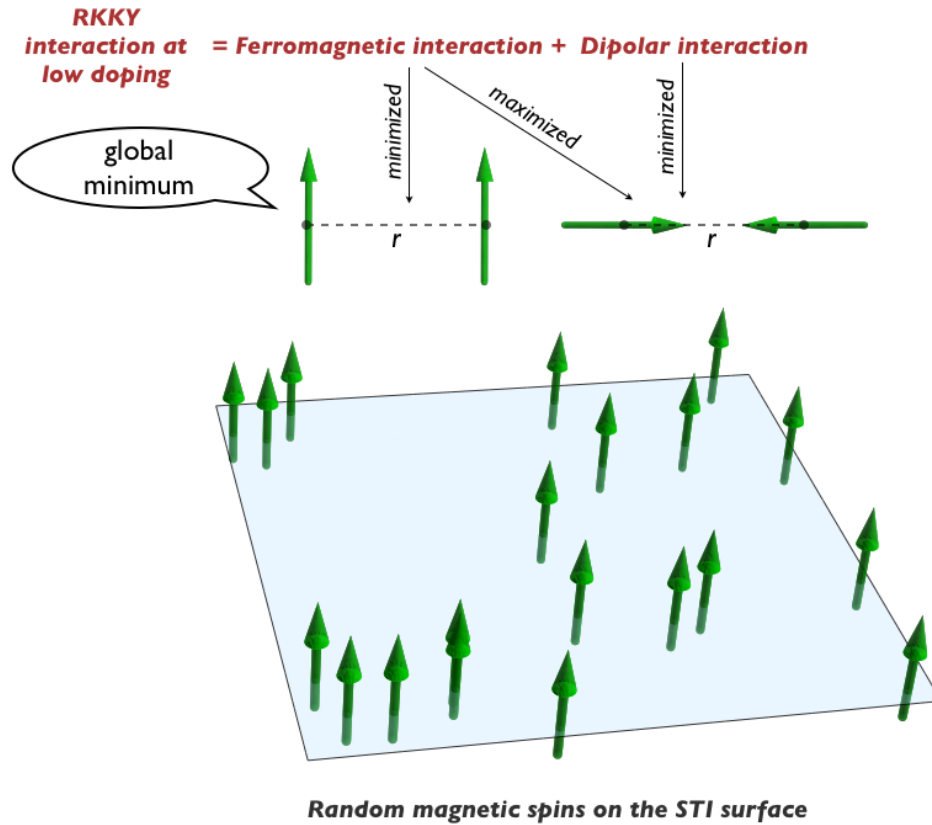


Figure 1.4: Consequences of the RKKY interaction between impurity spins on an undoped strong topological insulator.

### Step edges

Aside from point-like local impurities, step edges on the STI surface have been observed and their effects measured in recent experiments[179, 114, 5]. In Chapter 6, we take a look at the effects of a step edge on the LDOS of the STI surface. Using a scattering matrix formulation and time reversal symmetry, we can show that a suitably defined reflection amplitude is antisymmetric in the angle of incidence, which is zero at normal incidence. This, coupled with the spin-momentum locking of the TI surface states, enables us to deduce the power laws that should appear in the

distance-dependent decay of the induced LDOS oscillations, far from the step edge. Many of these simple conclusions, which do not require a detailed modeling of the step edge, been vindicated in recent experiments<sup>g</sup>.

## 1.2 Spin Liquids

The traditional introduction to interacting spin systems is usually through classic examples broken-symmetry states: the ferromagnet and then the Néel antiferromagnet. However, quantum fluctuations can also favor orderless but strongly correlated ‘spin liquid’ states at low temperatures. One such example is that of the one dimensional anti-ferromagnetic Heisenberg spin half chain<sup>h</sup>, which has no long range order and power law correlations[27] in its ground state. The 1-D spin 1 antiferromagnetic chain was also shown by Haldane[48] to possess an orderless ground state with a gap to excitations. Another reason why magnetic long range order might be suppressed is the inclusion of frustration, for e.g., arising due to the geometry of the triangular lattice. Increasing the lattice dimension typically favors mean field effects and ordered states. However, there is speculation that quantum systems exist in two dimensions that exhibit no long range order – we will look at some such theoretical spin liquid states in the next two sections.

---

<sup>g</sup>Ref: unpublished data from the talk V35.00006 on “Power laws and STM image of standing wave of the topological surface states” given by the group of Qi-Kun Xue at the APS March Meeting, 2011.

<sup>h</sup>The one dimensional anti-ferromagnetic Heisenberg spin- $s$  is defined by the Hamiltonian  $\mathcal{H}_{1D} = J \sum_i \mathbf{S}_i \cdot \mathbf{S}_{i+1}$ , where  $J > 0$  and  $\mathbf{S}_i$  are spin  $s$  operators on the sites  $\{i\}$  of a one dimensional lattice.

### 1.2.1 The staggered flux spin liquid

A paradigm in the treatment of strongly correlated materials is the Hubbard model on the square lattice. In this model, usually considered near half filling, spin half electrons hop on a square lattice with a nearest neighbor hopping amplitude  $t$ . There is also a short range interaction between the electrons – there is an energy cost  $U$  when two electrons occupy the same site. The Hamiltonian is thus

$$\mathcal{H}_{\text{Hubb}} = \sum_{\mathbf{x}} \left[ \sum_{i=x,y,s=\uparrow,\downarrow} t (\psi_s^\dagger(\mathbf{x} + \mathbf{b}_i) c_s(\mathbf{x}) + h.c.) + U n_\uparrow(\mathbf{x}) n_\downarrow(\mathbf{x}) \right] \quad (1.13)$$

where  $c_s(\mathbf{x})$  ( $s = \uparrow, \downarrow$ ) denote the electron annihilation operator at site  $\mathbf{x}$ , etc. It has been argued[6] that the half-filled (exactly one electron per site) Hubbard model is a good model for the undoped phase of the cuprate high  $T_c$  superconductor compounds. Following Anderson's influential paper in 1987[6], it is believed that the ground state of the model at some small hole doping consists of fluctuating singlet pairs with various ranges of entanglement, in addition to charge vacancies (holons). Spin excitations of this system occur when the singlets are disrupted. In certain scenarios, the two spin halves created by this process may be able to move apart, i.e become *deconfined*, in which case this spin liquid state will have uncharged spin half excitations – called spinons.

In its hole-doped regime, the Hubbard model can be simplified to the  $t - J$  model:

$$\mathcal{H}_{tJ} = J \sum_{\langle \mathbf{x}\mathbf{y} \rangle} \left( \mathbf{S}(\mathbf{x}) \cdot \mathbf{S}(\mathbf{y}) - \frac{n(\mathbf{x})n(\mathbf{y})}{4} \right) + t \sum_{\mathbf{x},i=x,y,s=\uparrow,\downarrow} \psi_s^\dagger(\mathbf{x} + \mathbf{b}_i) c_s(\mathbf{x}) + h.c. \quad (1.14)$$

with the constraint of *no double occupation* per site, and  $J = 4t^2/U$ . Here  $\mathbf{S}$  are

the spin operators. One method to try and solve this model is to use the following representation of the electron annihilation operator[4, 159]. We begin by introducing auxiliary fermionic fields  $f_s(\mathbf{x})$  and bosonic fields  $b_s(\mathbf{x})$ , with  $s = 1, 2$ . These can be combined as follows

$$\Psi_1 = \begin{pmatrix} f_1 \\ f_2^\dagger \end{pmatrix}, \quad \Psi_2 = \begin{pmatrix} f_2 \\ -f_1^\dagger \end{pmatrix}, \quad b = \begin{pmatrix} b_1 \\ b_2 \end{pmatrix} \quad (1.15)$$

and used to represent the actual electron operators  $c$  via the relation

$$c_s = \frac{b^\dagger \Psi_s}{\sqrt{2}}, \quad s = (1 \text{ or } \uparrow), (2 \text{ or } \downarrow) \quad (1.16)$$

The Hilbert space for the t-J model is recovered through the constraints (per site)

$$\frac{1}{2} \Psi_s^\dagger \boldsymbol{\tau} \Psi_s + b^\dagger \boldsymbol{\tau} b = 0 \quad (1.17)$$

where  $\boldsymbol{\tau}$  are Pauli matrices that act in the index space of Eq. (1.15). This representation can now be substituted into Eq. (1.14) and a mean field analysis performed to find the spectrum for the spinons  $f_s$ . The constraints Eq. (1.17) along with a local  $SU(2)$  gauge symmetry of the mean field Hamiltonian defined by the transformations

$$\Psi_{1,2}(\mathbf{x}) \rightarrow W(\mathbf{x}) \Psi_{1,2}(\mathbf{x}), \quad b(\mathbf{x}) \rightarrow W(\mathbf{x}) b(\mathbf{x}), \quad W \in SU(2) \quad (1.18)$$

also lead to the appearance of an  $SU(2)$  gauge field  $A_\mu^\ell$ , where  $\ell$  runs over the three  $SU(2)$  generator indices and  $\mu$  are the space-time indices. The mean field ansatz consists of appropriately condensing the bosons  $b$ , finding the requisite mean field values for the  $SU(2)$  gauge fields and ascribing a mean field value to the spinon



hopping amplitudes

$$U_{\mathbf{x},\mathbf{y}} = \begin{pmatrix} -\chi_{\mathbf{x}\mathbf{y}}^* & \Delta_{\mathbf{x},\mathbf{y}} \\ \Delta_{\mathbf{x},\mathbf{y}} & \chi_{\mathbf{x}\mathbf{y}} \end{pmatrix}$$

$$\chi_{\mathbf{x}\mathbf{y}} = \langle f_s^\dagger(\mathbf{x}) f_s(\mathbf{y}) \rangle, \Delta_{\mathbf{x}\mathbf{y}} = \langle f_1(\mathbf{x}) f_2(\mathbf{y}) - f_2(\mathbf{x}) f_1(\mathbf{y}) \rangle \quad (1.19)$$

Wen and Lee found[159] found that there exists a parameter regime where the following ansatz (which does not break any lattice symmetry and is by construction invariant under spin rotations) has the lowest ground state energy:

$$U_{\mathbf{r},\mathbf{r}+\mathbf{b}_x} = -\tau^3 \chi - i(-1)^{r_x+r_y} \Delta \tau^1$$

$$U_{\mathbf{r},\mathbf{r}+\mathbf{b}_y} = -\tau^3 \chi + i(-1)^{r_x+r_y} \Delta \tau^1$$

$$A_0^\ell = \langle b \rangle = 0 \quad (1.20)$$

This is the staggered flux (sF) spin liquid, thus named due to the staggered configuration of the winding fluxes given by the hopping ansatz. The spinon dispersion in this phase has gapless Dirac nodes at the points  $(\pm\pi/2, \pm\pi/2)$  in the Brillouin zone. Wen showed[156] that this state partly breaks the  $SU(2)$  symmetry down to a  $U(1)$  symmetry group. Rantner and Wen[111] showed that these  $U(1)$  gauge fluctuations strongly modify the properties of the Dirac quasiparticles. The excitation spectrum, however, still remains gapless and spin correlations obey power laws – thus this strongly interacting phase was named the ‘algebraic spin liquid’.

In Chapter 2 we will consider the effects of a spin vacancy in such a staggered flux spin liquid. Following earlier arguments[122] we show that the relevant coupling to the impurity occurs through via an impurity electric charge for the  $U(1)$  gauge field. We show that the impurity spin contributes a Curie-like spin susceptibility

with an anomalous coefficient. We also find that no staggered magnetization (or other predicted competing orders[49]) is induced near the impurity.

### 1.2.2 The Majorana Spin Liquid on the triangular lattice

At the beginning of this chapter, we have seen how Dirac formulated his quantum theory of a relativistic particle. It turns out that the spectrum of the Dirac equation is unbounded from below. While that is not a physical enigma for solid state physics, where there is a physical filled valence band, it produces a paradox in elementary particle physics where the concept of a vacuum needs to exist such that one could add to it particles which require additional energy to create. Dirac postulated the concept of a vacuum where the lower branch of eigenstates  $E_- = -\sqrt{m^2c^4 + p^2c^2}$  was completely filled by fermionic particles. Excitations would arise in the form of particle-hole pairs when a particle from the lower branch was promoted to the upper energy branch.

Such a concept of ‘material’ vacuum was discomfiting for many physicists and another argument for an alternate quantum theory of elementary relativistic particle was put forth by the Italian physicist Ettore Majorana[80]. He considered ‘real’ fermions that had no classical analog. The particles – dubbed the Majorana fermions – that arose from this formulation had no charge and no distinct ‘antiparticles’. In particle physics, Majorana fermions have been considered as candidates for the neutrino and the ‘photino’, the supersymmetric partner of the photon, while in condensed matter physics they are candidates for bound vortex states in certain kinds of superconduc-

tors<sup>i</sup>.

The self-adjoint nature of a Majorana fermion  $\gamma = \gamma^\dagger$  has an interesting consequence – it is possible to write down Majorana theories without a  $U(1)$  gauge freedom. This can be very useful as we shall see below.

Recently, a couple of organic charge-transfer salts have been shown to possess interesting spin liquid-like ground states –  $[\kappa\text{-(BEDT-TTF)}_2\text{Cu}_2(\text{CN})_3]$ [134] and  $\text{EtMe}_3\text{Sb}[\text{Pd}(\text{dmit})_2]_2$ [58]. Both of these feature triangular lattices with spin 1/2s with strong antiferromagnetic Heisenberg interactions. In the latter case, which we shall henceforth refer to as dmit-131, the spin liquid is found to be gapless with a low temperature thermal conductance that is proportional to the temperature[168], presumably arising from the spin degrees of freedom. While a linear in temperature thermal conductivity is expected for a theory of free fermionic spinons with a finite Fermi surface<sup>j</sup>, it was shown that gauge fluctuations should modify[76] the temperature dependence. Also, Katsura and others argued[66] that the flux of the spinon  $U(1)$  gauge field should couple to a perpendicular magnetic field and this should lead to the observation of a finite thermal Hall conductance if indeed deconfined fermionic spinons were responsible for the observed thermal current. A measurement of the thermal Hall effect, however, gave a null result[168].

In keeping with the experimental observation of a zero thermal Hall effect, we have

---

<sup>i</sup>For a discussion, see [161].

<sup>j</sup>Ignoring charge fluctuations, fermionic spinons  $f_{1,2}$  are defined for spin 1/2-s through the relation  $\mathbf{S} = (f_\alpha^\dagger \boldsymbol{\sigma}_{\alpha\beta} f_\beta)/2$  along with a per-site single occupancy constraint  $\sum_s f_s^\dagger f_s = 1$  imposed using a  $U(1)$  gauge field, corresponding to the gauge freedom  $f_s \rightarrow e^{i\phi} f_s$ .

proposed in Chapter 7 a spin liquid theory composed of deconfined spin 1 Majorana fermion spinons. The analysis is based on the following parton representation of spin half[85, 146, 24, 133, 126]

$$S^\mu = \frac{i}{4} \epsilon^{\mu\alpha\beta} \gamma^\alpha \gamma^\beta, \quad (1.21)$$

where the various indices run over  $x, y, z$  and the  $\gamma^\alpha$  is a Majorana fermion

$$(\gamma^\alpha)^\dagger = \gamma^\alpha, \quad \{\gamma^\alpha, \gamma^\beta\} = 2\delta_{\alpha\beta} \quad (1.22)$$

There is a  $Z_2$  gauge redundancy in this formulation and the Majorana fermion is found to transform under spin rotations like a three-dimensional vector, i.e, it is a spin 1 particle. We write down a spin liquid state on the triangular lattice that is formed out of Majorana bilinears – requiring spin rotation invariance and adherence to all lattice symmetries, *modulo* a gauge transformation. This procedure is the same as that of using the projective symmetric group (PSG – see [157]). It turns out that any quadratic Majorana Hamiltonian breaks time reversal and inversion symmetries, and our theory is restricted to have the symmetry of combined time reversal and an elementary lattice rotation.

The Majorana spin liquid derived in Chapter 7 is found to have a characteristic Fermi surface that consists of three curves intersecting at  $\mathbf{k} = 0$ . The quasiparticles at this intersection point have a dispersion that goes as the *cube* of their momenta. This leads to a divergent density of states (DOS) at low energies which controls the low temperature thermodynamics of the spin liquid. We also study the effects of a magnetic field on this system. The Zeeman term gaps out two-thirds of these quasiparticles and this leads to a drop in the quasiparticle specific heat and magnetic susceptibili-

---

ties. We argue, however, that the longitudinal thermal transport is unaffected by the Zeeman coupling – an observation that is consistent with experiments on the gapless spin liquid in dmit-131[168]. The presence of dilute impurities is found to soften the DOS divergence at low energies, leading to a constant low temperature magnetic susceptibility and a specific heat that is proportional to the temperature. Finally, we show the thermal conductivity to also be proportional to the temperature, at low temperatures. There is no thermal ‘Hall’ effect due to the application of a magnetic field, since the usual mechanism of orbital coupling of the magnetic field to the spinon  $U(1)$  gauge field does not arise here. This was our original motivation for using Majorana fermions. The last couple of observations regarding thermal transport are also consistent with measurements in dmit-131[168].

# Chapter 2

## Theory of quantum impurities in the staggered flux spin liquid

### 2.1 Synopsis

We describe spin correlations in the vicinity of a generalized impurity in a class of fractionalized spin liquid states. We argue that the primary characterization of the impurity is its electric charge under the gauge field describing singlet excitations in the spin liquid. We focus on a gapless  $U(1)$  spin liquid described by a 2+1 dimensional conformal field theory (CFT): the staggered flux (sF) spin liquid. In ref. [69], the more extended body of work containing the results of this chapter, we also considered the case of the deconfined critical point between the Néel and valence bond solid (VBS) states. For such spin liquids, the electric charge is argued to be an exactly

marginal perturbation of the CFT. Consequently, the impurity susceptibility has a  $1/T$  temperature dependence, with an anomalous Curie constant which is a universal number associated with the CFT. One unexpected feature of the CFT of the sF state is that an applied magnetic field does not induce any staggered spin polarization in the vicinity of the impurity (while such a staggered magnetization is present for the Néel-VBS case). These results differ significantly from earlier theories of vacancies in the sF state, and we explicitly demonstrate how our gauge theory corrects these works. We discuss implications of our results for the cuprate superconductors, organic Mott insulators, and graphene.

## 2.2 Introduction

The response of a strongly interacting electronic system to impurities has long been a fruitful way of experimentally and theoretically elucidating the subtle correlations in its many-body ground state wavefunction. The most prominent example is the Kondo effect, which describes the interplay between a variety of impurities with a spin and/or ‘flavor’ degree of freedom and a system of free fermions with either a finite [51, 100, 60] or vanishing [38, 149] density of states at the Fermi energy.

More recently, the impurity responses of a variety of ‘non-Fermi-liquid’ bulk states have been studied. [62, 32, 33, 120, 127, 148, 121, 118, 182, 177, 138, 145, 122, 52, 35] The  $S = 1/2$  antiferromagnetic spin chain generically has a critical ground state, and displays interesting universal characteristics in its response to impurities or boundaries [32, 33]. Universality was also found in the general theory [120, 148, 122] of impurities

in ‘dimerized’ quantum antiferromagnets in spatial dimensions  $d \geq 2$  near a quantum critical point between a Néel state and a confining spin gap state. Such ‘dimerized’ antiferromagnets have an even number of  $S = 1/2$  spins per unit cell, and consequently their bulk quantum criticality is described within the conventional Landau-Ginzburg-Wilson (LGW) framework of a fluctuating Néel order parameter.[130, 128, 131] Away from the impurity, such systems only have excitations which carry integer spin.

It is the purpose of this chapter to extend the above theory [120, 148, 122] to fractionalized ‘spin liquid’ states in spatial dimensions  $d \geq 2$  with neutral  $S = 1/2$  excitations (‘spinons’) in the bulk. Such spinon excitations carry gauge charges associated with an ‘emergent’ gauge force (distinct from the electromagnetic forces), typically with the gauge group [113, 156]  $Z_2$  or  $U(1)$ , and we will argue shortly that such gauge forces play a key role in the response of spin liquid states to impurities. Earlier analyses[73, 67, 93, 92, 106, 107, 154] of the influence of impurities in the  $U(1)$  ‘staggered-flux’ spin liquid ignored the crucial gauge forces; we will comment in detail on the relationship of our results to these works in Section 2.3.2.

There are a number of experimental motivations for our work. A large number of experiments have studied Zn and Ni impurities in the cuprates,[18, 104, 173, 105, 55] and much useful information has been obtained on the spatial and temperature dependence of the induced moments around the impurity. It would clearly be useful to compare these results with the corresponding predictions for different spin liquid states, and for states proximate to quantum critical points. In [69] we showed that there are significant differences in the experimental signatures of the different candidates, and this should eventually allow clear discrimination by a comparison



to experimental results. A second motivation comes from a recent nuclear magnetic resonance (NMR) study [135] of the  $S = 1/2$  triangular lattice organic Mott insulator  $\kappa$ -(ET)<sub>2</sub>Cu<sub>2</sub>(CN)<sub>3</sub>, which possibly has a non-magnetic, spin singlet ground state. The NMR signal shows significant inhomogeneous broadening, indicative of local fields nucleated around impurities. Our theoretical predictions here for the sF spin liquid (and for some other states, in [69]) for Knight shift around impurities should also assist here in selecting among the candidate ground states.

An important observation is that in situations with deconfinement in the bulk, the bulk spinons are readily available to screen any moments associated with an impurity atom (as has also been noted by Florens *et al.* [35]). Moreover, for a non-magnetic impurity (such as Zn on a Cu site), there is no *a priori* reason for the impurity to acquire a strongly localized moment. Consequently, it is very useful to consider the case where the impurity has local net spin  $S = 0$ . Naively, such a situation might seem quite uninteresting, as there is then no local spin degree of freedom which can interact non-trivially with the excitations of the spin liquid. Indeed, in a Fermi liquid, a non-magnetic impurity has little effect, apart from a local renormalization of Fermi liquid parameters, and there is no Kondo physics. However, in spin liquids the impurity can carry an *electric gauge charge*  $Q$ , and the primary purpose of the work presented in this chapter will be to demonstrate that a  $Q \neq 0$ ,  $S = 0$  impurity displays rich and universal physics.

We will primarily consider U(1) spin liquids here: then an important dynamical degree of freedom is a U(1) gauge field  $A_\mu$ , where  $\mu$  extends over the  $d + 1$  spacetime directions, including the imaginary time direction,  $\tau$ . Our considerations here can

also be easily extended to  $Z_2$  spin liquids, and this was done in [69]. We normalize the  $A_\mu$  gauge field such that the spinons have electric charges  $\pm 1$ . In the popular U(1) gauge theories of antiferromagnets on the square lattice (which we will describe more specifically below), a vacancy will carry a gauge charge  $Q = \pm 1$ . Thus, a Zn impurity on the Cu square lattice site has  $Q = \pm 1$ . This can be understood by thinking of the impurity as a localized ‘holon’ in the doped antiferromagnet, which also carries such gauge charges [92].

We will consider theories here with actions of the structure

$$\mathcal{S} = \mathcal{S}_b + \mathcal{S}_{\text{imp}}, \quad (2.1)$$

where  $\mathcal{S}_b$  is the bulk action of the spin liquid in the absence of any impurity, and  $\mathcal{S}_{\text{imp}}$  represents the perturbation due to an impurity which we assume is localized near the origin of spatial coordinates,  $x = 0$ . We will argue that the dominant term in  $\mathcal{S}_{\text{imp}}$  is the coupling of the impurity to the U(1) gauge field:

$$\mathcal{S}_{\text{imp}} = iQ \int d\tau A_\tau(x = 0, \tau). \quad (2.2)$$

We will demonstrate that additional terms in the impurity action are unimportant or ‘irrelevant’. The  $\mathcal{S}_{\text{imp}}$  above can be regarded as the remnant of the spin Berry phase that characterized the impurity in the previous theory [120, 148, 122] of dimerized antiferromagnets; the latter Berry phase for a spin  $S$  impurity was  $iS$  times the area enclosed by the path mapped on the unit sphere by the time history of the impurity spin. An explicit reduction in the spinon formulation of the spin Berry phase to Eq. (2.2) was presented in Ref. [119].

Our primary results will be for U(1) algebraic spin liquids, [111, 112] which are described by 2+1 dimensional conformal field theories (CFT) and we specialize our presentation to these CFT cases in the remainder of this section. An algebraic spin liquid has gapless spinon excitations which interact strongly with the  $A_\mu$  gauge field. An explicit realization appears in the deconfined quantum critical point [130, 128, 131] between Néel and valence bond solid (VBS) states, in which the spinons are relativistic bosons described by the  $CP^{N-1}$  field theory. Another is found in the ‘staggered flux’ (sF) phase of  $SU(N)$  antiferromagnets, where the spinons are Dirac fermions [111, 112, 50, 49, 96]. In all these cases, the algebraic spin liquid is described by a 2+1 dimensional conformal field theory, and our primary purpose here is to describe the *boundary conformal field theory* that appears in the presence of  $\mathcal{S}_{\text{imp}}$ .

Our central observation, forming the basis of our results, is that  $\mathcal{S}_{\text{imp}}$  in Eq. (2.2) is an *exactly marginal* perturbation to the bulk conformal field theory. This non-renormalization is a consequence of U(1) gauge invariance, which holds both in the bulk and on the impurity. We will verify this non-renormalization claim in a variety of perturbative analyses of the conformal field theory. The claim can also be viewed as a descendant of the non-renormalization of the spin Berry phase term, found in Ref. [122].

The exact marginality of  $\mathcal{S}_{\text{imp}}$  has immediate consequences for the response of the system to a uniform applied magnetic field  $H$ . The impurity susceptibility,  $\chi_{\text{imp}}$ , defined as the change in the total bulk susceptibility due to the presence of the

impurity, obeys

$$\chi_{\text{imp}} = \frac{\mathcal{C}}{T} \quad (2.3)$$

at finite temperature  $T$  above a conformal ground state; this can be extended by standard scaling forms (as in Ref. [148]) to proximate gapped or ordered phases, as we will describe in the next few sections. We set  $\hbar = k_B = 1$  and absorb a factor of the magneton,  $g\mu_B$ , in the definition of the Zeeman field. With this,  $\mathcal{C}$  is a dimensionless universal number, dependent only upon the value of  $Q$ , and the universality class of the bulk conformal field theory.

It is remarkable that the response of the impurity has a Curie-like  $T$  dependence, albeit with an anomalous Curie constant  $\mathcal{C}$  (which is likely an irrational number). This anomalous Curie response appears even though there is no spin moment localized on the impurity. In contrast, the earlier results for the LGW quantum critical point presented in Ref. [148] had an unscreened moment present and so a Curie response did not appear as remarkable. Here, it is due to the deformation of a continuum of bulk excitations by the impurity, and the  $1/T$  power-law is a simple consequence of the fact that  $H$  and  $T$  both scale as an energy. Indeed any other external field, coupling to a total conserved charge, will also have a corresponding universal  $1/T$  susceptibility.

A Curie-like response of an impurity in the staggered flux phase was also noted early on by Khalliulin and collaborators, [73, 67] and others.[93, 106, 107] However, in their mean-field analysis, they associated this response with a zero energy ‘bound state’, and hence argued that  $\mathcal{C} = 1/4$ . As noted above, the actual interpretation

is different: there is a critical continuum of excitations, and its collective boundary critical response has a Curie temperature dependence as a consequence of hyperscaling properties. Consequently,  $\mathcal{C}$  does not equal the Curie constant of a single spin, and is a non-trivial number which is almost certainly irrational. We will discuss the earlier work more explicitly in Section 2.3.2.

We will also consider the spatial dependence of the response to a uniform applied field,  $H$ , in the presence of an impurity, as that determines the Knight shift in NMR experiments. The uniform magnetization density induced by the applied field leads to a Knight shift  $HK_u(x)$ ; at  $T$  above a conformal ground state this obeys (the scaling form is also as in Ref. [148]):

$$K_u(x) = \frac{(T/c)^d}{T} \Phi_u(xT/c) \quad (2.4)$$

where  $c$  is the spinon velocity in the bulk (we assume the bulk theory has dynamic critical exponent  $z = 1$ , and henceforth set  $c = 1$ ),  $\Phi_u$  is a universal function, and the Knight shift is normalized so that

$$\int d^d x K_u(x) = \chi_{\text{imp}}. \quad (2.5)$$

The function  $\Phi_u(y)$  has a power-law singularity as  $y \rightarrow 0$ , with the exponent determined by a ‘boundary scaling dimension’: we shall come back to this in the sections below.

In addition to the locally uniform Knight shift, an impurity in the presence of a uniform applied field also induces a ‘staggered’ moment which typically oscillates at the wavevector associated with a proximate magnetically ordered state. This

leads to a staggered Knight shift,  $HK_s(x)$ , which we will also consider here. Such a staggered Knight shift does appear for the deconfined critical theory describing the Néel-VBS transition, and it has a spatial distribution associated with that of the Néel state (for more details, see [69]). However, the response for the U(1) sF spin liquid is dramatically different. One of our primary results is that for the scaling limit theory of the U(1) sF spin liquid, an applied magnetic field in the presence of an impurity induces *none* of the many competing orders [49] associated with the spin liquid. Thus there is no analog of the ‘staggered’ Knight shift. A subdominant induction of competing orders can arise upon including irrelevant operators associated with corrections to scaling; the primary response, however, is just the induction of a ferromagnetic moment, which has a slowly-varying, space-dependent envelope in the vicinity of the impurity specified by  $K_u(x)$ .

Our conclusions above for the impurity response of the U(1) sF spin liquid differ from the earlier mean-field theories.[73, 67, 93, 92, 106, 107, 154] They found an induced moment which had a strong oscillation between the two sublattices of the square lattice. We demonstrate here that this oscillation disappears in the continuum field theory which accounts for the gauge fluctuations. We are not aware of any reason why fluctuation corrections to the mean-field predictions should be considered small.

## 2.3 Theory and Results

This section will examine the response of a second algebraic spin liquid to impurities: the staggered flux spin liquid with fermionic spinon excitations. [111, 112, 50, 49,

96]. The low energy excitations of the spin liquid are described by  $N_f$  flavors of 2-component Dirac fermions,  $\Psi$ , coupled to the U(1) gauge field  $A_\mu$  with the action

$$\mathcal{S}_b = \int d^3y \bar{\Psi} [-i\gamma^\mu (\partial_\mu + iA_\mu)] \Psi. \quad (2.6)$$

As before,  $y = (\tau, \vec{x})$  is the spacetime coordinate, and  $\mu$  extends over the  $D = 3$  spacetime indices. The Dirac matrices  $\gamma^\mu = (\tau^3, \tau^2, -\tau^1)$ , where  $\tau^\mu$  are the Pauli matrices, and the field  $\bar{\Psi} = i\Psi^\dagger \tau^3$  — we follow the notation of Hermele *et al.*[49]. The number of flavors is  $N_f = 4$  for the staggered flux state, and our results are also extended to the so-called  $\pi$ -flux state, which has  $N_f = 8$ . Our analysis will be carried out, as in the previous works, in a  $1/N_f$  expansion. We have not included a bare Maxwell term for the gauge field in  $\mathcal{S}_b$  because it turns out to be irrelevant at all orders in the  $1/N_f$  expansion.

### 2.3.1 Bulk theory

The structure of the bulk theory has been described in some detail in Refs. [111, 112, 49], and we will not repeat the results here. In the large  $N_f$  limit, the propagator of the gauge field in the Lorentz gauge is

$$D_{\mu\nu}(p) = \left( \delta_{\mu\nu} - \frac{p_\mu p_\nu}{p^2} \right) \frac{16}{N_f p} \quad (2.7)$$

This propagator arises from the vacuum polarization of the fermions. Notice that it is suppressed by a power of  $1/N_f$ , so the  $1/N_f$  expansion can be setup as a perturbation theory in the fermion-gauge field interaction.

A large number of order parameters can be constructed out of fermion bilinears, and a detailed catalog has been presented. [49] Among these are the  $SU(N_f)$  flavor currents

$$J_\mu^a = -i\bar{\Psi}\gamma^\mu T^a\Psi, \quad (2.8)$$

certain components of which are the magnetization density and current. Conservation of this current implies the scaling dimension

$$\dim[J_\mu^a] = 2, \quad (2.9)$$

Also considered were the following quantities:

$$N^a = -i\bar{\Psi}T^a\Psi, \quad M = -i\bar{\Psi}\Psi, \quad (2.10)$$

which relate to additional order parameters including the Néel order (note that  $M$  does *not* correspond to the physical magnetization). Their scaling dimensions have been computed in the  $1/N_f$  expansion:

$$\dim[N^a] = 2 - \frac{64}{3\pi^2 N_f} + \mathcal{O}(1/N_f^2) \quad (2.11)$$

### 2.3.2 Relationship to earlier work

Before describing the results of our analysis of the impurity in the  $U(1)$  sF phase, it is useful to describe the earlier analyses in Refs. [73, 67, 93, 92, 106, 107, 154]. They ignored the  $A_\mu$  fluctuations, but instead considered a theory of fermionic spinons  $f_{i\alpha}$  on the sites,  $i$ , of the square lattice;  $\alpha$  is a spin index. These spinons obey  $\sum_\alpha \langle f_{i\alpha}^\dagger f_{i\alpha} \rangle = 1$  on every lattice site except at the impurity  $i = 0$ . Here, they inserted



a vacancy (representing *e.g.* a Zn impurity) by including a potential term in the Hamiltonian

$$\mathcal{H}_{\text{imp}} = V \sum_{\alpha} f_{0\alpha}^{\dagger} f_{0\alpha} \quad (2.12)$$

and taking the limit  $V \rightarrow \infty$  to prohibit any spinons from residing on the vacancy.

The key physical ingredient in these analyses is the difference in the spinon occupation number between the impurity and the bulk:

$$\sum_{\alpha} \langle f_{i\alpha}^{\dagger} f_{i\alpha} \rangle - 1 = -\delta_{i0}. \quad (2.13)$$

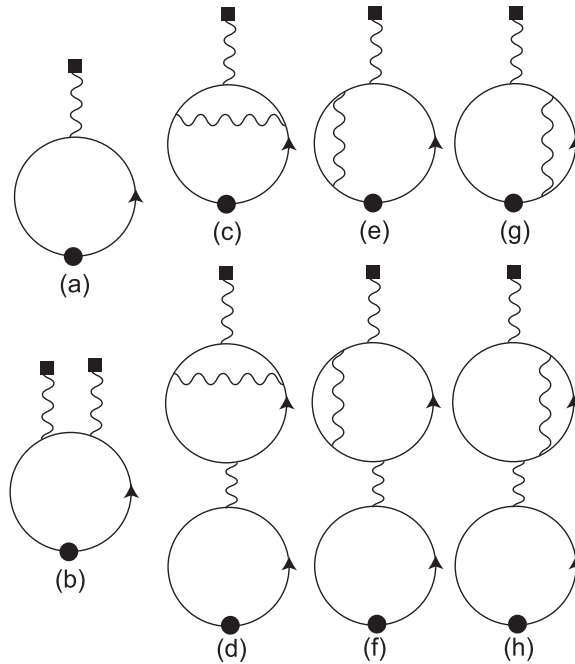


Figure 2.1: Feynman diagrams to order  $1/N_f$  for the lhs of Eq. (2.14). The full line is the Dirac fermion propagator, the wave line is the photon propagator, the filled square is the impurity source term in  $\mathcal{S}_{\text{imp}}$ , and the filled circle is  $\Psi^{\dagger}\Psi$  vertex. As noted in the text, the diagram in (b) has an odd number of photon vertices, and so vanishes by Furry's theorem.[59] Here, and henceforth, we do not show a number of other diagrams which vanish because of Furry's theorem.

In our approach the analog of the  $V = \infty$  limit is obtained by the functional integral over  $A_{\tau}$ . In the bulk theory, the continuum field  $\Psi$  is defined so that  $\langle \Psi^{\dagger}\Psi \rangle = 0$  in

the absence of the impurity, and the continuum analog of Eq. (2.13) is

$$\langle \Psi^\dagger \Psi(r) \rangle = -Q\delta^2(r) \quad (2.14)$$

where the rhs has a Dirac delta function. The constraint in Eq. (2.14) is imposed not by adding a potential energy, but by the functional integral over  $A_\tau$ , which appears in the Lagrangian density of  $\mathcal{S}_b + \mathcal{S}_{\text{imp}}$  (with  $\mathcal{S}_b$  given in Eq. (2.6)) as  $iA_\tau(\Psi^\dagger \Psi + Q\delta^2(r))$ . Our treatment of gauge fluctuations ensures that the constraint on the spinon occupations is imposed not just on the average, but dynamically on all states and on all sites. The equality in Eq. (2.14) holds to all orders in the  $1/N_f$  expansion: this follows from the ‘equation of motion’ for  $A_\tau$

$$\left\langle \frac{\delta}{\delta A_\tau} (\mathcal{S}_b + \mathcal{S}_{\text{imp}}) \right\rangle = 0. \quad (2.15)$$

It is instructive to also test Eq. (2.14) by explicitly evaluating the lhs of Eq. (2.14) in the  $1/N_f$  expansion. The corresponding Feynman diagrams are shown in Fig. 2.1. At leading order, we have the diagram Fig 2.1(a), which is easily evaluated to yield the rhs of Eq. (2.14). At order  $1/N_f$ , the diagrams shown in Fig. 2.1(b-g) contribute. Of these, Fig. 2.1(b) vanishes by Furry’s theorem.[59] Of the remaining, it is easy to show that they cancel in pairs: this requires only the knowledge that the photon propagator is the inverse of the fermion vacuum polarization bubble. Thus Figs. 2.1(c) and (d), (e) and (f), and (g) and (h), all cancel against each other, and Eq. (2.14) is thus established to this order. It is not difficult to extend these arguments to all orders in  $1/N_f$ . Note that it is possible to satisfy Eq. (2.14) in a perturbative treatment of gauge fluctuations, without the need to appeal to bound states: the delta function at  $r = 0$  arises from a superposition of the contribution of many extended states, rather than from a bound state claimed earlier.[73, 67, 93, 92]

It is clear that our approach yields a systematic and controlled treatment of the spinon deficit at the impurity, in contrast to the earlier ad-hoc mean-field approaches.[73, 67, 93, 92, 106, 107, 154] Our analysis implies that the Curie constant  $\mathcal{C}$  is a non-trivial number, with contributions at all orders in  $1/N_f$ , and is not given simply by the Curie constant of a single spin.

The proper analysis of a potential term like that in Eq. (2.12) requires the scaling analysis of perturbations to the conformal field theory defined by  $\mathcal{S}_b + \mathcal{S}_{\text{imp}}$ . The action for such a perturbation takes the form

$$\mathcal{S}'_b = V \int d\tau \Psi^\dagger \Psi(x=0, \tau) \quad (2.16)$$

A simple analysis of scaling dimensions shows that

$$\dim[V] = -1 + \mathcal{O}(1/N_f). \quad (2.17)$$

So, potential scattering is an irrelevant perturbation at all orders in the  $1/N_f$  expansion.

A further distinction between our results and the earlier work[73, 67, 93, 92, 106, 107, 154] appears in the response to a uniform magnetic field. This has significant experimental consequences, and will be discussed in Section 2.3.4.

### 2.3.3 Impurity exponents

We now turn to an analysis of spin correlations in the vicinity of the impurity. The general method is very similar to that followed in Ref. [122].

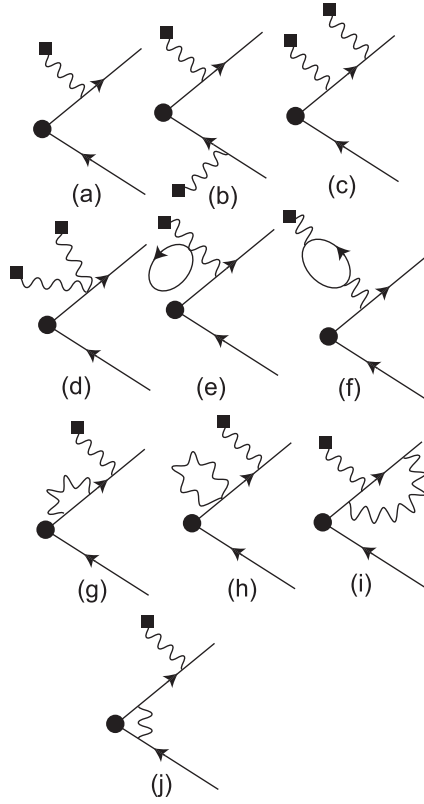


Figure 2.2: Feynman diagrams which contribute to the impurity-dependent renormalization of vertices. The full line is the  $\Psi$  propagator, the wavy line is the  $A_\mu$  propagator, and the filled square is the source term in  $\mathcal{S}_{\text{imp}}$ .

We assume here that monopole tunneling events remain irrelevant at the impurity at the quantum critical point, as they do in the bulk. [130, 128, 131] Such monopole tunneling events are defined only in  $d = 2$ , and so their scaling dimensions are not easily estimated in the  $\epsilon$  expansion. However, the monopoles are irrelevant at large  $N$  in the bulk because their action is proportional to  $N$ , and the same reasoning applies also in the presence of the impurity.

Here, we will determine the impurity renormalization to the order  $1/N_f^2$ . To this order, we find that all the operators introduced above, the  $J_\mu^a$  and  $N^a$  acquire a

common correction,  $\Delta_{\text{imp}}$ , to their bulk scaling dimension. This correction is given by the single diagram in Fig 2.2(c), which (along with its symmetry related partner) evaluates to

$$\begin{aligned} & \frac{512Q^2}{N_f^2} \int \frac{d^2q}{(2\pi)^2} \frac{d^2k}{(2\pi)^2} \frac{(-i\omega + \vec{q} \cdot \vec{\tau})(-i\omega + (\vec{k} + \vec{q}) \cdot \vec{\tau})}{kq(q^2 + \omega^2)((q + k)^2 + \omega^2)} \\ & = \frac{128Q^2}{N_f^2\pi^2} \ln(\Lambda/\omega) \end{aligned} \tag{2.18}$$

where  $\vec{\tau} = (\tau^1, \tau^2)$  and  $\Lambda$  is an ultraviolet cutoff; here and henceforth we are using the fermion lines to represent the propagator  $(i\omega + \vec{\tau} \cdot \vec{q})^{-1}$  from  $\Psi$  to  $\Psi^\dagger$  (rather than the Dirac propagator from  $\Psi$  to  $\bar{\Psi}$ ). There are a number of other diagrams, like those shown in Fig. 2.2, which could contribute to the vertex renormalization; however they do not contribute either because of Furry's theorem. From this we obtain the impurity correction to the scaling dimension

$$\Delta_{\text{imp}} = -\frac{128Q^2}{N_f^2\pi^2} + \mathcal{O}(1/N_f^3) \tag{2.19}$$

We expect that the higher order corrections will not be the same for the  $J_\mu^a$  and  $N^a$ .

### 2.3.4 Linear response to a uniform applied field

We apply a uniform magnetic field  $H_a$ , associated with the  $\text{SU}(N_f)$  generator  $T^a$ , which couples linearly to the conserved total spin density  $J_\tau^a$ . In principle, in the presence of the impurity, the linear response to this applied field can induce time-independent, space-dependent average values of not only the spin density,  $J_\tau^a$ , but also of the other order parameters  $M$ , and  $N^a$ . This would be analogous to the non-zero averages of the uniform and staggered magnetizations induced by an applied magnetic

field on the  $\text{CP}^{N-1}$  model (which led to the uniform and staggered Knight shifts). However, here we will find a crucial difference. In the scaling limit of the algebraic spin liquid represented by Eq. (2.6),  $H_a$  induces *only* a non-zero  $J_\tau^a$ , and average values of all the  $N^a$  and  $M$  are zero. Thus there is only a uniform Knight shift,  $K_u(x)$ , and all the ‘staggered’ Knight shifts,  $K_s(x)$ , associated with the many competing orders are zero. The staggered Knight shift can appear only if some corrections to scaling are included, associated with irrelevant operators which reduce the symmetry of the conformal theory to that of the lattice model, and so can be expected to be weaker than the uniform Knight shift.

The vanishing of  $\langle M(x) \rangle$  and  $\langle N^a(x) \rangle$  in the presence of  $H_a$  can be established by a careful consideration of the symmetries of the Dirac fermion theory. First  $\langle M \rangle = 0$ , to linear order in  $H_a$ , simply by  $\text{SU}(N_f)$  symmetry. Establishing the value of  $\langle N^a \rangle$  requires more complicated considerations. Let us consider the leading contribution to  $\langle N^a \rangle$ , to linear order in  $H_a$ , in the  $1/N_f$  expansion, represented by the graph in Fig 2.3(a). The value of the fermion loop is proportional to

$$T \sum_{\omega_n} \int \frac{d^2 k}{4\pi^2} \text{Tr} [(i\omega_n + \vec{\tau} \cdot \vec{k})^{-1} \tau^3 (i\omega_n + \vec{\tau} \cdot \vec{k})^{-1} \times (i\omega_n + \vec{\tau} \cdot (\vec{k} + \vec{q}))^{-1}] \quad (2.20)$$

Evaluating the trace over the Dirac matrices, we obtain an identical zero. This can be understood as a consequence of time-reversal invariance. Both  $H_a$  and  $N^a$  are odd under the time reversal, [50] as is the charge of the impurity  $Q$ . So an expansion of  $\langle N^a \rangle / H_a$  can only involve even powers of  $Q$ . Proceeding to order  $1/N_f^2$ , we obtain diagrams like those shown in Fig. 2.3(b-d), which have a pre-factor of  $Q^2$ , and so

are potentially non-zero. However, these diagrams have a fermion loop with an odd number of  $\gamma^\mu$  vertices, and so vanish by Furry's theorem. [59] By a combination of Furry's theorem and time-reversal invariance we can now easily see that all terms vanish and so  $\langle N^a \rangle = 0$ . Because of the  $T^a$  matrices in the definitions of  $N^a$  and  $J_\tau^a$ , there must be a single fermion loop which connects the external vertices. By Furry's theorem, this loop must have an odd number of photon vertices. All other fermion loops can only have an even number of photon vertices. Consequently, there must be an odd number of photon vertices remaining to connect to the external impurity source term. However, by time-reversal, there must be an even number of impurity terms; hence the result.

Our conclusion that  $\langle N^a \rangle = 0$  is starkly different from the mean-field prediction [73, 67, 93, 92, 106, 107, 154] of an induced moment which oscillated strongly between the two square sublattices. Such oscillations can only appear upon including irrelevant operators.

It remains only to compute the uniform Knight shift  $K_u(x)$ , or equivalently, its Fourier transform  $\chi_u(q)$  defined as:

$$K_u(x) = \int \frac{d^d q}{(2\pi)^d} \chi_u(q) e^{iqx}, \quad (2.21)$$

The scaling analysis of Section 2.3.3 implies that this Knight shift obeys the scaling form in Eq. (2.4), with the  $x \rightarrow 0$  behavior given by

$$K_u(x \rightarrow 0) \sim T^{d-1+\Delta_{\text{imp}}} \frac{1}{|x|^{-\Delta_{\text{imp}}}}. \quad (2.22)$$

Here we expect that the  $\Delta_{\text{imp}}$  exponent is that associated with  $J_\tau^a$ , and not (unlike the situation with the  $\text{CP}^{N-1}$  model) that associated with the  $N^a$ , because there is

no ‘mixing’ between the staggered and uniform magnetizations near the impurity for the sF spin liquid.

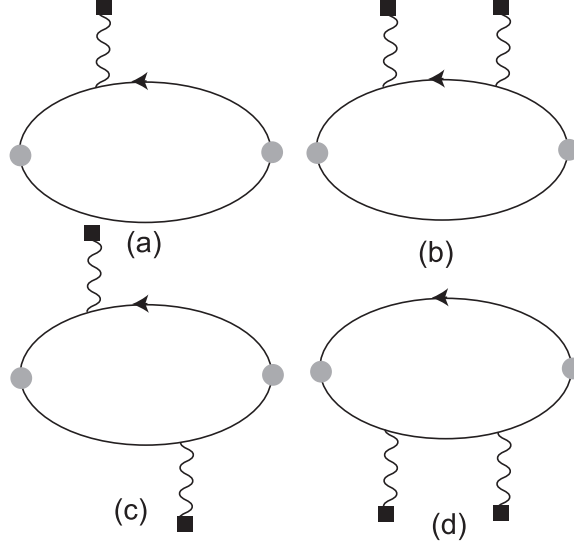


Figure 2.3: Feynman diagrams for the impurity susceptibility and Knight shifts of the staggered flux spin liquid. The grey circle vertices depend upon the correlator being evaluated: they equal (i)  $T^a \gamma_\tau$  for the ferromagnetic spin density  $J_\tau^a$ , (ii)  $T^a$  for the order parameter  $N^a$ , and (iii) unity for  $M$ .

At first order in  $1/N_f$ ,  $\chi_u(q)$  is given by the diagram in Fig 2.3(a), which vanishes by Furry’s theorem. The leading non-vanishing contribution is at order  $1/N_f^2$ , and is given by the diagrams in Fig 2.3(b-d) (a number of order  $1/N_f^2$  diagrams which vanish because of Furry’s theorem are not shown). The sum of these diagrams can be written in the following compact form

$$\begin{aligned} \chi_u(q) = & Q^2 \tilde{S} T \sum_{\omega_n} \int \frac{d^2 k}{4\pi^2} \frac{d^2 p}{4\pi^2} \frac{\partial}{\partial(i\omega_n)} \text{Tr} \left[ \left( i\omega_n + \vec{\tau} \cdot \vec{k} \right) \right. \\ & \times \left. \left( i\omega_n + \vec{\tau} \cdot (\vec{k} + \vec{q}) \right) \left( i\omega_n + \vec{\tau} \cdot (\vec{k} + \vec{p}) \right) \right]^{-1} \\ & \times D_{\tau\tau}(p) D_{\tau\tau}(|\vec{q} - \vec{p}|). \end{aligned} \quad (2.23)$$



Here  $D_{\tau\tau}$  is the  $\tau$  component of the photon propagator, representing the external lines connecting to the impurities, and  $\tilde{S}$  is the constant proportional to the SU(N) Casimir eigenvalue as defined below:

$$\tilde{S} = \frac{1}{N^2 - 1} \text{tr} \sum_{a=1}^{N^2-1} (T^a)^2 \equiv \frac{\tilde{\mathcal{C}}}{N^2 - 1}, \quad (2.24)$$

Here,  $\tilde{\mathcal{C}}$  is the eigenvalue of the Casimir operator of SU(N) which depends on the specific representation of the group. In the SU(2) case, this factor takes the familiar form  $\tilde{S} = S(S + 1)/3$ .

Notice that the expression (2.23) is a total frequency derivative; this immediately implies that  $\chi_u(q) = 0$  at  $T = 0$ , when the frequency summation can be converted to an integration. This vanishing is a consequence of the conservation of total spin.

A non-zero  $\chi_u(q)$  is obtained at  $T > 0$ , and we now compute this. First we need the photon propagator at  $T > 0$ . This is given by a single fermion loop and at this order we only need the  $\tau, \tau$  component at a spatial momentum  $\vec{q}$ :

$$\begin{aligned} D_{\tau\tau}^{-1}(q) &= -N_f T \sum_{\omega_n} \int \frac{d^2k}{4\pi^2} \text{Tr} \left[ \left( i\omega_n + \vec{\tau} \cdot \vec{k} \right) \right. \\ &\quad \left. \times \left( i\omega_n + \vec{\tau} \cdot (\vec{k} + \vec{q}) \right) \right]^{-1}. \end{aligned} \quad (2.25)$$

We first combine the denominators in Eq. (2.25) using the Feynman parameter  $u$ , perform the frequency summation, and finally integrate over  $k$ . This yields

$$D_{\tau\tau}^{-1}(q) = \frac{N_f T}{\pi} \int_0^1 du \ln \left[ 2 \cosh \left( \frac{q}{2T} \sqrt{u(1-u)} \right) \right]. \quad (2.26)$$

Eq. (2.26) interpolates between  $N_f q/16$  for  $T \ll q$  which agrees with the  $T = 0$  result in Eq. (2.7), to  $(T/\pi) \ln 2$  for  $q \ll T$ .

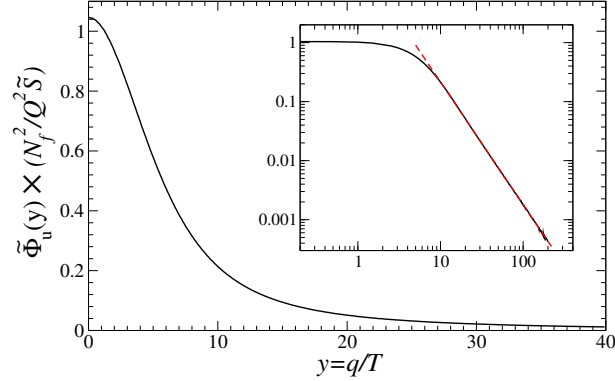


Figure 2.4: Numerically calculated scaling function  $\tilde{\Phi}_u(y)$  defined by (2.26-2.30). The inset shows large- $y$  behavior together with the least square fit (dashed line) to a power law for  $y > 40$ : the fit yields  $\tilde{\Phi}_u(y) \simeq C'/y^\alpha$  with  $C' = 24.7(1)$  and  $\alpha = 2.070(5)$ .

Inserting Eq. (2.26) into Eq. (2.23), we conclude that  $\chi_u(q)$  obeys the scaling form

$$\chi_u(q) = \frac{1}{T} \tilde{\Phi}_u(q/T) \quad (2.27)$$

where the scaling function  $\tilde{\Phi}_u$  is the Fourier transform of the scaling function  $\Phi_u$  in Eq. (2.4). Further,  $\mathcal{C}$ , the anomalous Curie constant appearing in Eq. (2.3), equals  $\tilde{\Phi}_u(0)$ . To determine the scaling function  $\tilde{\Phi}_u$ , we need to evaluate Eq. (2.23). We combined the Green's functions using two Feynman parameters  $u, v$ , evaluated the integral over  $k$ , differentiated with respect to frequency, and finally evaluated the summation over  $\omega_n$ . This yields

$$\begin{aligned} \chi_u(q) = & -\frac{Q^2\tilde{S}}{\pi} \int_0^1 du \int_0^{1-u} dv \int \frac{d^2p}{4\pi^2} \left\{ f'(\Delta) \right. \\ & + \left. \left[ 2\Delta^2 - uq^2 - vp^2 - (1 - 2(u+v))\vec{p} \cdot \vec{q} \right] \right. \\ & \left. \times \frac{f''(\Delta)}{4\Delta} \right\} D_{\tau\tau}(p) D_{\tau\tau}(|\vec{q} - \vec{p}|) \end{aligned} \quad (2.28)$$

where

$$\Delta^2 = q^2u(1-u) + p^2v(1-v) - 2uv\vec{p} \cdot \vec{q} \quad (2.29)$$

and  $f$  is the Fermi function

$$f(\varepsilon) = 1/(e^{\varepsilon/T} + 1). \quad (2.30)$$

The remaining integrals have to be evaluated numerically. From such an evaluation at  $q = 0$  we found

$$\mathcal{C} = \frac{1.0460(5)\tilde{S}Q^2}{N_f^2} + \mathcal{O}(1/N_f^3) \quad (2.31)$$

for the universal Curie constant appearing in Eq. (2.3). The calculated shape of the scaling function  $\tilde{\Phi}_u(y)$  is shown in Fig. 2.4. From the numerical analysis of its behavior for large arguments, we deduce that  $\tilde{\Phi}_u(y)$  has a power-law decay  $\tilde{\Phi}_u(y) \propto 1/y^\alpha$  at  $y \gg 1$ , where the exponent  $\alpha \approx 2$  within the accuracy we were able to achieve when calculating the four-dimensional integral in (2.28). Therefore, we obtain that at small distances the uniform Knight shift  $K_u(x)$  tends to a (lattice cutoff-dependent) constant as  $x \rightarrow 0$ , which is consistent, to the leading order in  $1/N_f$ , with Eq. (2.22) and the fact that  $\Delta_{\text{imp}}$  vanishes at this order (see Eq. (2.19)).

## 2.4 Conclusions

Let us summarize the basic physical characteristics of the impurity response of the Staggered flux spin liquid. This spin liquid is generically critical, and so has an anomalous Curie response; the Curie constant is given, to the leading order in the  $1/N_f$  expansion, by Eq. (2.31). The Knight shift now has only a uniform component, but no staggered component in the scaling limit. The absence of any staggered Knight shift is a defining characteristic of the sF spin liquid, and is a consequence of its large emergent symmetry.[49] There is a large number of competing order parameters, and

the leading impurity action  $\mathcal{S}_{\text{imp}}$  has no natural way of choosing among them, leading to a response which is restricted to the ferromagnetic moment alone. The behavior of the ferromagnetic Knight shift upon approaching the impurity is specified by the impurity exponent (2.19) found in Section 2.3.3; to the leading order in  $1/N_f$ , the Fourier transform of the ferromagnetic Knight shift is computed in Sect. 2.3.4.

Apart from their applications to spin liquids, the results in this chapter also have a direct application to the physics of charged impurities in two-dimensional graphene. It is well known that the low energy electronic excitations in graphene are described by 2 species of Dirac fermions. There is no fluctuating gauge field  $A_\mu$  as in Eq. (2.6). However in the presence of charged impurity, the *three-dimensional* Coulomb potential the electrons experience has the form  $C/r$ , where  $C$  is a constant. Interestingly, this is exactly the form of the static potential found in Section 2.3 in the presence of an impurity, where  $\langle A_\tau \rangle \sim 1/r$ . Thus, as long as we ignore quantum-electrodynamic loop corrections, the results of Section 2.3 apply also to graphene; specifically, in Fig. 2.1, (a) and (b) apply to graphene while (c)-(h) do not. One of our important results for this system was Eq. (2.14): that the induced charge density due to the Coulomb potential is a delta function, with  $Q$  a non-trivial universal function of  $C$ . This results therefore applies also to graphene. It disagrees with the earlier result of Ref. [30], which found a  $1/r^2$  decay in the induced charge density. We believe their results suffers from a cavalier treatment of the ultraviolet cutoff, which does not preserve gauge invariance.

Finally, we comment on the experimental implications of our work.

For the cuprates, NMR experiments [18, 104] show a large Knight shift response at the Néel wavevector in the vicinity of the impurity, and strong temperature-dependent enhancement of such correlations. These features are consistent with the Néel-VBS transition (considered in [69]) and also with the transition in dimerized antiferromagnets considered earlier. [120, 148, 122] The absence of a staggered response for the sF case is potentially a serious deficiency of this model's applicability to the cuprates. It remains to be seen if corrections to scaling (such as those in Eq. (2.16)) can remedy the situation.

For the organic Mott insulator  $\kappa$ -(ET)<sub>2</sub>Cu<sub>2</sub>(CN)<sub>3</sub>, the NMR Knight shift [135] has an appreciable  $T$  independent component at low  $T$ . This can potentially be fit either by the spinon Fermi surface or by a weakly magnetically ordered state (see [69]), but not by the sF spin liquid phase.

# Chapter 3

## Coulomb impurity in graphene

### 3.1 Synopsis

We consider the problem of screening of an electrically charged impurity in a clean graphene sheet. When electron-electron interactions are neglected, the screening charge has a sign opposite to that of the impurity, and is localized near the impurity. Interactions between electrons smear out the induced charge density to give a large-distance tail that follows approximately, but not exactly, an  $r^{-2}$  behavior and with a sign which is the *same* as that of the impurity.

## 3.2 Introduction

With the recent explosion of interest in graphene, there are numerous experimental motivations for understanding the influence of impurities on its electronic and transport properties. For non-interacting electrons, the influence of a dilute concentration of impurities on transport properties has been investigated in some depth [103]. Here we shall instead study in some detail the physics associated with a *single* impurity carrying electrical charge  $Z$ . Nanoscale studies of the electronic properties of a single graphene sheet have recently become possible [84, 141], and so it should eventually be possible to observe the variation in the charge density and the local density of states as a function of distance from the impurity. We shall show here that this spatial structure is a sensitive probe of the strong correlations between the electrons in graphene, and of the unusual nature of screening in a two-dimensional semi-metal with a Dirac dispersion spectrum.

For non-interacting electrons, the influence of a Coulomb impurity exerting a potential  $Ze^2/(4\pi\epsilon_0r)$  (where  $r$  is the distance from the impurity) was studied some time ago [30]. This case is equivalent to the familiar “Friedel problem” but for Dirac fermions. However, even for this seemingly simple case, there are subtleties which were overlooked in the initial treatment [30], and corrected in Ref. [69]. A number of papers appeared [136, 97, 108] while this research was being written up for publication, presenting additional results on this non-interacting problem. We shall review and extend the results of Ref. [69] for non-interacting electrons in Section 3.3. We shall then proceed to the full treatment of the impurity problem, and allow for

electron–electron Coulomb interactions.

In short, our results are as follows. For noninteracting electrons, the screening charge is a local delta-function in space to all orders in perturbation theory over the impurity charge. The sign of this screening charge is opposite to that of the impurity, as is usually the case. However, once interaction between electrons is turned on, the screening charge develops a long-range tail, even for small impurity charges. The tail follows approximately an  $r^{-2}$  law, with a coefficient which varies quite slowly with  $r$ . Notably, the sign of this tail is the same as that of the impurity. The long-range tail of the screening charge, thus, is a sensitive probe of the interaction between electrons, in particular to the renormalization of the fermion velocity and the “quantum critical” aspects [139] of the interacting Dirac fermion problem.

Let us begin with a statement of the problem. After taking the continuum limit to  $N = 4$  species of two-component Dirac fermions  $\Psi_a$  ( $a = 1 \dots N$ ) we have the theory defined by the Euclidean partition function

$$\begin{aligned}
\mathcal{Z} &= \int \mathcal{D}\Psi_\alpha \mathcal{D}A_\tau \exp(-\mathcal{S} - \mathcal{S}_{\text{imp}}), \\
\mathcal{S} &= \sum_{a=1}^N \int d^2r \int d\tau \Psi_a^\dagger(\mathbf{r}, \tau) \left[ \frac{\partial}{\partial \tau} + iA_\tau(\mathbf{r}, \tau) + iv\sigma^x \frac{\partial}{\partial x} + iv\sigma^y \frac{\partial}{\partial y} \right] \Psi_a(\mathbf{r}, \tau) \\
&\quad + \frac{1}{2g^2} \int \frac{d^2q}{4\pi^2} \int d\tau 2q |A_\tau(\mathbf{q}, \tau)|^2, \\
\mathcal{S}_{\text{imp}} &= -iZ \int d\tau A_\tau(\mathbf{r} = 0, \tau).
\end{aligned} \tag{3.1}$$

The functional integral is over fields defined in two spatial dimensions  $\mathbf{r} = (x, y)$  and imaginary time  $\tau$ ,  $\sigma^{x,y}$  are Pauli matrices acting on the Dirac space, and  $v$  is the Fermi velocity. The scalar potential which mediates the  $e^2/(4\pi\epsilon_0|\mathbf{r}|)$  Coulomb



interaction between the electrons is  $iA_\tau(\mathbf{r}, \tau)$ ; after a spatial Fourier transform to two-dimensional momenta  $\mathbf{q}$ , this interaction requires the  $2q$  ( $= 2|\mathbf{q}|$ ) co-efficient of the term quadratic in  $A_\tau$ , with the coupling  $g^2 = e^2/\epsilon_0$ . The screening due to a substrate of dielectric constant  $\epsilon$  can also be included by modifying the coupling to [139]  $g^2 = 2e^2/(\epsilon_0(1 + \epsilon))$ . The action  $\mathcal{S}$  therefore represents the physics of an ideal graphene layer. The influence of an impurity of net charge  $Z$  at  $\mathbf{r} = 0$  is described by  $\mathcal{S}_{\text{imp}}$ .

Many essential aspects of the theory above follow from its properties under the renormalization group (RG) transformation under which  $\mathbf{r} \rightarrow \mathbf{r}/s$  and  $\tau \rightarrow \tau/s$ . A standard analysis shows that all three couplings in  $\mathcal{Z}$ , namely  $v$ ,  $Z$ , and  $g$ , are invariant under this transformation at tree level. Indeed, for two of the couplings, this invariance extends to all orders in perturbation theory: the coupling  $g$  does not renormalize because of the non-analytic  $q$  co-efficient, while  $Z$  remains invariant because it is protected by gauge invariance [69]. So we need only examine the RG flow of a single coupling, the velocity  $v$ . Because  $v$  is a bulk coupling, its flow cannot be influenced in the thermodynamic limit by a single impurity, and so can be computed in the absence of the impurity. Such a RG flow was initially examined in the more general context of theories with Chern-Simons couplings in Ref. [175], but a complete presentation was given in the present context in Ref. [139]: we shall use the notation and results of the latter paper here, with the exception that we use two-component Dirac fermions with  $N = 4$  while Ref. [139] uses four-component Dirac fermions with  $N = 2$ .

It will be useful for our analysis to introduce two combinations of the above couplings

which also have engineering dimension zero, and hence are pure numbers. These are

$$\lambda = \frac{g^2 N}{32\hbar v} \quad ; \quad \alpha = \frac{g^2 Z}{4\pi\hbar v} \quad (3.2)$$

(we have set  $\hbar = 1$  elsewhere in the chapter). As we will see, the coupling  $\lambda$  is a measure of the strength of the electron-electron Coulomb interactions, while  $\alpha$  measures the strength of the electron-impurity Coulomb interaction.

We shall limit our explicit results here to the spatial form of the charge density

$$n(r) = - \sum_a \text{Tr} \langle \Psi_a^\dagger(\mathbf{r}, \tau) \Psi_a(\mathbf{r}, \tau) \rangle, \quad (3.3)$$

(where Tr acts on the Dirac space) induced by the impurity. However, our RG strategy can be extended to other observables of experimental interest, such as the local density of states.

As noted above, we will begin in Section 3.3 by considering only the electron-impurity Coulomb interaction, while electron-electron Coulomb interactions will be accounted for in Section 3.4.

### 3.3 Non-interacting electrons

This section will ignore the electron-electron Coulomb interactions. Formally, we work in the limit  $\lambda \rightarrow 0$ , but  $\alpha$  is kept fixed. The problem reduces to that of a single Dirac electron in the attractive impurity potential

$$V(r) = -\frac{Zg^2}{4\pi r}. \quad (3.4)$$

This problem was originally studied in Ref. [30]. However, they introduced an arbitrary cutoff at high energy to regulate the problem at short distances, and this leads to spurious results [69]. As we will demonstrate here, there is no dependence upon a cutoff energy scale at all orders in perturbation theory, provided the high energy behavior is regulated in a proper gauge-invariant manner. With no cutoff energy scale present, a number of results can be deduced by simple dimensional analysis. The Fourier transform of the charge density  $n(r)$  is dimensionless, and therefore we can write

$$n(q) = -NF(\alpha), \quad (3.5)$$

where  $F(\alpha)$  is a universal function of the dimensionless coupling  $\alpha$ . Note that  $n(q)$  is required by this dimensional argument to be  $q$ -independent, and so  $n(r) \propto \delta^2(\mathbf{r})$ .

The arguments so far are perturbative, but non-perturbative effects can be deduced by solving the full Dirac equation in the potential in Eq. (3.4). This solution has appeared elsewhere [142, 136, 97, 108], and so we will not reproduce it here. Such an analysis shows that the perturbative arguments apply for  $\alpha < 1/2$ , but new physics appears for  $\alpha > 1/2$ . In particular, Shytov *et al.* [136] and Terekhov *et al* [142] showed that  $n(r) \sim -r^{-2}$  for  $\alpha > 1/2$  (the sign of this tail is opposite to that of the impurity).

We shall limit our discussion in this section to the  $\alpha < 1/2$  case. One reason for doing so is that electron-electron Coulomb interactions act to reduce the effective value of  $\alpha$ . This will become clearer in Section 3.4, but we note here that a standard RPA screening of the potential  $V(r)$  in Eq. (3.4) can be simply accounted for by applying

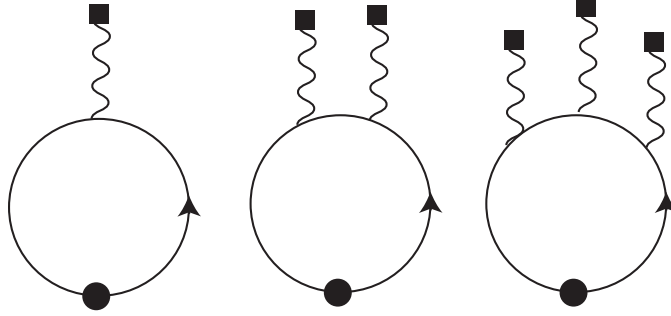


Figure 3.1: Feynman diagrams for the charge density without electron-electron interactions to order  $\alpha^3$ . The filled square is the impurity site, the wavy line is the  $A_\tau$  propagator, the line is the fermion propagator, and the filled circle is the charge density operator.

the mapping

$$\alpha \rightarrow \frac{\alpha}{1 + \lambda} \quad (3.6)$$

to the results of the present section. The value of  $\lambda$  in graphene is not small [139].

We shall now establish the existence of the universal function  $F(\alpha)$  in Eq. (3.5) to all orders in  $\alpha$ . The existence of a universal  $F(\alpha)$  is a consequence of the non-renormalization of the impurity charge  $Z$  [69]. We compute  $n(q)$  diagrammatically, and the needed diagrams all have one fermion loop and are shown in Fig. 3.1.

To first order in  $\alpha$  we have

$$n(q) = -\frac{Z}{2q} \Pi_0(q), \quad (3.7)$$

where  $\Pi_0(q)$  is the bare polarization operator

$$\begin{aligned} \Pi_0(q) &= -g^2 N \int \frac{d^2 k}{4\pi^2} \int \frac{d\omega}{2\pi} \text{Tr} [(-i\omega + v\mathbf{k} \cdot \vec{\sigma})^{-1} (-i\omega + v(\mathbf{k} + \mathbf{q}) \cdot \vec{\sigma})^{-1}] \\ &= \frac{g^2 N q}{16v}, \end{aligned} \quad (3.8)$$

and so we have  $F(\alpha) = (\pi/8)\alpha + \mathcal{O}(\alpha^2)$ .

The order  $\alpha^2$  graph in Fig. 3.1 vanishes by Furry's theorem, and at order  $\alpha^3$  we write the contribution to  $n(q)$  in the form

$$N(Zg^2)^3 \int \frac{d^2k_1}{4\pi^2} \frac{d^2k_2}{4\pi^2} \frac{d^2k_3}{4\pi^2} \frac{A(\mathbf{k}_1, \mathbf{k}_2, \mathbf{k}_3)}{8k_1k_2k_3} (2\pi)^2 \delta^2(\mathbf{k}_1 + \mathbf{k}_2 + \mathbf{k}_3 + \mathbf{q}), \quad (3.9)$$

where

$$\begin{aligned} A(\mathbf{k}_1, \mathbf{k}_2, \mathbf{k}_3) = & \int \frac{d^2p}{4\pi^2} \int \frac{d\omega}{2\pi} \text{Tr} [(-i\omega + v\mathbf{p} \cdot \vec{\sigma})^{-1} (-i\omega + v(\mathbf{p} + \mathbf{q}) \cdot \vec{\sigma})^{-1} \\ & \times (-i\omega + v(\mathbf{p} + \mathbf{q} + \mathbf{k}_1) \cdot \vec{\sigma})^{-1} (-i\omega + v(\mathbf{p} + \mathbf{q} + \mathbf{k}_1 + \mathbf{k}_2) \cdot \vec{\sigma})^{-1}] \end{aligned} \quad (3.10)$$

where it is understood here and below that  $-\mathbf{q} = \mathbf{k}_1 + \mathbf{k}_2 + \mathbf{k}_3$ . We now want to symmetrize this by placing the external vertex with momentum  $\mathbf{q}$  at different points on the loop — this should not change the final result for  $n(q)$ . In this manner we obtain

$$\begin{aligned} 3A(\mathbf{k}_1, \mathbf{k}_2, \mathbf{k}_3) = & \int \frac{d^2p}{4\pi^2} \int \frac{d\omega}{2\pi} \left\{ \text{Tr} [(-i\omega + v\mathbf{p} \cdot \vec{\sigma})^{-1} (-i\omega + v(\mathbf{p} + \mathbf{q}) \cdot \vec{\sigma})^{-1} \right. \\ & \times (-i\omega + v(\mathbf{p} + \mathbf{q} + \mathbf{k}_1) \cdot \vec{\sigma})^{-1} (-i\omega + v(\mathbf{p} + \mathbf{q} + \mathbf{k}_1 + \mathbf{k}_2) \cdot \vec{\sigma})^{-1}] \\ & + \text{Tr} [(-i\omega + v\mathbf{p} \cdot \vec{\sigma})^{-1} (-i\omega + v(\mathbf{p} + \mathbf{k}_1) \cdot \vec{\sigma})^{-1} \\ & \times (-i\omega + v(\mathbf{p} + \mathbf{q} + \mathbf{k}_1) \cdot \vec{\sigma})^{-1} (-i\omega + v(\mathbf{p} + \mathbf{q} + \mathbf{k}_1 + \mathbf{k}_2) \cdot \vec{\sigma})^{-1}] \\ & + \text{Tr} [(-i\omega + v\mathbf{p} \cdot \vec{\sigma})^{-1} (-i\omega + v(\mathbf{p} + \mathbf{k}_1) \cdot \vec{\sigma})^{-1} \\ & \left. \times (-i\omega + v(\mathbf{p} + \mathbf{k}_1 + \mathbf{k}_2) \cdot \vec{\sigma})^{-1} (-i\omega + v(\mathbf{p} + \mathbf{q} + \mathbf{k}_1 + \mathbf{k}_2) \cdot \vec{\sigma})^{-1}] \right\} \end{aligned} \quad (3.11)$$

Now this expression has the important property that it vanishes at  $\mathbf{q} = 0$ , where we have

$$\begin{aligned} 3A(\mathbf{k}_1, \mathbf{k}_2, \mathbf{k}_3) = & \int \frac{d^2p}{4\pi^2} \int \frac{d\omega}{2\pi} \frac{\partial}{i\partial\omega} \text{Tr} [(-i\omega + v\mathbf{p} \cdot \vec{\sigma})^{-1} (-i\omega + v(\mathbf{p} + \mathbf{k}_1) \cdot \vec{\sigma})^{-1} \\ & \times (-i\omega + v(\mathbf{p} + \mathbf{k}_1 + \mathbf{k}_2) \cdot \vec{\sigma})^{-1}]. \end{aligned} \quad (3.12)$$

This property allows us to establish that the integral in Eq. (3.9) is convergent and cut-off independent. Let the loop momenta  $p$ ,  $k_1$ ,  $k_2$ , and  $k_3$  all become much larger than the external momentum  $q$ . The resulting integrand will scale as the power of momenta associated with a logarithmic dependence on the upper cutoff. However, in this limit of small  $q$  we have just established that the integrand is zero. It is clear that this argument can be extended to all orders in  $\alpha$ . We have thus established the existence of the cut-off independent function  $F(\alpha)$ . We computed the integral in Eq. (3.9) numerically, and so obtained

$$F(\alpha) = \frac{\pi}{8}\alpha + (0.19 \pm 0.01)\alpha^3 + \mathcal{O}(\alpha^5). \quad (3.13)$$

This has been verified using an exact solution in [142].

### 3.4 Interacting electrons

We will now consider the full problem defined in Eq. (3.1), and account for both the electron-electron and electron-impurity Coulomb interactions.

The problem can be solved in two limits: in the weak coupling limit  $\lambda \rightarrow 0$  and the large  $N$  limit,  $N \rightarrow \infty$  with fixed  $Z = O(1)$ . In both cases  $\alpha/(1 + \lambda) \ll 1$ , so one can limit oneself to linear response in which the induced charge is [generalizing Eq. (3.7)]

$$n(q) = -ZD(q)\Pi(q), \quad (3.14)$$

where  $D(q)$  is the full propagator of the Coulomb potential  $A_\tau$ , and  $\Pi(q)$  is the polarization tensor. The connection between  $D(q)$  and  $\Pi(q)$  is

$$D^{-1}(q) = D_0^{-1}(q) + \Pi(q), \quad (3.15)$$

where  $D_0(q)$  is the bare propagator,

$$D_0(q) = \frac{1}{2q}. \quad (3.16)$$

To leading order (either in coupling or  $1/N$ ), the polarization operator was given in Eq. (3.8), and we showed in Section 3.3 that this gives rise to a  $q$ -independent  $n(q)$ , or a screening charge localized at  $\mathbf{r} = 0$ .

However, if we compute corrections, we find logarithmically divergent diagrams, where the logarithms are cut off from above by the inverse lattice size and from below by  $q$ . The leading logarithms are summed by a standard RG procedure. Since the theory is renormalizable, we can eliminate the dependence on the cutoff by expressing the each diagram in terms of the renormalized parameters, instead of the bare parameters of the Lagrangian. Choosing the renormalization point to be  $q_0$ , and denote  $v_0$  as the fermion velocity at the scale  $v$ , the polarization tensor can be schematically written as

$$\Pi(q) = \Pi(q; q_0, v_0). \quad (3.17)$$

In  $\Pi$  there are logarithms of the ratio  $q/q_0$ . We notice that  $\Pi(q; q_0, v_0)$  is invariant under a change of the renormalization  $q_0$ , given that  $v_0$  is changed correspondingly (the particle density has no anomalous dimension). To eliminate the powers of  $\log(q/q_0)$  we can choose  $q_0 = q$ , hence

$$\Pi(q) = \Pi(q; q, v(q)), \quad (3.18)$$

where in the perturbative expansion of the right hand side there is no large logarithms. Thus to leading order it is given by a single diagram, which was computed previously

[Eq. (3.8)],

$$\Pi(q) = \frac{g^2 N}{16v(q)} q. \quad (3.19)$$

All the leading logarithms are contained in the function  $v(q)$ , which satisfies the equation

$$q \frac{\delta}{\delta q} v(q) = \beta(v), \quad (3.20)$$

with the boundary condition  $v(q_0) = v_0$ . The screening charge is then

$$n(q) = -Z \frac{\lambda(q)}{1 + \lambda(q)}, \quad \lambda(q) = \frac{g^2 N}{32v(q)}. \quad (3.21)$$

The problem is now reduced to the problem of finding  $v(q)$  [or, equivalently,  $\lambda(q)$ ]. This problem has a long history [44, 45]; most recently it has been revisited in Ref. [139] (see also below).

To find the spatial charge distribution  $n(\mathbf{r})$  one needs to take Fourier transform of Eq. (3.21). First one notices that if the velocity does not run then  $n(\mathbf{r})$  is proportional to  $\delta(\mathbf{r})$ . Only when  $v$  runs with the momentum scale does  $n(\mathbf{r})$  differ from 0 away from the origin. When the running is slow (as at weak coupling or at large  $N$ ), the amount of screening charge enclosed inside a circle of radius  $r$  (assumed to be much larger than the lattice spacing), to leading order, is

$$\int d\mathbf{r}' n(r') \approx n(q)|_{q=1/r} = -Z \frac{\lambda(q)}{1 + \lambda(q)} \Big|_{q=1/r}. \quad (3.22)$$

The total screening charge is small if  $\lambda$  at the scale  $1/r$  is small, and close to  $-1$  if  $\lambda$  is large. Differentiating both sides of Eq. (3.22) with respect to  $r$ , one finds

$$n(r) = -\frac{Z}{2\pi r^2} \frac{\lambda(q)}{[1 + \lambda(q)]^2} \frac{\beta(v(q))}{v(q)}. \quad (3.23)$$



Note that the beta function for  $v$  is negative, therefore we arrive to a counterintuitive result the screening charge is *positive*. To see what is happening, let us take the limit  $r \rightarrow \infty$  in Eq.(3.22). This limit corresponds to the infrared limit  $q \rightarrow 0$ . We know that asymptotically  $v(q)$  grows to  $\infty$  in this limit (although only logarithmically), hence

$$\int^{\infty} d\mathbf{r}' n(\mathbf{r}') = 0. \quad (3.24)$$

i.e., the total screening charge is zero when integrated over the whole space (although the integral goes to zero very slowly). The presence of an external ion, therefore, only leads to charge redistribution: a fraction of the unit charge is pushed from short distance (of order of lattice spacing) to longer distances, but none of the charge goes to infinity. Therefore, there is a finite negative screening charge localized near  $\mathbf{r} = 0$ . Its value can be found by taking  $r$  to be of order of inverse lattice spacing  $a^{-1}$  in Eq. (3.22). The final result for the screening charge density can be written as

$$n(r) = -Z \frac{\lambda(a^{-1})}{1 + \lambda(a^{-1})} \delta(\mathbf{r}) - \frac{Z}{2\pi r^2} \frac{\lambda(q)}{[1 + \lambda(q)]^2} \frac{\beta(v(q))}{v(q)}. \quad (3.25)$$

In the rest of the note we will concentrate our attention on the long-distance tail of  $n(r)$ , ignoring the delta function at the origin.

At weak coupling ( $\lambda \ll 1$ ), the beta function for  $v(q)$  is

$$\beta(v) = -\frac{g^2}{16\pi}. \quad (3.26)$$

The solution to the RG equation, with the boundary condition  $v = v_0$  at  $q = q_0$ , is

$$v(q) = v_0 + \frac{g^2}{16\pi} \ln \frac{q_0}{q}, \quad (3.27)$$

and the screening charge density is

$$n(r) = \frac{Z}{Nr^2} \left( \frac{g^2 N}{32\pi} \right)^2 \left( v_0 + \frac{g^2}{16\pi} \ln q_0 r \right)^{-2}. \quad (3.28)$$

Notice that the result is proportional to the square of the small coupling constant  $\lambda = g^2 N / 32v$ , although we have performed the calculation to leading order in the coupling. The reason is that for the charge density  $n(r)$  to be nonzero, it is necessary that the coupling constant runs. The density  $n(r)$  therefore contains the beta function  $\beta(v)$ , as seen in Eq. (3.23), and hence is second order in the coupling constant.

In the  $1/N$  expansion the beta function for  $v(q)$  was computed in Ref. [139]:

$$\beta(v) = \begin{cases} -\frac{8v}{\pi^2 N} \left( \frac{\ln(\lambda + \sqrt{\lambda^2 - 1})}{\lambda \sqrt{\lambda^2 - 1}} + 1 - \frac{\pi}{2\lambda} \right), & \lambda > 1, \\ -\frac{8v}{\pi^2 N} \left( \frac{\arccos \lambda}{\lambda \sqrt{1 - \lambda^2}} + 1 - \frac{\pi}{2\lambda} \right), & \lambda < 1. \end{cases} \quad (3.29)$$

The two expressions smoothly match each other at  $\lambda = 1$ .

It is instructive to analyze two regimes where the RG equation can be solved analytically. The first regime is  $\lambda \ll 1$  where the result is the same as in Eq. (3.28). The second regime is the strong-coupling regime  $\lambda \gg 1$ . This regime corresponds to a quantum critical point characterized by a dynamic critical exponent  $z$ , whose value at large  $N$  is [139]

$$z = 1 - \frac{8}{\pi^2 N} + O(N^{-2}). \quad (3.30)$$

In this regime  $\beta = (z - 1)v$ . The solution to the RG equation, with the initial condition  $v = v_0$  at  $q = q_0$ , is

$$v(q) = v_0 \left( \frac{q_0}{q} \right)^{1-z}, \quad 1 - z \approx \frac{8}{\pi^2 N}. \quad (3.31)$$

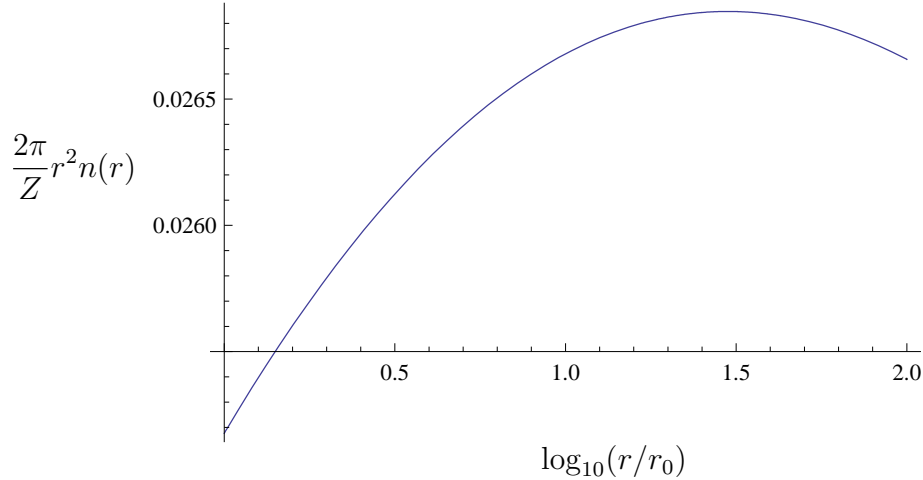


Figure 3.2: The dependence of  $2\pi Z^{-1}r^2n(r)$  on the distance  $r$  for suspended graphene. Note that coordinate  $r$  is on a logarithmic scale.

In this regime

$$n(r) = \frac{Z}{2\pi r^2} \frac{1-z}{\lambda_0} (q_0 r)^{1-z}, \quad \lambda_0 = \frac{g^2 N}{32v_0}, \quad (3.32)$$

i.e., the charge density follows a power law behavior  $n(r) \sim r^{-1-z}$ . The power is slightly different from  $-2$ .

In real graphene  $\lambda$  is of order 1, so one has to solve numerically the RG equation. We chose the scale  $q_0$  to be comparable to the inverse lattice spacing,  $r_0^{-1}$ , and  $v_0$  to be  $10^6$  m/s, a typical value found in experiments. We then run  $v$  according to the leading (in  $1/N$ ) RG equation in two cases, in vacuum and when graphene is on a  $\text{SiO}_2$  substrate with dielectric constant  $\epsilon = 4.5$ . We then plot  $2\pi r^2 n(r)$  as a function of the distance  $r$  on Figs. (3.2) and (3.3).

As seen from the figures, the charge density  $n(r)$  roughly follows the  $r^{-2}$  law: when  $r$  changes by two orders of magnitude, the product  $r^2 n(r)$  changes by a factor of less than 1.5 in both cases.

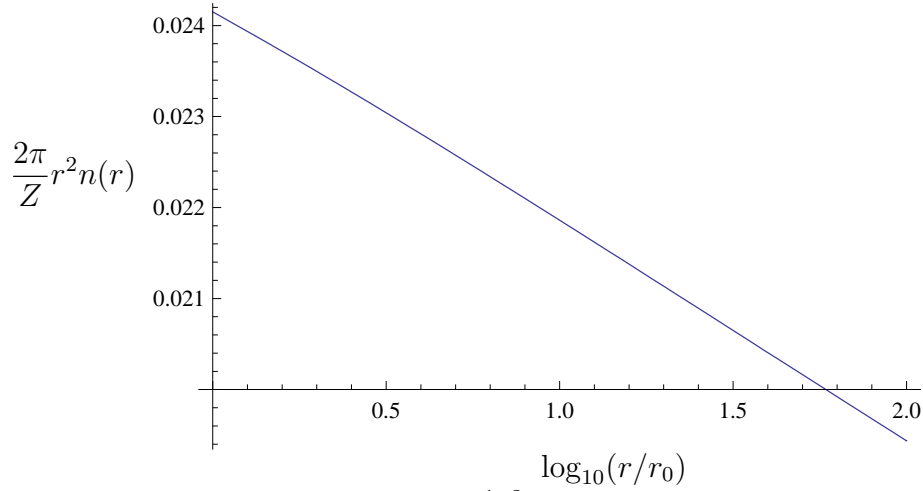


Figure 3.3: The dependence of  $2\pi Z^{-1}r^2n(r)$  on the distance  $r$  for graphene on a substrate with  $\epsilon = 4.5$ . Note that coordinate  $r$  is on a logarithmic scale.

### 3.5 Conclusions

In this chapter we have considered the problem of screening of a Coulomb impurity in graphene. We show that there is a qualitative difference between screening by non-interacting and interacting electrons. In the case of non-interacting electrons the induced charge density is localized at the position of the impurity when the impurity charge is small. The interaction between electrons lead to a long-distance tail in the induced charge distribution, with a counterintuitive sign which is the same as that of the impurity.

## Chapter 4

# Quasiparticle Interference and Landau Level Spectroscopy in Graphene in the presence of a Strong Magnetic Field

### 4.1 Synopsis

We present a calculation of the modulation in the Local Density Of electronic States (LDOS) caused by an impurity in graphene in the presence of an external magnetic field. We focus on the spatial Fourier Transform (FT) of this modulation around the impurity. The FT due to the low energy quasiparticles is found to be nonzero over the

reciprocal lattice corresponding to graphene. At these lattice spots the FT exhibits well-defined features at wavevectors that are multiples of the inverse cyclotron orbit diameter (see Figure 4.2) and is cut off at the wavevector corresponding to the energy of observation. Scanning Tunneling Spectroscopy (STS) on graphene and the energy-resolved FT fingerprint obtained therefrom may be used to observe the quasiparticle interference of Dirac particles in graphene in the presence of magnetic field.

## 4.2 Introduction

Graphene is a monatomic layer of carbon atoms arranged in a hexagonal lattice. It was first isolated by the mechanical exfoliation of graphite in 2004[99]. The electronic band structure of graphene is characterized by two points  $K$  and  $K^*$  (at wavevectors  $\pm\mathbf{K}$ )[83] in the reciprocal space where the valence and conduction bands touch each other. The gapless low energy excitations that exist at those points can be described by theories of massless Dirac quasiparticles with opposite chirality in (2+1) dimensions [151]. An interesting consequence of such a band structure is the formation of Landau levels (in a perpendicular magnetic field) whose energies vary as the square root of the Landau level index as well as that of the magnitude of the perpendicular magnetic field [86, 95]. The unconventional Quantum Hall Effect seen in transport measurements in graphene is another profound physical consequence of the Dirac nature of these quasiparticles[180, 98]. Till date, the only evidence of the Landau quantization of Dirac particles has come from bulk transport measurements. Alternately, one might look at the evidence from Landau level spectroscopy using

the Scanning Tunneling Microscope (STM). In addition to the real space imaging of Landau levels local spectroscopic tools can be a very sensitive probe of QuasiParticle Interference (QPI) that often reveals details about the underlying band structure and the quasiparticle wavefunctions[7, 140]. Applications of these ideas to graphene are natural and promising. Experiments are currently in progress that probe the signatures of QPI in graphene in the presence of a magnetic field. In this chapter we focus on QPI in magnetic field in graphene. We use the theory of non-interacting Dirac quasiparticles in a magnetic field and calculate the change in the electronic LDOS in response to weak impurities. We find that i) the LDOS FT displays characteristic rings whose size is set by the inverse cyclotron diameter  $d_{cyc}$  – indeed, in the limit of a strong magnetic field when effects of disorder and line broadening are secondary the main feature of quasiparticle motion will be the cyclotron orbits – and ii) these rings will form a lattice in Fourier space that is the same as the graphene reciprocal lattice. Also, depending on the detailed impurity potential structure this FT could have additional angular dependence in  $k$ -space determined by off-diagonal (sublattice mixing terms) in impurity scattering matrix. These ring-like signatures could be observed in STM experiments.

### **4.3 Theory**

In this work we have followed the lattice-related conventions used in [83]. The hamiltonian near the  $K^*$ -point is related to that near the  $K$ -point by a parity transformation of the lattice:  $\mathcal{H}(-K + k) = \sigma_x \mathcal{H}(K - k) \sigma_x$ . Since the low energy theory describing

free excitations near the  $K/K^*$  points obey a (2+1)-dimensional Dirac theory[151, 86], we can again use the parity operator  $\sigma_z$  for the dirac fields within a given valley to relate the stationary eigenstates of and the contributions to the propagator/Green's function from the two valleys (*modulo* the  $e^{\pm i\mathbf{K}\cdot\mathbf{r}}/e^{\pm 2i\mathbf{K}\cdot\mathbf{r}}$  factors; these are expressed as  $2\times 2$  matrices in sublattice space below – spin is ignored):

$$\begin{aligned}\psi_{\mathbf{k},s}^{-\mathbf{K}} &\propto i\sigma_y\psi_{\mathbf{k},s}^{\mathbf{K}} \\ \mathbb{G}_{-\mathbf{K}} &= \sigma_y\mathbb{G}_{\mathbf{K}}\sigma_y^\dagger \equiv -\sigma_y\mathbb{G}_{\mathbf{K}}\sigma_y\end{aligned}\quad (4.1)$$

The total low-energy electronic green's function will finally be given by:

$$\mathbb{G} = \mathbb{G}_{\mathbf{K}} + \mathbb{G}_{-\mathbf{K}} \quad (4.2)$$

When a finite perpendicular magnetic field  $B\hat{z}$  is present, in a convenient gauge choice the energy eigenstates at the  $K$ -point are given by (for  $B > 0$ ):

$$\chi_{n,k}^{\mathbf{K}}(\mathbf{r}) = \frac{e^{ikx}e^{i\mathbf{K}\cdot\mathbf{r}}}{\sqrt{\gamma_n L_x}} \begin{pmatrix} -\sigma_n\phi_{|n|-1}(y - k\ell^2) \\ \phi_{|n|}(y - k\ell^2) \end{pmatrix} \quad (4.3)$$

where  $\sigma_n = \text{sgn}(n)(1 - \delta_{n0})$ ,  $\ell = \sqrt{\hbar/(eB)}$ ,  $\gamma_n = 2 - \delta_{n,0}$ ,  $\omega_c = \sqrt{2}v/\ell$ ,  $E_{n,k} = \sigma_n\sqrt{|n|}\hbar\omega_c$  and  $n \in \mathbb{Z}$ . The  $\phi_n$ 's are the orthonormal eigenfunctions of the 1D Simple Harmonic Oscillator<sup>a</sup> (take  $\phi_{-1} \equiv 0$ ). The  $k$ 's are consistent with periodic boundary conditions in the  $x$ -direction. Since the SHO eigenfunctions need to be confined inside the sample, we end up with a degeneracy of  $\mathcal{N} = L_x L_y / (2\pi\ell^2)$  per Landau level.

---

<sup>a</sup> $\phi_n(x) = \frac{1}{\sqrt{2^n n! \sqrt{\pi}\ell}} e^{-\frac{x^2}{2\ell^2}} H_n(x/\ell)$  where  $H$  are the Hermite polynomials.



The green's function may be calculated as:

$$\begin{aligned}
 \mathbb{G}_{\mathbf{K}}(\mathbf{r}', \mathbf{r}, z) &= \sum_{n,k} \frac{\chi_{n,k}^{\mathbf{K}}(\mathbf{r}') \chi_{n,k}^{\mathbf{K}\dagger}(\mathbf{r})}{z - E_{n,k}} \\
 &= \frac{e^{i\mathbf{K}\cdot\boldsymbol{\varrho}}}{2\pi\ell^2} \sum_n \frac{e^{-\frac{\rho^2}{4\ell^2} - i\xi(y+y')/2}}{\gamma_n(z - E_n)} \times \\
 &\quad \left( \begin{array}{cc} \sigma_n^2 L_{|n|-1} & i\sigma_n \frac{\rho}{\sqrt{2|n|\ell}} e^{-i\theta} L_{|n|-1}^1 \\ i\sigma_n \frac{\rho}{\sqrt{2|n|\ell}} e^{i\theta} L_{|n|-1}^1 & L_{|n|} \end{array} \right) \\
 &\equiv \frac{e^{i\mathbf{K}\cdot\boldsymbol{\varrho}}}{2\pi\ell^2} \sum_n \frac{e^{-\frac{\rho^2}{4\ell^2} - i\xi(y+y')/2}}{\gamma_n(z - E_n)} \mathbb{M}_n^{\mathbf{K}}(\boldsymbol{\varrho}) \\
 &\equiv e^{-i\xi(y+y')/2} \mathbb{N}^{\mathbf{K}}(\boldsymbol{\varrho}, z)
 \end{aligned} \tag{4.4}$$

where  $\rho$  and  $\theta$  are the modulus and the argument respectively of the complex number  $\boldsymbol{\varrho} = (x' - x) + i(y' - y)$  and  $\boldsymbol{\varrho} = (x' - x, y' - y)$ ; the argument of the (associated) Laguerre polynomials, denoted by  $L$ , is  $\frac{\rho^2}{2\ell^2}$  and we have defined the matrices  $\mathbb{M}$  and  $\mathbb{N}$  for later reference.

We note here that we haven't found this convenient elementary result in the literature till date.

The  $K^*$  point eigenfunctions as well as the Green's functions are related to those at the  $K$  point by the aforesaid relations (4.1).

It is instructive to compare the zero field and finite field free electronic green's functions. A comparative plot of the angular average of one of their components is shown in Figure 4.1, plotted against the spatial separation as a fraction of the cyclotron diameter  $d_{cyc} = 2|E|/(evB) = 2\sqrt{2n_{LL}}\ell_B$ .

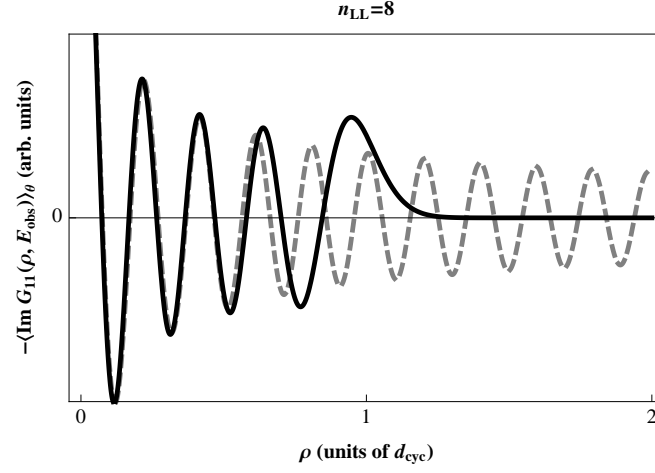


Figure 4.1: Comparison of the Green’s functions when  $B = 0$  (dashed gray) and  $B \neq 0$  (continuous black), at an energy  $E_{\text{obs}}$  corresponding to the Landau level index  $n_{LL} = 8$ . The distance propagated is measured in units of the classical cyclotron orbit diameter  $d_{cyc} = 2|E|/(evB) = 2\sqrt{2n_{LL}}\ell_B$ . At small distances these oscillate together at the wavevector  $E_{\text{obs}}/(\hbar v)$  but after  $n_{LL}/2$  oscillations the green’s function for  $B \neq 0$  decays exponentially since the particle ‘turns’ in its cyclotron orbit and cannot propagate further than  $d_{cyc}$ .

We now consider the case when an impurity potential  $\mathbb{V}(\mathbf{r})$  (whose spatial fourier transform is given by  $\tilde{\mathbb{V}}(\mathbf{q})$ ) is present in graphene. We consider the general form of  $\mathbb{V}(\mathbf{r})$  in what follows — i.e,  $\mathbb{V}(\mathbf{r})$  is a *general hermitian  $2 \times 2$  matrix function* of  $\mathbf{r}$  ( $\mathbb{V}(\mathbf{r}) = \mathbb{V}^\dagger(\mathbf{r})$ ).

## 4.4 Results

Scanning Tunneling Microscopes (STMs) give a signal corresponding to the local value of the spectral function [19]. We can use the Green’s function derived above to obtain the spatial FT of the change in the LDOS (given by the change in the spectral

function) to the linear order in the impurity potential strength as follows:

$$\begin{aligned}
 \delta A(\mathbf{r}, \omega) &= -2\text{ImTr} \left[ \int d\mathbf{r}' \mathbb{G}(\mathbf{r}, \mathbf{r}', \omega + i\eta) \mathbb{V}(\mathbf{r}') \mathbb{G}(\mathbf{r}', \mathbf{r}, \omega + i\eta) \right] \\
 \Rightarrow \delta \tilde{A}(\mathbf{k}, \omega) &= -2\text{ImTr} \left[ \tilde{\mathbb{X}}(\mathbf{k}, \omega + i\eta) \tilde{\mathbb{V}}(\mathbf{k}) \right]
 \end{aligned} \tag{4.5}$$

In the above,  $\tilde{\mathbb{X}}(\mathbf{k}, z)$  is the fourier transform (w.r.t  $\boldsymbol{\rho}$ ) of

$$\begin{aligned}
 \mathbb{X}(\boldsymbol{\rho}, z) &= \mathbb{N}(-\boldsymbol{\rho}, z) \mathbb{N}(\boldsymbol{\rho}, z) \\
 &= \mathbb{N}^{\mathbf{K}}(-\boldsymbol{\rho}, z) \mathbb{N}^{\mathbf{K}}(\boldsymbol{\rho}, z) + \mathbb{N}^{-\mathbf{K}}(-\boldsymbol{\rho}, z) \mathbb{N}^{-\mathbf{K}}(\boldsymbol{\rho}, z) \\
 &\quad + \mathbb{N}^{\mathbf{K}}(-\boldsymbol{\rho}, z) \mathbb{N}^{-\mathbf{K}}(\boldsymbol{\rho}, z) + \mathbb{N}^{-\mathbf{K}}(-\boldsymbol{\rho}, z) \mathbb{N}^{\mathbf{K}}(\boldsymbol{\rho}, z)
 \end{aligned} \tag{4.6}$$

From (4.3) and (4.4) we see that  $\mathbb{N}^{\pm\mathbf{K}}(\boldsymbol{\rho}, z)$  possess the prefactors  $e^{\pm i\mathbf{K}\cdot\boldsymbol{\rho}}$ . We thus deduce that scattering by the impurity potential  $\mathbb{V}$  will yield spatial LDOS oscillations around the wavevectors  $\mathbf{0}$  (terms in the first row of (4.6)) and  $\pm 2\mathbf{K}$  (second row of (4.6)) as well as those joined to these by reciprocal lattice vectors, due to intra and intervalley scattering respectively. The resulting lattice is identical to the reciprocal lattice (see Figure 4.2(C)).

Since scattering around the zero wavevector can also arise from many slowly varying unknown environmental potentials, we expect that LDOS oscillations around the wavevectors  $\pm 2\mathbf{K}$  near isolated atomically sharp defects will better reproduce the LDOS profiles that our theory predicts and for this reason we'll focus on explaining how to calculate the features around  $\pm 2\mathbf{K}$ . To do this we need to isolate in (4.5) the part due to intervalley scattering, which amounts to using the terms in the last line of (4.6) that we shall refer to as  $e^{\mp 2i\mathbf{K}\cdot\boldsymbol{\rho}} \mathbb{X}_{\mp}$  respectively.

The Landau levels have been assumed to be sharp in the treatment so far and so direct evaluation of (4.4) and the subsequent calculations will yield a sum of delta functions in energy. To be able to resolve the spatial functional forms and to reflect realistic experimental conditions we can either assume that the Landau levels are broadened or that the STM has a finite detection window. We have chosen to take a gaussian detection window with width  $\Gamma^b$ :

$$\delta\tilde{A}(\mathbf{k}, \omega)_{\text{obs}} \propto \int d\omega' e^{-\frac{(\omega' - \omega)^2}{2\Gamma^2}} \frac{1}{\sqrt{2\pi}\Gamma} \delta\tilde{A}(\mathbf{k}, \omega') \quad (4.7)$$

It is now possible to write down the LDOS as a series expansion in  $\frac{\Gamma}{\Delta E}$ , where  $\Delta E$  is of the order of the difference between the energy levels that are incorporated into the calculation. To see this, we note that upon substituting the expression (4.4) of the green's function we come across sums of the following structure ( $g$  represents the gaussian in (4.7);  $f_{mn}$  is proportional to Fourier transforms of the form  $\int d^2q \text{Tr}[\tilde{\mathbb{M}}_m^{\pm\mathbf{K}}(\mathbf{q} - \mathbf{k}) \tilde{\mathbb{M}}_n^{\mp\mathbf{K}}(\mathbf{q}) \tilde{\mathbb{V}}(\mp 2\mathbf{K} + \mathbf{k})]$  that satisfy the condition  $\text{Im}f_{mn} = -\text{Im}f_{nm}$  when  $\mathbb{V}$  is *invariant under spatial inversion*):

$$\begin{aligned} & \text{Im} \int d\omega' g(\omega' - \omega) \sum_{m,n} \frac{f_{mn}}{(\omega' - \epsilon_m + i\eta)(\omega' - \epsilon_n + i\eta)} \\ & \stackrel{\text{Im}f_{mn} = -\text{Im}f_{nm}}{=} \pi \sum_{m \neq n} \text{Re}f_{mn} \frac{g(\epsilon_n - \omega) - g(\epsilon_m - \omega)}{\epsilon_m - \epsilon_n} - 2\pi \sum_n f_{nn} g'(\epsilon_n - \omega) \\ & = \pi \sum_n g(\epsilon_n - \omega) \sum_{m(\neq n)} \frac{\text{Re}(f_{mn} + f_{nm})}{\epsilon_m - \epsilon_n} - 2\pi \sum_n f_{nn} g'(\epsilon_n - \omega) \end{aligned} \quad (4.8)$$

The ‘diagonal’ term involving  $f_{nn}$  above (that corresponds to the particle ejected by the STM tip remaining in the same Landau level on both legs of its journey before

---

<sup>b</sup>If the Landau levels are sharper than the lock-in AC voltage amplitude applied to the STM, this approach is more appropriate. It is easy to calculate the case of broadened Landau levels (or non-gaussian profiles) and does not affect our general conclusions.

and after scattering off the defect) gives the main contribution and the other members in the sum are suppressed by the aforesaid factors of  $\frac{\Gamma}{\Delta E}$ . The numerical calculations that we subsequently perform are taking only the first few terms of this series into account and work well for large magnetic fields when  $\Delta E \propto \sqrt{B} \gg \Gamma$ .

From (4.5) and subsequent discussions we find that we can write  $\delta\tilde{A}_{\text{obs}}$  in the form  $\delta\tilde{A}(\pm 2\mathbf{K} + \mathbf{k}, \omega)_{\text{obs}} = \text{Tr}[\tilde{\mathbb{D}}_{\pm}(\mathbf{k}, \omega)\tilde{\mathbb{V}}(\pm 2\mathbf{K} + \mathbf{k})]$ , where  $\mathbb{D}_{\pm} = i(\mathbb{X}_{\pm} - \mathbb{X}_{\pm}^{\dagger})$ . We can make the following general comments regarding the functional dependence of the components of  $\tilde{\mathbb{D}}_{\pm}(\mathbf{k}, \omega)$  as a function of  $\mathbf{k}$ . Let  $n_{LL}(\omega)$  denote the Landau level index corresponding to the Landau level nearest to the energy of observation  $E_{\text{obs}} = \hbar\omega$  — it is thus the integer closest to  $\text{sgn}\omega(\omega/\omega_c)^2$ . The ‘diagonal’ term in (4.8) that is the most important contribution then corresponds to  $n = n_{LL}(\omega)$ . From the definition of  $\mathbb{D}$  and using (4.4) we see that  $\mathbb{D}$  consists of products of two oscillatory functions (like those shown in Figure 4.1). We thus expect spatial oscillation scales set by the wavevectors  $2\pi/(2\sqrt{2}|n_{LL}|\ell)$  and twice of  $|\omega|/v$  to appear in  $\mathbb{D}(\mathbf{r})$ . Our calculation confirms this expectation — we find that  $\tilde{\mathbb{D}}(\mathbf{k})$  displays a set of about  $|n_{LL}|$  oscillatory peaks starting at  $k = 0$  and separated by a period  $\Delta k$  (see below); it then decays rapidly after a maximum wavevector  $k_{\text{max}}$ , where

$$\Delta k \sim \frac{2}{\ell} \sqrt{\frac{2}{|n_{LL}|}} = \frac{8}{d_{\text{cyc}}}, \quad k_{\text{max}} = \frac{2|\omega|}{v} \sim 2\sqrt{2} \frac{|n_{LL}|}{\ell} \quad (4.9)$$

The off-diagonal elements in (4.4) possess an angular dependence and for this reason  $\tilde{\mathbb{D}}(\pm 2\mathbf{K} + \mathbf{k})$  exhibits sinusoidal oscillations in  $\theta_k$  and  $2\theta_k$  for a given  $k$ ,  $\theta_k$  being the orientation angle of  $\mathbf{k}$  with respect to the direction of  $\mathbf{K}$ . We find that when intravalley scattering is considered, only the off-diagonal components of  $\mathbb{V}$  give rise

to  $\theta_k$ -oscillations while in the case of intervalley scattering, the diagonal components of  $\mathbb{V}$  can, in addition, lead to  $2\theta_k$ -oscillations.

The results of our calculations have been summarized in the Figure 4.2. The FT of the LDOS oscillations is plotted near a short-ranged diagonal impurity potential  $\tilde{\mathbb{V}}(\mathbf{k}) \propto \mathbb{I}$  (the  $2 \times 2$  identity matrix). Given any other nontrivial form of this potential, the LDOS modulations may be found straightforwardly from the above prescription.

It is worth noting here that we have only quantified the oscillation parameters that may be observed in the spatial Fourier transform and *not the Power Spectrum*, examples of which are however also shown in Figure 4.2 (L1, R1). Upon squaring the FT modulus to obtain the power spectrum the result could have twice as many oscillations – this needs to be kept in mind when comparing the foregoing results with experimental signatures.

## 4.5 Conclusion

In conclusion, in this work we have laid out the framework for calculating the LDOS modifications around an impurity in graphene in the presence of a strong magnetic field. We use the linearly dispersing chiral quasiparticle theory. To calculate the QPI we have derived the graphene green's function in a magnetic field. There are two distinct regimes – in case of a strong field we have a situation of QHE while in the opposite case of a weak field the level broadening  $\Gamma$  (due to lock-in modulation of STM voltage or due to impurity scattering, etc) will be larger than the Landau level

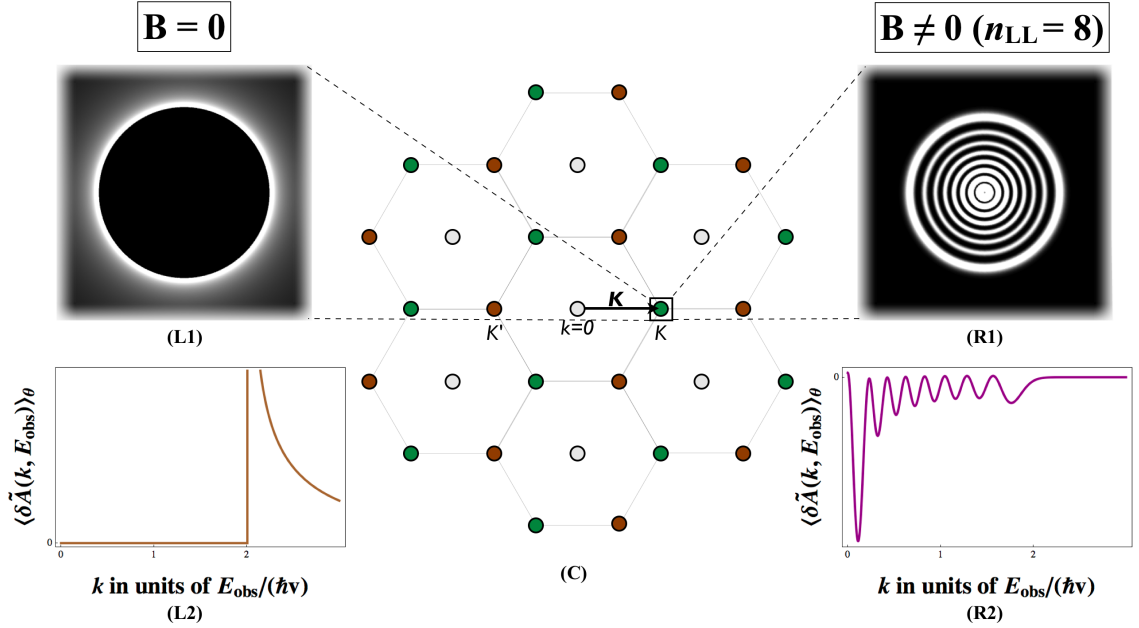


Figure 4.2: (Color online) Comparison of the *angular averages* of the spatial FT and power spectrum of LDOS modulations around a short-ranged impurity potential  $\tilde{V}(\mathbf{k}) \propto \mathbb{I}$ , for the cases when the magnetic field is zero and when it's nonzero (and the nearest Landau level has an index  $n_{LL} = 8$ ). The center figure (C) shows part of the reciprocal lattice formed by regions in  $k$ -space where the Fourier transform may be nonzero. The green and red 'spots' arise from  $K \rightarrow K'$  scattering and vice versa respectively. The grey spots arise from intravalley scattering. One green region is enlarged to show the angle-averaged *Power Spectrum* on a scale where the oscillations are better resolved (the density maps have edges of length  $6E_{\text{obs}}/(\hbar v)$ ), for the  $B \neq 0$  (R1) and  $B = 0$  (L1) cases. Below these are the corresponding variation of the *Fourier transforms* with  $k$  — the deviation from the  $K$ -point, for the  $B \neq 0$  (R2 – see (4.9) for parameters) and  $B = 0$  (L2) cases. All plots were made using Mathematica[1].

splitting  $\Delta E \sim B^{1/2}$ . We considered the case of a strong magnetic field. To this end we established a series expansion in  $\Gamma/\Delta E$ . In this limit our approach can be used to obtain the LDOS oscillations for any impurity potential. While the exact form of these oscillations vary by impurity type, we have identified a few important characteristics that may be observed in the FT of these oscillations — impurity-induced LDOS modulations in a magnetic field thus offers an alternative avenue for Landau level spectroscopy using local probes.

(After the submission of our work, we became aware of the preprint [12] where similar questions have been addressed.)



# Chapter 5

## Impurity-induced states on the surface of 3D topological insulators

### 5.1 Synopsis

We calculate the modification of the local electronic structure caused by a single local impurity on the surface of a 3D Topological Insulator. We find that the LDOS around the Dirac point of the electronic spectrum at the surface is significantly disrupted near the impurity by the creation of low-energy resonance state(s) – however, this is not sufficient to (locally) destroy the Dirac point. We also calculate the non-trivial spin textures created near the magnetic impurities and discover anisotropic RKKY coupling between them.

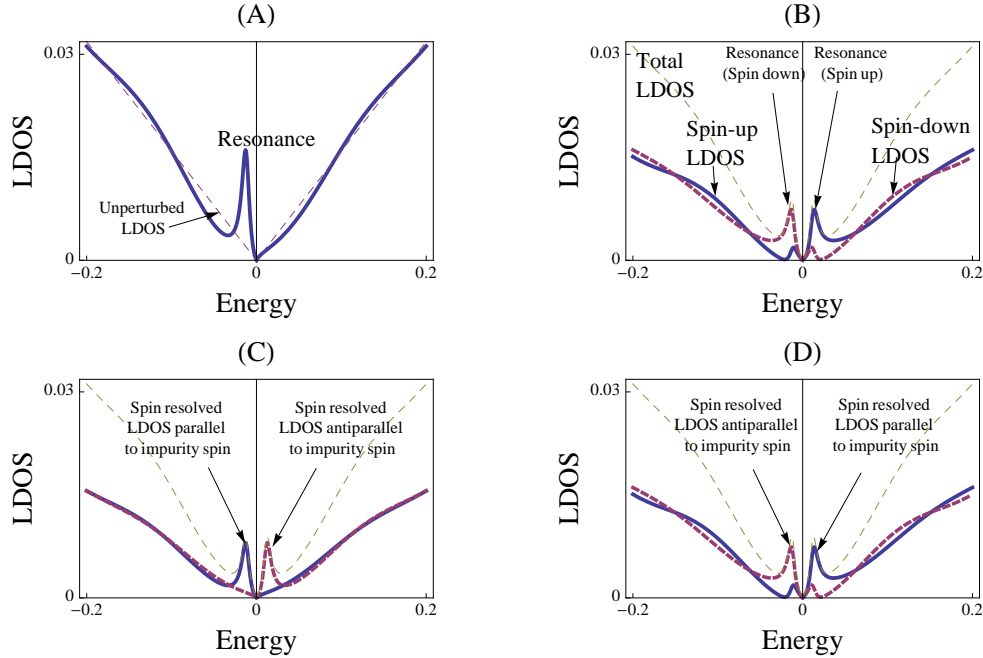


Figure 5.1: (Color Online) LDOS plots showing the low energy resonance(s) near (A) the scalar/potential impurity, (B) the  $z$ -polarized and (C,D) the  $x$ -polarized magnetic impurities. (C) and (D) show the  $x$ -spin projected LDOS, at a point on the  $x$  and  $y$ -axis respectively. Note from (C) that on the  $x$ -axis, the negative energy states have excess states with spins *parallel* to the  $x$ -polarized impurity. In all these cases,  $U = 100$ ,  $r = 20$ . In the system of units used above,  $\hbar$ ,  $v_F$  and  $W$  are unity.

## 5.2 Introduction

The Dirac spectrum of chiral excitations are realized in a wide range of materials including d-wave superconductors[7], graphene[95], semiconductors[36] and superfluid  $^3\text{He-A}$ [150]. The Dirac spectrum brings in substantial similarities in electronic properties – like response to defects as well as low energy and low temperature properties. It is thus natural to combine these materials into a category of ‘Dirac materials’. A recent exciting realization of the Dirac spectrum is on the surface of 3D Strong Topological Insulators (STI)[166, 115, 178]. These materials have an ungapped spectrum at

the surface while being fully gapped in the bulk. In addition, STIs are unique because the topology of their bulk band structure constrains their surface states to possess an odd number of Dirac nodes[42, 124]. Suppressed backscattering inside the odd Dirac cone guarantees that the Dirac dispersion remain essentially unperturbed for any perturbation to the Hamiltonian that preserves time reversal symmetry. This is a manifestation of the topological protection enjoyed by this kind of surface band crossing and makes these materials an attractive candidate for spintronics applications[91] as well as a possible platform for topological quantum computation[41]. In this context an important issue is the stability of the STI surface nodes to the presence of impurities[124, 94, 46]. We contribute to this discussion by looking at the modification of surface states around a *single* local potential/magnetic impurity and calculate the change in the Local Density of States (LDOS) as well as the spin density near the impurity site. These quantities should be accessible by STM measurements. We find the following.

(i) There is substantial modification of the LDOS near the impurity site for both the nonmagnetic (time reversal preserving) and magnetic impurities (time reversal breaking), especially when impurity scattering is strong (unitary). Near the potential/magnetic impurity, a single/a pair of low energy resonances form near the Dirac point (Figs. 5.1, 5.2). These become very sharp and their energies  $\Omega \rightarrow 0$  as the impurity strength (5.3)  $|U| \rightarrow \infty$  :

$$|\Omega| \approx \frac{5 \operatorname{sgn}|U|}{|U| \ln |U|} \quad (5.1)$$

The scalar impurity resonance is doubly degenerate due to Kramers' theorem[155, 7, 13]. The magnetic impurity breaks time reversal symmetry and splits the low energy

impurity resonance into two spin-polarized resonances on either side of the Dirac point (Fig. 5.1).

(ii) Modification of the LDOS vanishes quickly for energies less in magnitude than the resonance energy (approaching the Dirac point) for *both* magnetic and nonmagnetic impurities. Thus, modifications to the low energy LDOS does not provide us with a signature of any incipient gap in the spectrum for both potential and magnetic impurities. For  $r \gg 1/\omega$ , these decay as  $1/r^2$ .

(iii) In addition to LDOS modifications, magnetic scattering produces non-trivial spin textures near the impurity site (Figure 5.3) that can be imaged with a magnetic force microscope or spin-resolved STM. These non-trivial spin textures lead to the propagation of unconventional antiferromagnetic (AF) RKKY coupling between magnetic impurities, when they are polarized along the line joining them and when the chemical potential is close to the Dirac point. When the spins are perpendicular to the line joining them, they interact strongly and ferromagnetically (FM). The Dzyaloshinskii-Moriya (DM) interaction between the spins[174] vanishes at the Dirac point. We thus conclude that random magnetic impurities will tend to align parallel to the normal to the STI surface.

### 5.3 Theory

We will model the STI surface states as a single species of non-interacting 2-D Dirac quasiparticles[78] with a high energy band cutoff  $W$ . We shall work in units of  $W$ ,  $\hbar$

and  $v_F$  (the Fermi velocity). The Hamiltonian becomes:

$$\mathcal{H}_0 = \boldsymbol{\sigma} \cdot \mathbf{p} \quad (5.2)$$

where  $\boldsymbol{\sigma}/2$  is the *actual* spin of the electron (or related by a rotation about  $\hat{z}$ ). We shall consider local impurities of the potential and classical types respectively:

$$\hat{V}_{\text{pot}} = U \mathbb{I} \delta(\hat{\mathbf{r}}), \quad \hat{V}_{\text{mag}} = U \mathbf{S} \cdot \boldsymbol{\sigma} \delta(\hat{\mathbf{r}}) \quad (5.3)$$

For the magnetic case we have assumed a local Heisenberg exchange  $J$  between the band electrons and the impurity spin  $S$ , whose direction is given by the *unit vector*  $\mathbf{S}$ . Thus,  $U = JS/2$  in  $\hat{V}_{\text{mag}}$ .

To address the effect of impurity scattering we use the T-matrix technique [7]. The T-matrix is defined via:

$$\hat{T}(\omega) = \hat{V} + \hat{V} \hat{G}_0^{\text{ret}}(\omega) \hat{T}(\omega) \quad (5.4)$$

where  $G_0^{\text{ret}}$  is the retarded Green's function for the impurity-free material and  $\omega$  is the energy. For  $\omega \ll 1$  and  $\rho \gg 1/W$  ( $\rho \equiv \mathbf{r} - \mathbf{r}'$ ), it has the following form:

$$\langle \mathbf{r} | G_0^{\text{ret}}(\omega) | \mathbf{r}' \rangle = \frac{|\omega|}{4} [f_0(\omega, \rho) \mathbb{I} + f_1(\omega, \rho) (\boldsymbol{\sigma} \cdot \hat{\boldsymbol{\rho}})] \quad (5.5)$$

where

$$f_0(\omega, \rho) = s(\omega) Y_0 - i J_0 \theta, \quad f_1(\omega, \rho) = i Y_1 + s(\omega) J_1 \theta \quad (5.6)$$

and  $|\omega|\rho$  is the argument of the Bessel functions  $J_{0/1}$  and  $Y_{0/1}$ . Also,  $s(\cdot) \equiv \text{sgn}(\cdot)$  and  $\theta \equiv \Theta(1 - |\omega|)$ . We shall also require the unperturbed on-site Green's function

valid for short distances  $\lesssim 1$ :

$$\begin{aligned} \mathbb{G}_0(\omega) &\equiv \langle \mathbf{0} | G_0^{\text{ret}}(\omega) | \mathbf{0} \rangle = -(g_0(\omega) + ig_1(\omega)) \mathbb{I}, \text{ where} \\ g_0(\omega) &= \frac{\omega}{4\pi} \ln \left| \frac{1}{\omega^2} - 1 \right|, g_1(\omega) = \frac{|\omega|}{4} \Theta(1 - |\omega|) \end{aligned} \quad (5.7)$$

In (5.3), we have used a local form for the impurity potential  $\langle \mathbf{r} | \hat{V} | \mathbf{r}' \rangle = \mathbb{V} \delta(\mathbf{r}) \delta(\mathbf{r}')$ , where  $\mathbb{V}$  is a  $2 \times 2$  matrix in spin-space. The T-matrix also becomes  $\langle \mathbf{r} | \hat{T} | \mathbf{r}' \rangle = \mathbb{T} \delta(\mathbf{r}) \delta(\mathbf{r}')$ , with  $\mathbb{T}$  satisfying the following equation

$$\mathbb{T} = \mathbb{V} + \mathbb{V} \mathbb{G}_0 \mathbb{T} = (\mathbb{I} - \mathbb{V} \mathbb{G}_0)^{-1} \mathbb{V} \quad (5.8)$$

From the algebraic relations involving (5.3), (5.7) and (5.8), we analytically calculate the T-matrix, the full Green's function  $\hat{G}^{\text{ret}}$ ,

$$\hat{G}^{\text{ret}}(\omega) = \hat{G}_0^{\text{ret}}(\omega) + \hat{G}_0^{\text{ret}}(\omega) \hat{T}(\omega) \hat{G}_0^{\text{ret}}(\omega) \quad (5.9)$$

the full (spin-unresolved) LDOS,

$$\rho(\mathbf{r}, \omega) = -\frac{1}{\pi} \text{ImTr} \left\langle \mathbf{r} \left| \hat{G}^{\text{ret}}(\omega) \right| \mathbf{r} \right\rangle, \quad (5.10)$$

the local density of spin up/down states (in direction  $\mu$ ),

$$\rho_{\pm}^{\mu}(\mathbf{r}, \omega) = -\frac{1}{\pi} \text{ImTr} \left\langle \mathbf{r} \left| \hat{G}^{\text{ret}}(\omega) \left( \frac{1 \pm \sigma_{\mu}}{2} \right) \right| \mathbf{r} \right\rangle \quad (5.11)$$

and the energy-resolved spin density averages:

$$\mathbf{s}(\mathbf{r}, \omega) = -\frac{1}{\pi} \text{ImTr} \left\langle \mathbf{r} \left| \hat{G}^{\text{ret}}(\omega) \frac{\boldsymbol{\sigma}}{2} \right| \mathbf{r} \right\rangle \quad (5.12)$$

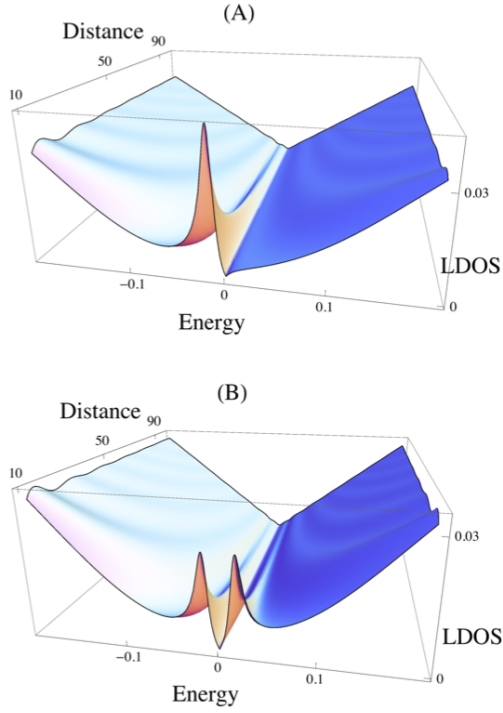


Figure 5.2: (Color Online) Low energy LDOS near the (A) scalar impurity and (B) the  $x$ -polarized magnetic impurity for  $U = 80$ .  $\hbar$ ,  $v$  and  $W$  have been set to unity.

## 5.4 Results

For the scalar and magnetic impurity cases, we find that the additional  $GTG \equiv \delta G$  pieces in the Green's function (5.9) evaluate respectively to (using  $g \equiv g_1 + ig_2$ )

$$\delta G_{\text{pot}} = \frac{U\omega^2}{16} \frac{f_0^2 - f_1^2}{1 + Ug} \quad (5.13)$$

and

$$\begin{aligned} \delta G_{\text{mag}} = \frac{U\omega^2}{16(1 - U^2g^2)} & \left[ -2if_0f_1\boldsymbol{\sigma} \cdot (\mathbf{S} \times \hat{\mathbf{r}}) + \right. \\ & \left. (f_0^2 + f_1^2)\boldsymbol{\sigma} \cdot \mathbf{S} - 2f_1^2(\boldsymbol{\sigma} \cdot \hat{\mathbf{r}})(\mathbf{S} \cdot \hat{\mathbf{r}}) - Ug(f_0^2 - f_1^2) \right] \end{aligned} \quad (5.14)$$

As shown in Figures (5.1) and (5.2), for both the magnetic and non-magnetic cases

we obtain low energy resonance(s) in the LDOS (arising from the minima of the denominators in (5.13) and (5.14)) that approach the Dirac point for large impurity strengths according to (5.1) [155, 7]. These resonances become sharper as they approach the Dirac point with increasing potential strength and while doing so, also increase in amplitude relative to the unperturbed LDOS. For  $r \gg 1/\omega$  and  $\omega \ll 1$ , the strength of LDOS modulations diminish with distance as  $1/r^2$ [11].

Topological stability of the surface Dirac spectrum in TIs is often discussed as a crucial property of these materials. An important question in this context is whether the appearance of these low-energy resonances is related to the local creation of a gap at/destruction of the Dirac point. Naïve scaling analysis tells us that the potential strength  $U$  has a dimension of  $-1$  (same as length) near the fixed point corresponding to (6.10). As we approach the Dirac point, we should thus see the effects of the impurity become negligible. Indeed, we find that if we move from the resonances to the Dirac point, the density of states gradually settles down to the impurity-free value. We cannot, therefore, find signatures of gap-opening at the Dirac point at the stage of one-impurity scattering. We also note here that the appearance of these resonances *at* the Dirac point is a consequence of the band cutoff being symmetric on the particle and hole sides – in realistic materials[166] the band structure is asymmetric and depending on the degree of asymmetry, these resonances may appear at other region(s) of the bands[7].

In addition to the impurity resonances at small energy we find new states that lie outside the effective band edges – a consequence of using a hard cutoff. These true bound/anti-bound states are located at the positive/negative side for posi-



tive/negative sign of a scalar impurity potential  $U$ . For a magnetic impurity they are located on both sides outside the effective band edges. For large  $|U|$ , these are located approximately at a distance  $U$  from the Dirac point, while as  $|U| \rightarrow 0$  they approach the band edge as  $e^{-4/|U|}$ . In real STI SSSs, these may well be located at the same energy as the bulk bands, will hybridize with them and delocalize into the bulk.

Near a magnetic impurity, entanglement of the electron spin and momentum lead to the creation of spin textures, as shown in Figure 5.3. The energy-resolved spin average is found to be:

$$\begin{aligned} \mathbf{s}(\mathbf{r}, \omega) & \quad (5.15) \\ & = U\omega^2 \text{Im} \left( \frac{2if_0f_1\mathbf{S} \times \hat{\mathbf{r}} - (f_0^2 + f_1^2)\mathbf{S} + 2f_1^2\hat{\mathbf{r}}(\mathbf{S} \cdot \hat{\mathbf{r}})}{16\pi(1 - U^2g^2)} \right) \end{aligned}$$

The first term in (5.15) gives rise to a DM interaction between two impurity spins. When the chemical potential  $\mu$  is at the Dirac point, considering only the perturbative result (obtained cheaply by putting  $g \rightarrow 0$  in the above expression), the strength of this interaction becomes zero

$$\begin{aligned} & \int_{-\infty}^0 \text{Re}(f_0f_1)\omega^2 d\omega \\ & \sim -\frac{1}{r^3} \int_0^\infty \frac{d}{dx} (J_0Y_0)\Theta(r-x)x^2 dx \stackrel{r \gg 1}{\approx} 0 \end{aligned} \quad (5.16)$$

For a finite chemical potential  $|\mu| \ll 1$ , the amplitude of the DM interaction becomes

$$\begin{aligned} \frac{U}{8\pi} \int_{-\infty}^\mu \text{Re}(f_0f_1)\omega^2 d\omega & = \frac{U \text{sgn}\mu}{8\pi} \int_0^{|\mu|} \text{Re}(f_0f_1)\omega^2 d\omega \\ & = \frac{U\mu|\mu|J_1(|\mu|r)Y_1(|\mu|r)}{8\pi r} \end{aligned} \quad (5.17)$$

At large distances, the amplitude of this interaction decays as  $\sim U\mu/r^2$ .

The second term in (5.15) leads to FM RKKY interactions when  $\mu = 0$ , in the perturbative approximation. The corresponding spin component is

$$-\frac{U\mathbf{S}}{16\pi} \int_{-\infty}^0 \text{Im}(f_0^2 + f_1^2)\omega^2 d\omega = -\frac{U}{32\pi r^3} \mathbf{S} \quad (5.18)$$

Finally, the third term in (5.15) leads to AF RKKY interaction between impurity spin components pointing along the line joining the impurities, when  $\mu = 0$ . In the perturbative limit, the corresponding induced spin component is:

$$\frac{U\hat{\mathbf{r}}(\mathbf{S} \cdot \hat{\mathbf{r}})}{8\pi} \int_{-\infty}^0 \text{Im}(f_1^2)\omega^2 d\omega = \frac{3U}{64\pi r^3} \hat{\mathbf{r}}(\mathbf{S} \cdot \hat{\mathbf{r}}) \quad (5.19)$$

From these two expressions we calculate that at  $\mu = 0$  the interaction energy between two impurity spins  $\mathbf{S}_{1,2}$ :

$$\begin{aligned} \Delta E_{12}(\mathbf{r}_{21})_{\mu=0} &= \langle U\mathbf{S}_1 \cdot \mathbf{s}_1 + U\mathbf{S}_2 \cdot \mathbf{s}_2 \rangle_{\text{cross terms}} \\ &= \frac{U^2}{16r^3} \left( -\mathbf{S}_1 \cdot \mathbf{S}_2 + \frac{3}{2} (\mathbf{S}_1 \cdot \hat{\mathbf{r}}_{21})(\mathbf{S}_2 \cdot \hat{\mathbf{r}}_{21}) \right) + \mathcal{O}(U^4) \end{aligned} \quad (5.20)$$

is *minimized* when they are aligned parallel to each other and perpendicular to the line joining them. Thus, when many impurities are present (and  $\mu = 0$ ), they will tend to point in the common direction where all gain the FM interaction energy – along the  $z$ -direction, normal to the surface. This kind of FM ordering will be conducive to opening a gap in the STI surface state spectrum – an example of which has been observed in a recent experiment [164]. Also, we note here that this state does not arise due to the spontaneous breaking of a continuous symmetry and hence is not forbidden by the Mermin-Wagner theorem[87].

We would like to note here that the foregoing results are not obvious when observing the energy-resolved spin densities at low energies  $\omega \rightarrow 0-$ , because of the low density

of states there. Naïvely, one would have expected the low energy long wavelength features to determine the  $r \rightarrow \infty$  spin textures, but the low energy spin textures predict, incorrectly, antiferromagnetic RKKY interactions with short distance ferromagnetic contributions arising from non-perturbative effects. We would also like to note here that we assumed a smooth cutoff when adding up the spin textures at different energies to eliminate cutoff-dependence[123]. We have used multiplicative functions like  $e^{-\eta|\omega|}$  and  $(1 - e^{-\eta\omega^2})/(\eta\omega^2)$  (having different characters as  $|\omega| \rightarrow \infty$ ) in the energy integrals and then taken the limit  $\eta \rightarrow 0+$  — both these procedures gave the same limit<sup>a</sup>.

When we consider the full nonperturbative spin average obtained by integrating (5.15) numerically, the aforementioned behaviors seems to hold qualitatively if we look beyond the ‘ringing’ introduced by a sharp cutoff.

## 5.5 Conclusion

In summary, we find that local impurities can strongly disrupt the structure near the Dirac node of 2-D surface states in 3-D topological insulators by forming low energy resonance(s). However, in the asymptotic approach to the Dirac point, the linear DOS is preserved, consistent with the negative scaling dimension of the impurity strength. Thus, the gap-opening mechanism for magnetic impurities is not evident at this stage of analysis. We also find that the induction of non-trivial spin

---

<sup>a</sup>Calculations by the authors, on the lines of [137], have confirmed these results. These calculations will be presented in a later work.

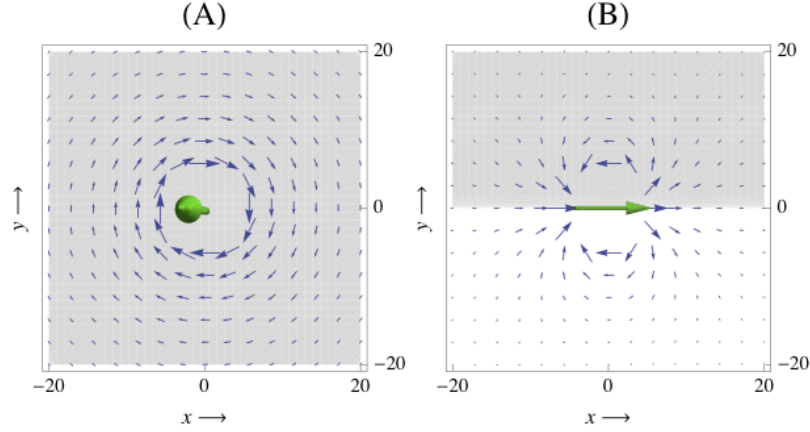


Figure 5.3: (Color Online) Spin textures near spin impurities ( $U = 80$ ,  $E = \Omega = -0.014$ ) when the impurity is (A)  $z$ -polarized and when it is (B)  $x$ -polarized (solid green arrows). The component in the  $xy$  plane is denoted by a vector while the background shade gives the sign of  $s_z(r, E)$  (clear  $\equiv$  positive). The arrows are normalized to the longest field-of-view total spin length in (A) and  $xy$  spin length in (B), indicating respectively the sign of the  $z$  polarization and the anisotropic  $x$  polarization around the impurities in accordance with (5.15) (these mediate *anisotropic* RKKY interactions between two impurity spins).

textures near magnetic impurities leads to the mediation of antiferromagnetic RKKY coupling between impurity spin components parallel to the lines joining them, especially if the chemical potential is at the Dirac point (in which case the interaction does not oscillate in sign). The spin components perpendicular to the line joining the impurities, however, exhibit strong FM interaction. While there is, in general, a DM component in the spin interactions, it vanishes at the Dirac point. We predict that when many impurities are present (and  $\mu \approx 0$ ), they will tend to point in the common direction where all gain the FM interaction energy – along the  $z$ -direction, normal to the surface. This kind of ordering will be conducive to opening a gap in the STI surface state spectrum – an example of which has been observed in a recent experiment [164] where iron atoms were deposited on the surface of  $\text{Bi}_2\text{Se}_3$ .

# Chapter 6

## Scattering from Surface Step Edges in Strong Topological Insulators

### 6.1 Synopsis

We study the characteristics of scattering processes at step edges on the surfaces of Strong Topological Insulators (STI), arising from restrictions imposed on the  $S$ -matrix *solely* by time reversal symmetry and translational invariance along the step edge. We show that the ‘perfectly reflecting’ step edge that may be defined with these restrictions allow modulations in the Local Density of States (LDOS) near the step edge to decay no slower than  $1/x$ , where  $x$  is the distance from the step edge. This is faster than in 2D Electron Gases (2DEG) — where the LDOS decays as  $1/\sqrt{x}$  — and shares the same cause as the suppression of backscattering in STI surface states. We

also calculate the scattering at a delta function scattering potential and argue that *generic* step edges will produce a  $x^{-3/2}$  decay of LDOS oscillations. Experimental implications are also discussed.

## 6.2 Introduction

Strong topological Insulators (STI) are three-dimensional band insulators that have an odd number of gapless chiral modes on their surfaces[42, 89, 178]. These have recently been realized experimentally[166, 115, 54, 43] and are an active area of current research. The chiral states on the STI surfaces consist of time-reversed pairs of states propagating in opposite directions, between which backscattering by time-reversal invariant impurities and perturbations[115] is forbidden. Because of this, we can expect scattering at impurities or step edges on the STI surface to lead to outcomes that are substantially different from the case of the 2D Electron Gas (2DEG). This suppression of backscattering is also often quoted as a major reason for the topological protection of the STI surface states against surface impurities. While this suppression is precise for the case of exact backscattering, it does not forbid scattering processes in which the particle gets reflected ‘almost’ backward – the formation of localized resonances/states near surface defects[176, 16] are still allowed. It is therefore instructive to test the response of these STI surface states to various surface defects and precisely quantify the restrictions imposed by the robust Time Reversal Symmetry (TRS). This knowledge will be an important ingredient in future attempts to design electronic devices based on these materials. We also discuss the relation of the

calculations in this chapter with a growing body of literature on the use of Scanning Tunneling Spectroscopy (STS) to investigate the role of isolated impurities and step edges on STI surfaces[5, 132].

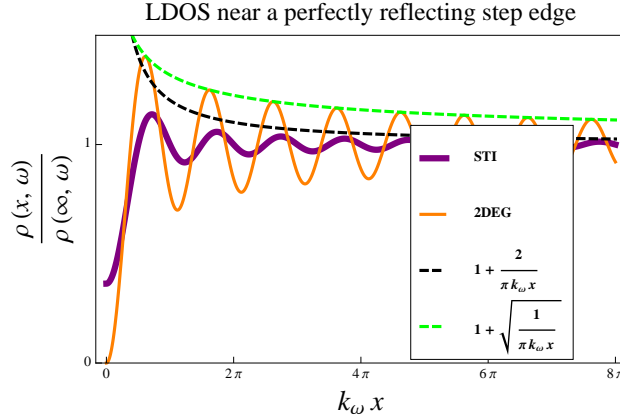


Figure 6.1: (Color Online) Comparison between the LDOS near a ‘perfectly reflecting’ step edge in the STI (6.16) and the 2DEG. Their envelopes, decaying as  $1/x$  and  $1/\sqrt{x}$ , respectively, are shown as dashed curves.  $k_\omega$  is the wave vector at energy  $\omega$ .

We shall address, in this chapter, the scattering physics characteristic of a *single* set of chiral states – such as the Dirac states present on the surface of  $\text{Bi}_2\text{Te}_3$  or  $\text{Bi}_2\text{Se}_3$ [54, 178] — in the context of scattering from a step edge. We find the following:

(i) TRS and unitarity impose a set of constraints on the reflection and transmission amplitudes (equation (6.5)) *irrespective* of the effective Hamiltonian describing the step edge. We only require that the step edge does not violate TRS and is translationally invariant along its length.

(ii) Suppressed backscattering leads to a substantial decrease of LDOS modulation near the step edge on the surface of the STI — the LDOS is found to decay at least

as fast as (Figure 6.1)

$$\frac{\delta\rho(\omega, x)}{\rho^{(0)}(\omega)} \sim \frac{1}{x} \quad (6.1)$$

In contrast, in 2DEGs this decay is slower  $\sim 1/\sqrt{x}$  [25].

(iii) We predict the existence of the ‘perfectly reflecting’ step edge (6.15) by using the scattering matrix restrictions. This perfectly reflecting wall produces LDOS modulations of the kind mentioned in (6.1) (shown in Figure 6.1).

(iv) For a sharp step edge, which we approximate using a delta function, we have evaluated the reflection amplitude explicitly as a function of the potential strength (6.18) and using this, find that for a ‘strong’ potential there are essentially no oscillations near the step edge. The LDOS decays monotonically as  $x^{-3/2}$  far from the edge, after an initial dip (Figure 6.3) – similar to the long wavelength scattering observed in [5]. The  $x^{-3/2}$  decay law is also true for *generic* step edges due to TRS.

Modulation in the density of states produced by defects can be imaged using local spectroscopy like Scanning Tunneling Microscopy (STM) and comparisons between theoretical calculations and experimental observations would allow one to verify the topological stability of states on the surface of a STI.

Our results can be viewed in the context of a broader discussion of scattering of Dirac quasiparticles in graphene. One of the striking features discussed in the past is the so called Klein paradox where particles can tunnel without backscattering under barrier [95, 65, 10]. The situation we address here is similar yet different: the additional symmetry which is present in our analysis but absent in graphene is the exact suppression of backscattering for *any* time reversal invariant potential due to



topological protection. In case of graphene large momentum scattering would allow inter-valley scattering and thus back-scattering is ultimately permitted. This add-on effect of the exact suppression of backscattering off the step edge is what we address in this chapter.

### 6.3 Theory

We begin by formulating the general scattering matrix framework for the case of scattering at a surface step edge. We label the STI surface states by their band index  $s = \pm 1$  and momentum  $\mathbf{k} = (k_x, k_y)$ , which together also determine their energies  $E_{s,\mathbf{k}}$ . We choose  $E = 0$  at the Dirac point and  $s = \text{sgn}E_{s,\mathbf{k}}$ . The defining characteristic of these states is that oppositely propagating states at a given energy are time-reversed partners ( $\Theta$  is the time reversal operator):

$$|s, -\mathbf{k}\rangle \propto \Theta |s, \mathbf{k}\rangle \quad (6.2)$$

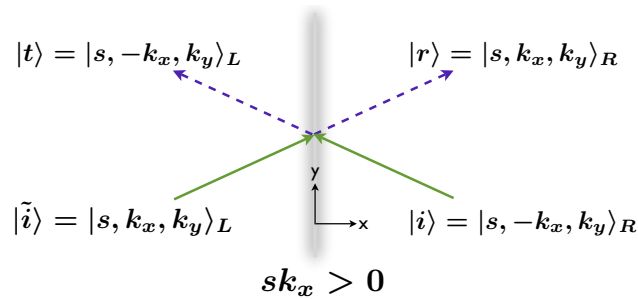


Figure 6.2: (Color Online) The scattering problem at a step edge, at an energy  $E_{s,\mathbf{k}}$  and a  $y$ -momentum  $k_y$ . The green (incoming) and dashed violet (outgoing) arrows label the ‘incoming’ and ‘outgoing’ states respectively.

We assume that there is translational invariance in the direction parallel to the step

edge, say  $y$  (See Figure 6.2). Thus, the step edge can be represented by a finite-range modification to the Hamiltonian that preserves the  $y$ -momentum[26, 25]. In some cases, it may be modeled as an electrostatic potential  $V(x)$  that is a function of only the perpendicular coordinate  $x$ . Scattering processes at the step leave  $k_y$  – the  $y$ -momentum – unchanged. In what follows, we shall first embody the effect of the step edge in a scattering matrix (the  $S$ -matrix). We label the scattering process as in Figure 6.2 and define the reflection and transmission coefficients to be  $(r, r')$  and  $(t, t')$  respectively. The energy of the scattering process is  $E_{sk}$ . The states are taken to belong to the  $s^{\text{th}}$  band – this is not mentioned explicitly, for brevity, in the following equations.  $R/L$  denotes the half-space (right/left) these states belong to. The  $S$ -matrix is

$$\begin{aligned} \mathbb{S}(k_x, k_y) &= \begin{pmatrix} r(k_x, k_y) & t'(k_x, k_y) \\ t(k_x, k_y) & r'(k_x, k_y) \end{pmatrix} \\ &\equiv \begin{pmatrix} {}_R\langle k_x, k_y | \hat{S} | -k_x, k_y \rangle_R & {}_R\langle k_x, k_y | \hat{S} | k_x, k_y \rangle_L \\ {}_L\langle -k_x, k_y | \hat{S} | -k_x, k_y \rangle_R & {}_L\langle -k_x, k_y | \hat{S} | k_x, k_y \rangle_L \end{pmatrix} \end{aligned} \quad (6.3)$$

Step-edges don't usually break time-reversal symmetry unless, for e.g, they have embedded magnetic impurities. We can use this fact to find relations between the reflection/transmission amplitudes defined above. For simplicity, we fix the phases of the *incoming* states by defining them to be the time-reversed versions of the appropriate outgoing states:

$$\begin{aligned} | -k_x, k_y \rangle_R &\stackrel{sk_x > 0}{\equiv} \Theta | k_x, -k_y \rangle_R \\ | k_x, k_y \rangle_L &\stackrel{sk_x > 0}{\equiv} \Theta | -k_x, -k_y \rangle_L \end{aligned} \quad (6.4)$$

Using this convention and the relation  $\Theta^2 = -1$ , we can prove the following constraints that are similar to the Stokes' relations in Optics:

$$\begin{aligned} r(k_x, k_y) &= -r(k_x, -k_y), \quad r'(k_x, k_y) = -r'(k_x, -k_y) \\ t(k_x, k_y) &= -t'(k_x, -k_y) \end{aligned} \quad (6.5)$$

As an example, we prove the first relation explicitly:

$$\begin{aligned} r(k_x, k_y) &\equiv_R \langle k_x, k_y | \hat{S} | -k_x, k_y \rangle_R \\ &=_R \langle \Theta(-k_x, -k_y) | \hat{S} | -k_x, k_y \rangle_R \\ &=_R \langle \Theta(-k_x, k_y) | \hat{S} | \Theta^2(-k_x, -k_y) \rangle_R \\ &= -_R \langle k_x, -k_y | \hat{S} | -k_x, -k_y \rangle_R = -r(k_x, -k_y) \end{aligned} \quad (6.6)$$

The antiunitary nature of the time reversal operator was used in the third line and  $\Theta^2 = -1$ , corresponding to spin-1/2 states, was used in the last step.

The unitary nature of the scattering process requires  $\mathbb{S}\mathbb{S}^\dagger = \mathbb{I}$  and so:

$$\begin{aligned} |r|^2 + |t|^2 &= |r'|^2 + |t'|^2 = 1 \\ r^*t' + r't^* &= 0 \\ (\Rightarrow |r|^2 + |t'|^2 &= |r'|^2 + |t|^2 = 1 \text{ also}) \end{aligned} \quad (6.7)$$

If we are able to specify  $\mathbb{S}$ , the asymptotic forms of the new energy eigenstates, i.e., the wavefunctions outside the influence of  $V(x)$ , are given by:

$$\begin{aligned} |\mathbf{k}\rangle_R^{\text{new}} &= \frac{|-k_x, k_y\rangle_R + r(\mathbf{k})|k_x, k_y\rangle_R + t(\mathbf{k})|-k_x, k_y\rangle_L}{\sqrt{2}} \\ |\mathbf{k}\rangle_L^{\text{new}} &= \frac{|k_x, k_y\rangle_L + r'(\mathbf{k})|-k_x, k_y\rangle_L + t'(\mathbf{k})|k_x, k_y\rangle_R}{\sqrt{2}} \end{aligned} \quad (6.8)$$

The normalizations follow from (6.7). Since we have these new eigenstates of the Hamiltonian, it is straightforward to calculate the modified LDOS away from the step edge:

$$\begin{aligned} \rho(\omega, x > 0) &= \sum_{s=\pm 1} \int_0^{s\cdot\infty} \frac{dk_x}{\pi} \int_{-\infty}^{\infty} \frac{dk_y}{2\pi} (|\psi_{s,\mathbf{k},R}^{\text{new}}(x, y)|^2 + |\psi_{s,\mathbf{k},L}^{\text{new}}(x, y)|^2) \delta(\omega - E_{s,\mathbf{k}}) \\ &= \rho^{(0)}(\omega) + \iint_0^{\infty} \frac{dk_x dk_y}{\pi^2} \text{Re} \left[ r(s, sk_x, k_y) \psi_{s,-sk_x, k_y}^{(R)}(x, y)^\dagger \psi_{s, sk_x, k_y}^{(R)}(x, y) \right] \delta(\omega - E_{s,\mathbf{k}})_{s=\text{sgn}\omega} \end{aligned} \quad (6.9)$$

Here,  $\rho^{(0)}$  is the LDOS in the absence of the step and simplifications have been made using time reversal symmetry. At this stage we can approximate the band structure near the Dirac point as that arising from the Dirac hamiltonian<sup>a</sup>

$$\mathcal{H} = v\boldsymbol{\sigma} \cdot \mathbf{k} \quad (6.10)$$

Here,  $\boldsymbol{\sigma}$  is the actual spin operator, up to a rotation. The *outgoing eigenstates* of this Hamiltonian are given by ( $sk_x \geq 0$  for the *R/L* cases):

$$\psi_{s,\mathbf{k}}^{(R/L)}(x, y) = \frac{1}{\sqrt{2}} \begin{pmatrix} e^{i\theta_{\mathbf{k}}} \\ s \end{pmatrix} e^{i\mathbf{k}\cdot\mathbf{r}}, \quad E_{s,\mathbf{k}} = svk \quad (6.11)$$

The phases of the *incoming eigenstates* are set by (6.4):

$$\psi_{s,\mathbf{k}}^{(R/L)}(x, y) = \frac{1}{\sqrt{2}} \begin{pmatrix} s \\ e^{-i\theta_{\mathbf{k}}} \end{pmatrix} e^{i\mathbf{k}\cdot\mathbf{r}} \quad (6.12)$$

We have used  $\Theta = i\sigma_y K$ ,  $K$  being the complex conjugation operator, in the above equation. Using this setup, (6.9) can be simplified to yield (for  $x > 0$ ):

$$\frac{\delta\rho(\omega, x)}{\rho^{(0)}(\omega)} = -\frac{2\text{sgn}\omega}{\pi} \int_0^{\pi/2} d\theta \sin\theta \text{Im} [r_\omega(\theta) e^{2ik_\omega x \cos\theta}] \quad (6.13)$$

---

<sup>a</sup>The linear nature of the dispersion is not important – the chiral nature of the Hamiltonian is.

Here,  $\rho^{(0)}(\omega) = |\omega|/(2\pi v^2)$ ,  $k_\omega = \omega/v$  is the momentum at energy  $\omega$  and the reflection amplitude  $r_\omega(\theta_{\mathbf{k}}) \equiv r(\text{sgn}\omega, \mathbf{k}_\omega)$  needs to obey the property (6.6)

$$r_\omega(-\theta) = -r_\omega(\theta) \quad (6.14)$$

## 6.4 Results

### 6.4.1 The perfect reflector

We now note that the ‘perfect’ reflector needs to have the form (no transmittance except at normal incidence)

$$r_\omega^{\text{perf}}(\theta) = e^{i\delta_{\omega,|\theta|}} \text{sgn}(\theta) \quad (6.15)$$

which tells us that the LDOS becomes ( $x > 0$ ):

$$\begin{aligned} \frac{\delta\rho(\omega, x)}{\rho^{(0)}(\omega)} &= -\frac{2\text{sgn}\omega}{\pi} \int_0^{\pi/2} d\theta \sin\theta \sin(2k_\omega x + \delta_{\omega,|\theta|}) \\ &= -\frac{(\cos(2k_\omega x + \delta_\omega) - \cos\delta_\omega)}{\text{sgn}\omega \pi k_\omega x} \quad (\text{when } \delta \text{ is } \theta\text{-indep.}) \end{aligned} \quad (6.16)$$

In Figure 6.1, these LDOS modulations are compared with those near a perfectly reflecting step edge in a 2DEG. We see that even for ‘perfect’ reflection the step edge is only able to create LDOS oscillations that decay as  $1/x$ , as opposed to the slower  $1/\sqrt{x}$  decay in the 2DEG case[25].

The exact shape of the potential that would provide perfect reflection is hard to calculate based only on the specific form of reflection coefficient. One can easily see that the abrupt change of the  $r_\omega^{\text{perf}}(\theta)$  as a function of angle is not possible in any

realistic scattering problem. Hence at a moment this can be viewed as an idealized calculation. We would like to stress here that what we have shown above is that the concept of perfect reflection (except at normal incidence) is not antithetical to the existence of suppressed backscattering. Also, we did not have to consider an actual potential modeling of a step edge that would realize such a case. We guess that if we consider a potential that is noisy in the  $x$ -direction, it may not afford the incident wave much scope of penetration and reflect most of it. In practice, even if a very good reflector is realized, near normal incidence the reflection amplitude will become linear in  $k_y$  over a small region of size  $\Delta k_y$ . We should then observe a  $1/x$  decay till a distance of  $\sim 1/\Delta k_y$  and beyond that a  $x^{-3/2}$  decay (see 6.4.3).

### 6.4.2 Discussion of recent experiments

In a recent paper (Figures 3a-e in [5]) oscillations of the form given by (6.16) have been observed at energies far from the Dirac point where the wavefunction wavelength is comparable to or shorter than the width of the step edge. However, in that region the band surface exhibits hexagonal warping[39] and the dominant scattering signature comes from the scatterings between the states at the adjacent  $M$ -points (the step edge is oriented perpendicular to the  $\Gamma M$  direction). These do *not* involve the special processes near perfect backscattering in the STI that we have considered above. The  $1/x$  behavior arises simply because the bands are not perpendicular to the  $\Gamma K$  direction near the hexagon vertices<sup>b</sup>[17]. In Figures 3f-h of the above-mentioned paper

---

<sup>b</sup>For scattering between the hexagonal vertices,  $r$  and the spin overlaps are finite and  $\Delta k_x$  is a linear function of  $k_y$ ; a scaling analysis of (6.9) yields the  $1/x$  law

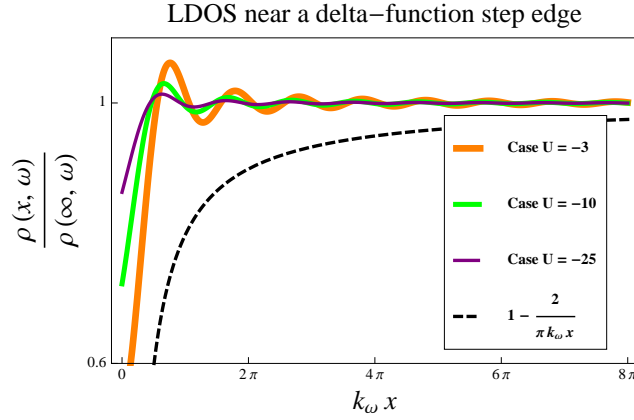


Figure 6.3: (Color Online) LDOS *above* the Dirac point near a *strong attractive*  $\delta$ -function step edge potential (6.17) for various values of  $U$  (solid curves with different colors and thicknesses). Notice how the oscillations get damped for large  $U$ . The dashed curve is the envelope for the ‘perfectly reflecting’ step edge on the STI (Figure 6.1), shown here for comparison.

[5] the authors also observed that at lower energies, closer to the Dirac point, the character of these LDOS modulations change qualitatively. They are much less pronounced exhibit an almost oscillation-less decay. We propose to explain this behavior by modeling the step edge as a delta-function potential

$$V(x) = U\delta(x) \quad (6.17)$$

when considering the scattering of long wavelength states near the Dirac point. Using this with the original Hamiltonian (6.10), we obtain the reflection amplitude[65]:

$$r_\omega^\delta(\theta) = \frac{4U \sin(\theta)}{(U^2 - 4) \cos(\theta) - 4i \operatorname{sgn} \omega U} \quad (6.18)$$

Note that the reflection amplitude is antisymmetric about  $\theta = 0$ , and is also linear around that region. The LDOS obtained for this delta-function potential is shown in Figure 6.3 and displays minimal oscillations when  $U$  is large and *negative* and  $E > 0$ . There is a dip in the LDOS near the wall followed by an almost oscillation-less decay

(for large potential strength) away from the wall – similar to what was observed in [5]. The dip can be explained by the existence of *bound states* near the wall: for  $U < -2$  these occur at negative energies but the transferred spectral weight leads to the dip at positive energies.

### 6.4.3 Generic step edges

The long-distance decay of the above oscillations is found to be given by  $x^{-3/2}$ , which arises out of the proportionality between  $r(\theta)$  and  $\theta$  near  $\theta = 0$ . Because of the antisymmetry of  $r(\theta)$  about  $\theta = 0$  (6.14), for *generic* step edges we will also have  $r(\theta) \propto \theta$  near  $\theta = 0$  and this will result in the almost coherent scatterings near  $\theta = 0$  interfering far away from the edge to yield a spatial decay law of  $x^{-3/2}$ [181]. This power law may be obtained by considering the scaling behavior of the integrand in (6.13), near  $\theta = 0$ .

It is possible that for high energies, near a step edge perpendicular to the  $\Gamma M$  direction in  $\text{Bi}_2\text{Te}_3$  (or with *any* orientation in  $\text{Bi}_2\text{Se}_3$  which has no hexagonal warping), one will observe a  $1/x$  decay of oscillations at the wave-vector equal to the diameter of the band surface along the  $K - \Gamma - K$  direction *if* the step edge is perfectly non-reflecting – a quality that possibly arises due to roughness along its normal direction. Generically, due to the scaling relation  $r(\theta) \propto \theta$  near  $\theta = 0$ , one should be able to observe a faster  $x^{-3/2}$  decay of the oscillations.



## 6.5 Conclusion

In summary, we have used the *chiral nature* of the STI surface states and *time reversal invariance* to impose restrictions on the reflection and transmission amplitudes of the scattering process at a step edge on the surface of a Strong Topological Insulator. This allowed us to define the ‘perfect reflecting step edge’ for these chiral surface states and we found that the amplitude of LDOS ripples caused by such an edge decay no slower than  $1/x$  — faster than in the analogous case for a 2DEG, where the decay occurs as  $1/\sqrt{x}$ . For a *generic* smooth step edge, the decay law is  $x^{-3/2}$ . We give possible reasons for the LDOS features seen in experiments[5] — damped oscillations and a monotonic decay of the LDOS modulation far from the step edge for small energies and a  $1/x$  decay at higher energies – by arguing that the scattering of long wavelength states near the Dirac point occurs due to an effective  $\delta$ -function local potential (6.17) while the shape of the band surface yields the  $1/x$  decay at higher energies. To the best of our knowledge, this is the first application of this general  $S$ -matrix formalism (with the imposition of TRS) to the scattering of STI surface states.

# Chapter 7

## SU(2)-invariant spin liquids on the triangular lattice with spinful Majorana excitations

### 7.1 Synopsis

We describe a new class of spin liquids with global SU(2) spin rotation symmetry in spin 1/2 systems on the triangular lattice, which have real Majorana fermion excitations carrying spin  $S = 1$ . The simplest translationally-invariant mean-field state on the triangular lattice breaks time-reversal symmetry and is stable to fluctuations. It generically possesses gapless excitations along 3 Fermi lines in the Brillouin zone. These intersect at a single point where the excitations scale with a dynamic exponent

$z = 3$ . An external magnetic field has no orbital coupling to the  $SU(2)$  spin rotation-invariant fermion bilinears that can give rise to a transverse thermal conductivity, thus leading to the absence of a thermal Hall effect. The Zeeman coupling is found to gap out two-thirds of the  $z = 3$  excitations near the intersection point and this leads to a suppression of the low temperature specific heat, the spin susceptibility and the Wilson ratio. We also compute physical properties in the presence of weak disorder and discuss possible connections to recent experiments on organic insulators.

## 7.2 Introduction

The recent experimental evidence for spin liquids in the triangular lattice organic compounds  $\kappa$ -(ET)<sub>2</sub>Cu<sub>2</sub>(CN)<sub>3</sub> [169, 167, 109] and EtMe<sub>3</sub>Sb[Pd(dmit)<sub>2</sub>]<sub>2</sub> [58, 168, 57] has sparked much interest in characterizing the experimental signatures of the many candidate spin liquid states.

For the compound  $\kappa$ -(ET)<sub>2</sub>Cu<sub>2</sub>(CN)<sub>3</sub>, a theory [110] building upon the proximity of a magnetic ordering quantum critical point is compatible with the recent observation of magnetic order induced by a small external field [109].

On the other hand, EtMe<sub>3</sub>Sb[Pd(dmit)<sub>2</sub>]<sub>2</sub> is characterized [168] by a thermal conductivity,  $\kappa$ , for which  $\kappa/T$  reaches a non-zero limit as the temperature  $T \rightarrow 0$ , and this is strong evidence for the presence of gapless excitations across a Fermi surface. A spin liquid state with a spinon Fermi surface has been proposed [90, 76, 47], and so is a natural candidate for this material. However, this spinon Fermi surface state is also

expected to display a thermal Hall effect [66] and this effect has not been detected so far [168].

Here, we will examine another possibility for a spin liquid state with a Fermi surface of spin 1 excitations. We will assume that the Fermi surface excitations are real Majorana fermions and this, as we will see, allows us to retain the longitudinal thermal conductivity while suppressing the thermal Hall effect.

Our approach relies upon following representation of  $S = 1/2$  spins in terms of  $S = 1$  Majorana fermions [85, 146, 24, 133, 153]

$$S^\mu = \frac{i}{4} \epsilon^{\mu\alpha\beta} \gamma^\alpha \gamma^\beta. \quad (7.1)$$

Here we have suppressed site indices, and the Majorana fermion operators all anti-commute with each other, and have a unit square  $(\gamma^\alpha)^2 = 1$  (no sum over  $\alpha$ ). As explained by Shastry and Sen [133], such Majorana fermions provide a redundant but faithful realization of the Hilbert space of  $S = 1/2$  fermions. The redundancy is linked to a  $Z_2$  gauge invariance  $\gamma^\alpha \rightarrow -\gamma^\alpha$ , which then also plays a crucial role in the description of any spin liquid states; some related issues are discussed in Appendix A.

The representation in equation (7.1) has been used extensively in recent work [158, 34, 8, 75, 170, 20, 147, 172, 82, 165, 101, 9, 28, 162, 143, 144, 22, 152, 23, 74, 81, 171, 153], following the exactly solvable spin model proposed by Kitaev [68]. A rich variety of solvable models have been found on different types of lattices, some with global SU(2) symmetry, others with Fermi surfaces. However, none of them are on the triangular lattice, and none of them have both SU(2) symmetry and a Fermi surface: these are clearly important requirements for making contact with the experiments on

$\text{EtMe}_3\text{Sb}[\text{Pd}(\text{dmit})_2]_2$ .

Here, we shall not attempt to find an exact solution to a particular model Hamiltonian. Instead, we will build upon the extensive experience that has been gained by parton constructions of mean-field spin liquid states, and the establishment of their stability by an effective gauge theory of fluctuations. Previous constructions of  $Z_2$  spin liquids relied upon writing the spins either in terms of Schwinger bosons [113] or fermions [156], and here we will apply an analogous analysis to the Majorana parton construction in equation (7.1). We will be aided in this analysis by the Projective Symmetry Group (PSG)[157] which we shall apply to the effective Hamiltonian for the Majorana excitations.

### 7.2.1 Low energy theory

We begin by postulating the existence of a  $SU(2)$  invariant spin liquid state on the triangular lattice, whose quasiparticles are described by a triplet Majorana field  $\gamma^\alpha(\mathbf{r})$ ,  $\alpha = x, y$  or  $z$ . Although we are using the same notation as in equation (7.1), the Majorana field operators used in the low energy field theory create the physical quasiparticles and so can be strongly renormalized from the underlying Majorana fermion in equation (7.1). Noting that the Majorana bilinear Hamiltonian has to change sign both under time reversal (TR) and under a lattice rotation by  $\pi$ , we assume that the  $\gamma^\alpha$  transform trivially, i.e.,  $\gamma^\alpha \rightarrow \gamma^\alpha$  (without a possible sign change) under all the PSG operations associated with a modified triangular lattice space group. In this modified triangular lattice space group the elementary operation of rotation by

$\pi/3$  is replaced by the same operation compounded with TR. Furthermore, the Majorana operators transform naturally in the  $S = 1$  representation of spin rotations and are real operators which are invariant under time reversal. These simple and general transformation rules are already sufficient to strongly constrain the effective low energy theory of the  $\gamma^\alpha(\mathbf{r})$ .

Let us begin by writing an effective Hamiltonian for the  $\gamma^\alpha$  bilinears as an expansion in spatial gradients.

Demanding invariance under by  $2\pi/3$  rotations (a double application of TR +  $\pi/3$  rotation) and hermicity, we are led to the Hamiltonian

$$\mathcal{H}_0 = iw_0 \int d^2\mathbf{r} \gamma^\alpha (\mathcal{D}_1 + \mathcal{D}_2 + \mathcal{D}_3) \gamma^\alpha \quad (7.2)$$

where the  $\mathcal{D}_i \equiv \boldsymbol{\delta}_i \cdot \boldsymbol{\nabla}$  are directional derivatives along the 3 principal directions  $\boldsymbol{\delta}_1$ ,  $\boldsymbol{\delta}_2$  and  $\boldsymbol{\delta}_3$  shown in Figure 7.2 and  $w_0$  is a real number. We remark here that there is no term without spatial gradients because the Majorana fermions square to unity and because of  $SU(2)$  spin rotation symmetry. However, we clearly have  $\boldsymbol{\delta}_1 + \boldsymbol{\delta}_2 + \boldsymbol{\delta}_3 = 0$  and so  $H_0$  vanishes identically. To obtain a non-zero contribution, we have to expand all the way to 3 derivatives<sup>a</sup>, when we obtain two independent terms which can be written as

$$\mathcal{H} = i \int d^2\mathbf{r} \gamma^\alpha [w_1 \mathcal{D}_1 \mathcal{D}_2 \mathcal{D}_3 - w_2 (\mathcal{D}_1^2 \mathcal{D}_2 + \mathcal{D}_2^2 \mathcal{D}_3 + \mathcal{D}_3^2 \mathcal{D}_1)] \gamma^\alpha \quad (7.3)$$

where both  $w_1$  and  $w_2$  are real parameters. The low energy Hamiltonian in equation (7.3) underlies all the results derived in this chapter. From this it follows that

---

<sup>a</sup>The Majorana bilinear Hamiltonian cannot have terms with an even number of derivatives as they are identically zero by integration by parts.

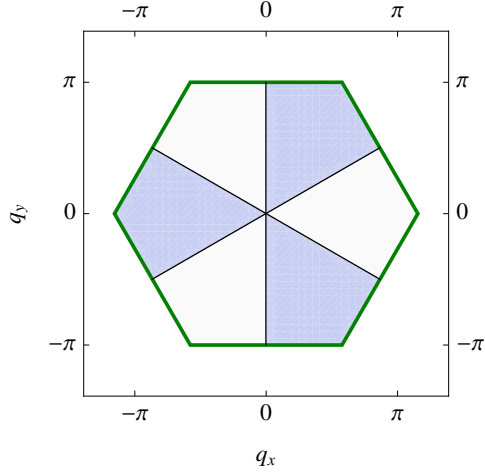


Figure 7.1: The Fermi surface (shown as black lines) corresponding to the lattice dispersion in equation (7.9) in Section 7.3 — equation (7.3) is the generic continuum version of the same theory. The BZ is bounded by the green border while the ‘occupied’ states are shaded.

the long wavelength excitations of this theory have the dispersion

$$E_{\mathbf{q}} \stackrel{q \rightarrow 0}{\simeq} t q^3 \cos(3\theta_{\mathbf{q}} + \phi) \quad (7.4)$$

$$\text{where } \begin{cases} t \cos \phi = \frac{3}{8}(2w_1 + w_2) \\ t \sin \phi = \frac{3\sqrt{3}}{8}w_2 \end{cases}$$

Next, let us describe the structure of the low energy excitations of  $\mathcal{H}$ . As we shall demonstrate shortly in Section 7.3 and as is illustrated in Figure 7.1, there are two classes of excitations. First, there are the excitations with momentum  $\mathbf{q} \approx 0$ , which have energy  $\sim |\mathbf{q}|^3$ , and so look like those of a quantum-critical theory with dynamic exponent  $z = 3$ . Second, there are the linearly dispersing gapless excitations along Fermi lines which meet at  $\mathbf{q} = 0$ .

It is now straightforward to establish the perturbative stability of  $\mathcal{H}$ . The collective modes arising from decoupling spin interaction terms like the four Majorana exchange

interactions in equation (7.5) constitute the gauge fluctuations of a  $Z_2$  gauge theory [113, 129]. These have a finite range of stability without a transition to confinement, when our theory as described above is valid. Next, we consider the influence of terms quartic in the Majorana fermions. These quartic couplings will lead to innocuous Fermi liquid renormalizations of quasiparticles along the Fermi lines, just as in any Fermi liquid. The influence of quartic couplings on the  $z = 3$  excitations near  $\mathbf{q} = 0$  is more subtle, but can be analyzed by a standard scaling argument. The scaling dimension of  $\gamma^\alpha$  is  $d/2$ , where  $d = 2$  is the spatial dimension<sup>b</sup>. Dimensional analysis now shows that a quartic coupling with  $p$  spatial derivatives has scaling dimension  $z - d - p$ . For  $z = 3$  and  $d = 2$ , this is irrelevant only if  $p > 1$ . With the requirements of  $SU(2)$  invariance, it is easy to show that any quartic term must have *at least*  $p = 2$  derivatives: the simplest non-vanishing term with  $SU(2)$  spin rotation invariance has the generic structure  $\sim (\gamma^\alpha \partial \gamma^\alpha)(\gamma^\beta \partial \gamma^\beta)$ . We emphasize that  $SU(2)$  spin rotation symmetry is crucial to the stability of the theory: in its absence, marginal quartic terms arise that could destabilize the postulated liquid.

The outline of the rest of this chapter is as follows. In Section 7.3 we shall derive the Majorana mean field theory corresponding to the Heisenberg antiferromagnet and reproduce the general low energy spectrum postulated in equation (7.3). We shall also demonstrate how any Majorana bilinear Hamiltonian on the triangular lattice gives rise to equation (7.3) in the low energy long wavelength limit. We will then describe the experimentally observable properties of this state in Section 7.4. The

---

<sup>b</sup>This is most easily seen in a Lagrangian formulation where the kinetic term is  $\gamma^\alpha \partial_\tau \gamma^\alpha$ ,  $\tau$  being the imaginary time.



influence of weak disorder will be presented in Section 7.5.

## 7.3 The mean field Majorana Hamiltonian on a triangular lattice

### 7.3.1 Majorana mean field theory from a spin Hamiltonian: an example

In this section we derive a Majorana mean field theory starting from the AF Heisenberg model on a triangular lattice, mainly to demonstrate the mechanics of such a derivation<sup>c</sup>. We choose a real space coordinate system such that one set of bonds point along the  $x$ -axis, as shown in Figure 7.2. The Hamiltonian has the form:

$$\begin{aligned} \mathcal{H}_{AF} &= J \sum_{\text{n.n}} \mathbf{S}(\mathbf{x}) \cdot \mathbf{S}(\mathbf{x}') \\ &= \frac{J}{8} \sum_{\mathbf{x}, \delta, \alpha \neq \beta} \gamma^\alpha(\mathbf{x}) \gamma^\alpha(\mathbf{x} + \delta) \gamma^\beta(\mathbf{x}) \gamma^\beta(\mathbf{x} + \delta) \end{aligned} \quad (7.5)$$

where  $\delta$  are the three nearest neighbor bonds labeled in Figure 7.2 which are related by rotations through  $2\pi/3$ . We perform a mean field analysis for the above Hamiltonian by assuming the mean field ansatz<sup>d</sup>

$$\langle \gamma^\alpha(\mathbf{x}) \gamma^\beta(\mathbf{x} + \delta) \rangle = ig \delta_{\alpha\beta} \quad (7.6)$$

---

<sup>c</sup>It is known[56] that the actual ground state of this model breaks spin rotation symmetry.

<sup>d</sup>This ansatz implies that the mean field theory breaks time reversal at the level of Majorana dynamics. If  $|\Psi\rangle$  is invariant under time reversal and *assuming* the fact that the spin 1  $\gamma$ 's are left invariant or change by a factor of  $-1$  under the action of time reversal,  $\langle \Psi | \gamma_{\mathbf{x}}^\alpha \gamma_{\mathbf{y}}^\alpha | \Psi \rangle = \langle \Psi | \gamma_{\mathbf{y}}^\alpha \gamma_{\mathbf{x}}^\alpha | \Psi \rangle = 0$  unless  $\mathbf{x} = \mathbf{y}$ .

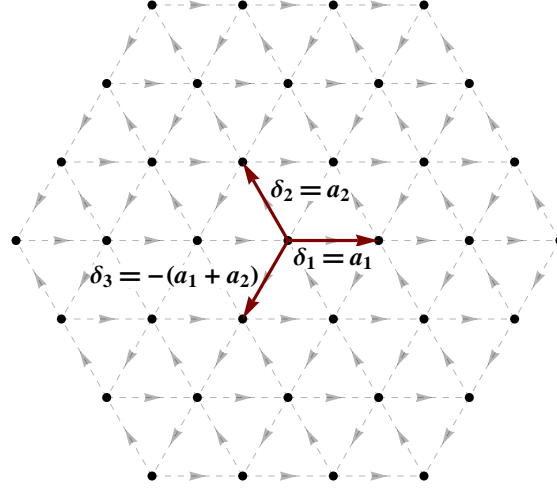


Figure 7.2: The triangular lattice showing the lattice vectors and the  $\boldsymbol{\delta}$  vectors used in the text. The arrows on the bonds define the mean field ansatz equation (7.6) that also becomes the scheme for assigning the same phase to hopping parameters. The amplitudes of hopping processes in the directions opposite to the specified bond directions pick up an additional factor of -1.

which is also graphically represented by directed bonds in Figure 7.2. Using this ansatz, equation (7.5) becomes:

$$\begin{aligned} \mathcal{H}_{MF} &= \frac{J}{8} \sum_{\mathbf{x}, \boldsymbol{\delta}, \alpha} [2 \times 2ig \gamma^\alpha(\mathbf{x}) \gamma^\alpha(\mathbf{x} + \boldsymbol{\delta}) + 2g^2] \\ &= \frac{iJg}{4} \sum_{\mathbf{x}, \boldsymbol{\delta}, \alpha} (\gamma^\alpha(\mathbf{x}) \gamma^\alpha(\mathbf{x} + \boldsymbol{\delta}) - \gamma^\alpha(\mathbf{x} + \boldsymbol{\delta}) \gamma^\alpha(\mathbf{x})) + \frac{9}{4} \mathcal{N} J g^2 \end{aligned} \quad (7.7)$$

where  $\mathcal{N}$  is the number of sites, assumed to be an even number. This Hamiltonian can be diagonalized using the momentum states defined over the Brillouin zone (BZ) of the triangular lattice:

$$b_{\mathbf{q}}^\alpha = \frac{1}{\sqrt{2\mathcal{N}}} \sum_{\mathbf{x}} \gamma^\alpha(\mathbf{x}) e^{-i\mathbf{q}\cdot\mathbf{x}} \Leftrightarrow \gamma^\alpha(\mathbf{x}) = \sqrt{\frac{2}{\mathcal{N}}} \sum_{\mathbf{q}} b_{\mathbf{q}}^\alpha e^{i\mathbf{q}\cdot\mathbf{x}} \quad (7.8)$$

These  $b$  operators are complex Fermions with  $b_{-\mathbf{q}} = b_{\mathbf{q}}^\dagger$  and  $\{b_{\mathbf{p}}^\alpha, b_{\mathbf{q}}^\beta\} = \delta_{\alpha\beta} \delta_{\mathbf{p}, -\mathbf{q}}$ , showing that independent  $b$  operators cover only half the BZ. Using these in equation (7.7),

we can diagonalize the Hamiltonian:

$$\begin{aligned}
 \mathcal{H}_{MF} &= \sum_{\alpha, \mathbf{q} \in BZ} \left( -Jg \sum_{\mathbf{q}} \sin \mathbf{q} \cdot \boldsymbol{\delta} \right) b_{-\mathbf{q}}^{\alpha} b_{\mathbf{q}}^{\alpha} + \frac{9}{4} \mathcal{N} J g^2 \\
 &= \sum_{\alpha, \mathbf{q} \in BZ} \frac{E_{\mathbf{q}}}{2} b_{-\mathbf{q}}^{\alpha} b_{\mathbf{q}}^{\alpha} + \frac{9}{4} \mathcal{N} J g^2 \quad \left( E_{\mathbf{q}} = 8Jg \sin \frac{q_x}{2} \sin \frac{(R_{2\pi/3}\mathbf{q})_x}{2} \sin \frac{(R_{4\pi/3}\mathbf{q})_x}{2} \right) \\
 &= \sum_{\alpha, \mathbf{q} \in BZ' | E > 0} \left( E_{\mathbf{q}} b_{-\mathbf{q}}^{\alpha} b_{\mathbf{q}}^{\alpha} - \frac{E_{\mathbf{q}}}{2} \right) + \frac{9}{4} \mathcal{N} J g^2 \quad (\text{using } E_{-\mathbf{q}} = -E_{\mathbf{q}}) \\
 &= \sum_{\alpha, \mathbf{q} \in BZ'} E_{\mathbf{q}} (b_{\mathbf{q}}^{\alpha})^{\dagger} b_{\mathbf{q}}^{\alpha} + \frac{9\mathcal{N}J}{4} g \left( g - \frac{2}{\pi} \right) \tag{7.9}
 \end{aligned}$$

Here we have introduced the notation  $BZ'$  to denote that half of the BZ where the quasiparticle energies of the spin rotation-invariant Hamiltonian are positive. The fermion creation operators in  $BZ'$  are related to those in the remaining half of the BZ by the particle-hole relation  $b_{-\mathbf{q}} = b_{\mathbf{q}}^{\dagger}$ . The structure of the Fermi sea obtained above is shown in Figure 7.1, where  $BZ'$  consists of the un-shaded regions of the BZ. It follows that near  $\mathbf{q} = \mathbf{0}$ , the quasiparticle energy has the same form as derived earlier in equation (7.4) using a gradient expansion

$$E_{\mathbf{q}} \stackrel{q \rightarrow 0}{\simeq} \left( \frac{Jg}{4} \right) q^3 \cos 3\theta_{\mathbf{q}} \tag{7.10}$$

The ground state energy  $\frac{9\mathcal{N}J}{4}g \left( g - \frac{2}{\pi} \right)$  is minimized when  $g = \frac{1}{\pi}$ <sup>e</sup>:

$$E_0 = -\frac{9}{4\pi^2} J\mathcal{N} = -0.22J\mathcal{N} \tag{7.11}$$

As expected,  $E_0$  is higher than the numerically calculated ground state energy of about  $-0.54J$  per site[15] for the best candidate spin-ordered ground state[56]. Additional interactions should be added to the Heisenberg Hamiltonian in equation (7.5) to stabilize the spin liquid state described by the non-interacting Majorana ground state.

---

<sup>e</sup>The same value is obtained from the definition equation (7.6), as a check.

### 7.3.2 The general low energy effective theory on the lattice

This subsection will give an alternative presentation of the ideas of Section 7.2.1, working directly with the lattice Hamiltonian, rather than the continuum theory.

A general spin  $SU(2)$  rotation-invariant and translation-invariant low energy effective Hamiltonian of Majorana bilinears has the form:

$$\mathcal{H}_{MF} = i \sum_{\mathbf{x}, \mathbf{d}, \alpha} t(\mathbf{d}) \gamma^\alpha(\mathbf{x}) \gamma^\alpha(\mathbf{x} + \mathbf{d}) \quad (7.12)$$

where Hermiticity requires that  $t(\mathbf{d})$  is real and *antisymmetric* in the hopping vector  $\mathbf{d}$ :

$$t(-\mathbf{d}) = -t(\mathbf{d}), \quad t(\mathbf{d}) \in \mathbb{R} \quad (7.13)$$

If this Hamiltonian describes a spin liquid, the observable quantities which are the spin correlation functions should not break any lattice symmetry, in addition to the spin rotation and lattice translation symmetries discussed above. However, since a lattice rotation by  $\pi$  and time reversal separately flip the sign of the mean field Hamiltonian equation (7.12), the theory can be invariant only under a combined application of the two. This uses the fact that the Majorana operators are hermitian and also that due to spin rotation symmetry, their bilinears cannot acquire any additional factor under symmetry operations. We require the maximum possible adherence to the lattice point group symmetry consistent with these observations — a lattice rotation by  $\pi/3$  combined with time reversal must leave the Hamiltonian invariant. This, along with invariance under lattice translations and reflection about a bond, are the elementary symmetry operations that define the class of effective Hamiltonians which

may possess the Majorana spin liquid ground state described in this work. Even with this reduced set of symmetry operations, all equal time correlation functions with an even number of spin operators will remain invariant under the full set of lattice symmetry operations.

These arguments motivate rewriting the Hamiltonian in a manner that makes the antisymmetry under a rotation by  $\pi/3$  apparent:

$$\mathcal{H}_{MF} = i \sum_{\mathbf{x}, \{\mathbf{d}\}, \alpha} t(\mathbf{d}) \sum_{n=0}^5 (-1)^n \gamma^\alpha(\mathbf{x}) \gamma^\alpha(\mathbf{x} + R_{n\pi/3}(\mathbf{d})) \quad (7.14)$$

where  $\{\mathbf{d}\}$  denotes the set of hopping vectors, modulo those that are related through rotations by multiples of  $\pi/3$ . In terms of the momentum state operators equation (7.8), we have:

$$\mathcal{H}_{MF} = i \sum_{\mathbf{k}, \alpha} \frac{\left( \sum_{\{\mathbf{d}\}} E_{\mathbf{d}}(\mathbf{q}) \right)}{2} b_{-\mathbf{q}}^\alpha b_{\mathbf{q}}^\alpha \quad (7.15)$$

where

$$E_{\mathbf{d}}(\mathbf{q}) = 16 t(\mathbf{d}) \sin \frac{\mathbf{q} \cdot \mathbf{d}}{2} \sin \frac{\mathbf{q} \cdot (R_{2\pi/3}\mathbf{d})}{2} \sin \frac{\mathbf{q} \cdot (R_{4\pi/3}\mathbf{d})}{2} \quad (7.16)$$

is the contribution to the Majorana dispersion from the hopping processes characterized by the hopping vector  $\mathbf{d}$ . This expression tells us that the dispersion of the long wavelength low energy modes near  $\mathbf{q} = 0$  have the form

$$E_{\mathbf{q}} \stackrel{\mathbf{k} \rightarrow 0}{\simeq} t q^3 \cos(3\theta_{\mathbf{q}} + \phi) \quad (7.17)$$

where  $t$  and  $\phi$  are real constants. These parameters are the analog of those in equation (7.4) obtained from corresponding continuum analysis. Figure 7.3 shows the Fermi sea and Fermi surface corresponding to a model with a next nearest neighbor

hopping amplitude that is one-fifth of the nearest neighbor hopping amplitude and demonstrates the existence of three Fermi curves intersecting at  $\mathbf{q} = \mathbf{0}$ , in this system.

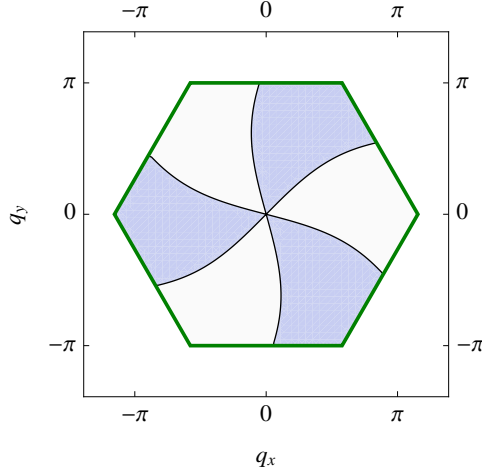


Figure 7.3: The Fermi surface (black curves) corresponding to equation (7.14) with a next-nearest-neighbor hopping amplitude that is 20% the nearest neighbor hopping amplitude. The BZ is bounded by the green border while the ‘occupied’ states are shaded.

From this calculation it is clear that the low energy mean field theory is composed of two kinds of excitations which are smoothly connected to each other, as was noted in Section 7.2.1. Excitations near  $\mathbf{q} = \mathbf{0}$  have a dispersion that varies as  $q^3$  and a dynamical exponent  $z = 3$  while those along the Fermi curves behave like the excitations of a 2D Fermi gas.

### 7.3.3 The low energy effective theory in the presence of a perpendicular magnetic field

Let us first consider orbital coupling terms which do not violate the  $SU(2)$  spin rotation symmetry. In this case the arguments that lead to the formulation of the

Hamiltonian will be no different that in the field free case considered in the previous sections and so the Hamiltonian will be invariant under rotations by  $2\pi/3$ . The transverse thermal conductivity, which involves averaging the product  $v_x v_y$  over momentum space, will be zero since the sum of  $v_x v_y$  over points related by  $2\pi/3$  rotations is zero. Equivalently, it may be noted that the PSG implies that there is no orbital coupling between the applied magnetic field and a fermion bilinear: it is not possible to find a fermion bilinear which is invariant under translations and by spatial rotations under  $\pi/3$ . It follows that orbital coupling of the magnetic field will not induce a thermal Hall effect [66] in our theory. This is in contrast to what happens in the case of the U(1) spin liquid with a spinon Fermi surface [90], where the  $B$  field does couple to fermion bilinear [66]: the coupling is of the form  $\mathbf{B} \cdot (\nabla \times \mathbf{J})$ , where  $\mathbf{J}$  is the U(1) spinon current.

The other way in which a perpendicular magnetic field  $B\hat{\mathbf{z}}$  enters the Hamiltonian is via terms that break the spin  $SU(2)$  symmetry down to a  $U(1)$  symmetry of rotations about the direction of the magnetic field. Such a coupling will not affect the  $\gamma^z$  fermions but will couple the  $\gamma^{x,y}$  Majoranas into  $S_z = \pm 1$  excitations. The most relevant term in that case is the Zeeman term  $-iB\gamma^x\gamma^y/2$  which does not break the three-fold rotation symmetry and thus does not lead to a thermal Hall effect.

### 7.3.4 The spectrum in the presence of the Zeeman coupling

The Zeeman term  $-\mu_0 B S_z$  does not affect the spectrum of the  $\gamma^z$  fermions because they carry spin  $S_z = 0$ . The Hamiltonian of the  $\gamma^{x,y}$  fermions, however, is modified:

$$\begin{aligned} \mathcal{H} &= \frac{1}{2} \sum_{\mathbf{k}} \begin{pmatrix} b_{-\mathbf{k}}^x & b_{-\mathbf{k}}^y \end{pmatrix} \cdot \begin{pmatrix} E_{\mathbf{k}} & i\mu_0 B \\ -i\mu_0 B & E_{\mathbf{k}} \end{pmatrix} \cdot \begin{pmatrix} b_{\mathbf{k}}^x \\ b_{\mathbf{k}}^y \end{pmatrix} \\ &= \frac{1}{2} \sum_{\mathbf{k}, s=\pm 1} (E_{\mathbf{k}} - s\mu_0 B) c_s^\dagger(\mathbf{k}) c_s(\mathbf{k}) \\ &\equiv \sum_{\mathbf{k}} (E_{\mathbf{k}} + \mu_0 B) c_-^\dagger(\mathbf{k}) c_-(\mathbf{k}) + \text{c-number} \end{aligned} \quad (7.18)$$

where the new fermionic excitations with spins  $S_z = s/2$ ,  $s = \pm 1$  are

$$c_s(\mathbf{k}) = \frac{b_{\mathbf{k}}^x + i s b_{\mathbf{k}}^y}{\sqrt{2}}; \quad c_{s,\mathbf{k}} = c_{-s,-\mathbf{k}}^\dagger \quad (7.19)$$

The Fermi surface now consists of arcs in three of the six wedges partitioning the BZ, as shown in Figure 7.4.

## 7.4 Properties of the clean Majorana spin liquid

The bilinear Majorana Hamiltonian which will be used in the following sections is

$$\mathcal{H}_{MF} = i \sum_{\mathbf{q}, \alpha} \frac{E_{\mathbf{q}}}{2} b_{-\mathbf{q}}^\alpha b_{\mathbf{q}}^\alpha \quad (7.20)$$



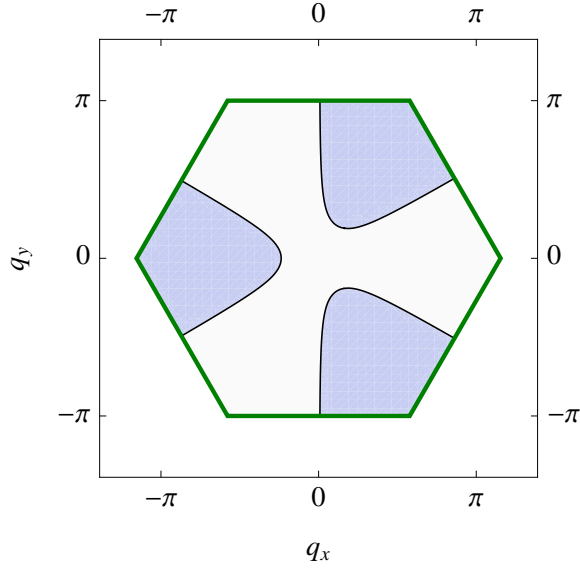


Figure 7.4: The Fermi sea of  $c_-$  fermions (shaded regions) in the presence of a Zeeman term (assuming  $\mu_0 B > 0$ ). The hexagon is the BZ for the triangular lattice. The  $\gamma^z$  fermions are not affected by a magnetic field in the  $z$  direction and will retain their original excitation structure as shown in Figure 7.1.

where the  $q \rightarrow 0$  form of  $E_q$  is given by equation (7.17). The propagator[146] for the Majorana excitations is given by<sup>f</sup>

$$\langle b_{\mathbf{p}}^{\alpha} b_{\mathbf{q}}^{\beta} \rangle = \frac{\delta_{\alpha\beta} \delta_{\mathbf{p}, -\mathbf{q}}}{z - E_{\mathbf{q}}} = \delta_{\alpha\beta} \delta_{\mathbf{p}, -\mathbf{q}} \mathcal{G}_{\mathbf{q}}(z) \quad (7.21)$$

### 7.4.1 The low energy density of states (DOS)

Because of the  $k^3$  dispersion, the contribution to the density of states from the states near  $\mathbf{k} = \mathbf{0}$  diverges as the energy  $E \rightarrow 0$ . The divergence may be calculated from

<sup>f</sup>The general analytic form has been provided here and from it the Matsubara, retarded and advanced Green's functions can be obtained by the substitutions  $z \rightarrow i\omega_n, \omega + i0+$  and  $\omega - i0+$  respectively.

the effective Hamiltonian in equation (7.17):

$$\begin{aligned}
 \rho(E) &= 3 \sum_{\mathbf{k}} \delta(E - tk^3 \cos 3\theta_{\mathbf{k}}) \\
 &\stackrel{E \rightarrow 0}{\simeq} 9 \int_0^\Lambda \frac{dk k}{4\pi^2} \int_{-\pi/6}^{\pi/6} d\theta \delta(|E| - |t|k^3 \cos 3\theta_{\mathbf{k}}) \\
 &= \frac{3}{2|t|\pi^2} \int_{|E/t|^{1/3}}^\Lambda \frac{dk k}{k^3} \frac{1}{\sqrt{1 - \frac{E^2}{t^2 k^6}}} = \frac{3}{2|t|\pi^2} \int_{|E/t|^{1/3}}^\Lambda \frac{dk k}{\sqrt{k^6 - (E/t)^2}} \\
 &\approx 0.18 (t^2|E|)^{-1/3} \equiv \rho_0 |E|^{-1/3}
 \end{aligned} \tag{7.22}$$

where  $\Lambda \simeq 1$  is the upper cutoff for the momentum integral.

## 7.4.2 Specific Heat

The specific heat, as  $T \rightarrow 0$  is given by

$$\begin{aligned}
 C &= \int_0^\infty dE \left( \frac{\partial n_F(E)}{\partial T} \right) E \rho(E) \\
 &\stackrel{T \rightarrow 0}{\simeq} \rho_0 \int_0^\infty dE \left( \frac{\partial n_F(E)}{\partial T} \right) |E|^{2/3} \simeq 1.18 \rho_0 T^{2/3}
 \end{aligned} \tag{7.23}$$

## 7.4.3 Magnetic susceptibility

Only the  $SU(2)$  spin rotation symmetry-breaking Zeeman term  $-\frac{i}{2}\mu_0 B^a \gamma^x \gamma^y$  will give rise to a magnetic moment due to the application of a magnetic field  $B\hat{\mathbf{z}}$ . The static

susceptibility may be calculated from the spin correlation function:

$$\begin{aligned}
 \chi_{zz} &= \mu_0 \int \frac{d^2k}{4\pi^2} \sum_{i\omega_n} \frac{1}{(i\omega_n - E_{\mathbf{k}})^2} \\
 &= 2\mu_0 \int_0^\infty dE \frac{\rho(E)}{3} \left( -\frac{\partial n_F(E)}{\partial E} \right) \\
 &\stackrel{T \rightarrow 0}{\simeq} \frac{2\mu_0\rho_0}{3} \int_0^\infty dE E^{-1/3} \left( -\frac{\partial n_F(E)}{\partial E} \right) \simeq 0.38\mu_0\rho_0 T^{-1/3} \quad (7.24)
 \end{aligned}$$

#### 7.4.4 The Wilson ratio – comparison with a 2DEG

For a spin 1/2 free fermion gas, the susceptibility and specific heat are given by

$$\chi_{xx} = \frac{\varrho_{2\text{DEG}}}{4}, \quad c_V = \frac{\pi^2}{3} \varrho_{2\text{DEG}} T \quad (7.25)$$

Thus, the Wilson ratio of this model is

$$\frac{0.38\rho_0 T^{-1/3}}{1.18\rho_0 T^{2/3}} \times \frac{\frac{\pi^2}{3} \varrho_{2\text{DEG}} T}{\frac{\varrho_{2\text{DEG}}}{4}} \simeq 4.2 \quad (7.26)$$

times that of the free spin 1/2 electron gas, assuming  $\mu_0 = \mu_B$ , the Bohr magneton.

A spin-1 non-interacting 2DEG has a Wilson ratio that is  $8/3 = 2.67$  times that of the spin-1/2 free 2DEG, i.e, *smaller* than that of our model.

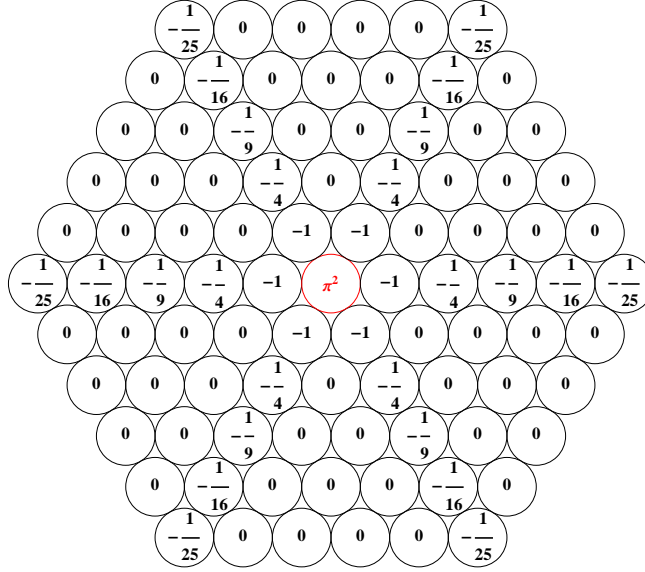


Figure 7.5: Variation of  $(\pi f(\mathbf{r}))^2 = 4\pi^2 \langle S^a(\mathbf{r})S^a(\mathbf{0}) \rangle$  on the real space lattice, at  $T = 0$  with only nearest neighbor hopping. The red circle at the center is  $\mathbf{r} = \mathbf{0}$  and there is no sum over  $a$ . We see that  $\langle S^a(\mathbf{r})S^a(\mathbf{0}) \rangle$  decays as an inverse square of the distance (the strongly directed nature is an artifact of nearest neighbor hopping).

#### 7.4.5 Static Structure Factor

The spin static structure factor is given by

$$\begin{aligned}
 \langle S^\mu(\mathbf{r})S^\nu(\mathbf{0}) \rangle &= -\frac{1}{16} \epsilon^{\mu ab} \epsilon^{\nu cd} \langle \gamma^a(\mathbf{r})\gamma^b(\mathbf{r})\gamma^c(\mathbf{0})\gamma^d(\mathbf{0}) \rangle \\
 &= \begin{cases} 0 & \text{for } \mu \neq \nu \\ \frac{\langle \gamma^\alpha(\mathbf{r})\gamma^\alpha(\mathbf{0}) \rangle^2}{4} & \text{for } \mu = \nu \text{ (no sum over } \alpha) \end{cases} \quad (7.27)
 \end{aligned}$$

This simplification occurs due to the absence of correlation between Majorana fermions of different flavors arising out of spin rotation invariance;  $\langle \gamma^\alpha(\mathbf{r})\gamma^\beta(\mathbf{0}) \rangle = f(\mathbf{r})\delta_{\alpha\beta}$ , where the function  $f(\mathbf{r})$  may be found as follows. Expressing the position vector  $\mathbf{r} = n_1\mathbf{a}_1 + n_2\mathbf{a}_2$  in terms of the lattice displacement vectors  $\mathbf{a}_{1,2}$  as well as the wave vector  $\mathbf{r} = p_1\mathbf{K}_1 + p_2\mathbf{K}_2$  in terms of the reciprocal lattice vectors  $\mathbf{K}_{1,2}$  defined through

$\mathbf{K}_i \cdot \mathbf{a}_j = \delta_{ij}$ , we find that

$$\begin{aligned}
 f(\mathbf{r}) &= \langle \gamma^\alpha(\mathbf{r}) \gamma^\alpha(\mathbf{0}) \rangle \quad (\text{no sum over } \alpha) \\
 &= \frac{2}{\mathcal{N}} \sum_{\mathbf{p}, \mathbf{q}} \langle b_{\mathbf{p}}^\alpha b_{\mathbf{q}}^\alpha \rangle e^{i\mathbf{p} \cdot \mathbf{r}} = \frac{2}{\mathcal{N}} \sum_{\mathbf{p}} (1 - n_F(E_{\mathbf{q}})) e^{i\mathbf{q} \cdot \mathbf{r}} \\
 &\stackrel{T=0}{=} \frac{1}{2\pi^2} \iint_{BZ'} d^2p e^{i(p_1 n_1 + p_2 n_2)} \\
 &\stackrel{n_1, n_2, n_1 - n_2 \neq 0}{=} \frac{e^{-i\pi(n_1 + 2n_2)}}{2\pi^2 n_1 n_2 (-n_1 + n_2)} \left[ (-1 + e^{i\pi n_1}) (1 + e^{i\pi(n_1 + 2n_2)}) n_2 \right. \\
 &\quad \left. + (1 - e^{i\pi n_2}) (1 + e^{i\pi(n_1 + 2n_2)}) (1 - e^{i\pi n_1} + e^{i\pi n_2}) n_1 \right] \quad (7.28)
 \end{aligned}$$

From the last expression, which is valid only for the case with nearest-neighbor hopping, we can prove that at  $T = 0$   $f(\mathbf{r})$  is zero when  $n_1, n_2, n_1 - n_2 \neq 0$ . Thus, the function is non-zero only along 3 lines defined by  $n_1, n_2, n_1 - n_2 = 0$ . The spatial variation of the squared value of this function at  $T = 0$ , which is proportional to the static spin correlation function, is shown in the Figure 7.5. We find that static spin correlations are negative and decay according to the *inverse square* law along the six directions (3 lines) discussed above. Inclusion of longer range hopping processes will modify the highly directional nature of the correlations.

#### 7.4.6 Effect of a perpendicular magnetic field

In the presence of a Zeeman term  $-\mu_0 B S_z$  which is small in comparison to the bandwidth, the DOS gets modified to

$$\rho_B(E) = \frac{\rho_0}{3} (|E|^{-1/3} + |E - \mu_0 B|^{-1/3} + |E + \mu_0 B|^{-1/3}) \quad (7.29)$$

where the three separate contributions come from the  $S_z = 0, \pm 1$  excitations respectively. The  $z = 3$  excitations for the  $S_z = \pm 1$  sector are gapped out and this results in a suppression of the low energy DOS and consequently also the specific heat and magnetic susceptibilities at low temperatures, as shown in Figures 7.6(a) and 7.6(b) respectively. As  $T \rightarrow 0$ , only the  $S_z = 0$  excitations contribute to the specific heat which thus gets reduced to a third of its zero field value. Since no excitations of the  $z = 3$  kind contribute to the magnetic susceptibility at  $T = 0$ , it is reduced to 0 in comparison to its zero field value. This leads to a suppression of the Wilson ratio at low temperatures, as shown in Figure 7.6(c). At temperatures much higher than the Zeeman energy, these quantities recover their zero field values.

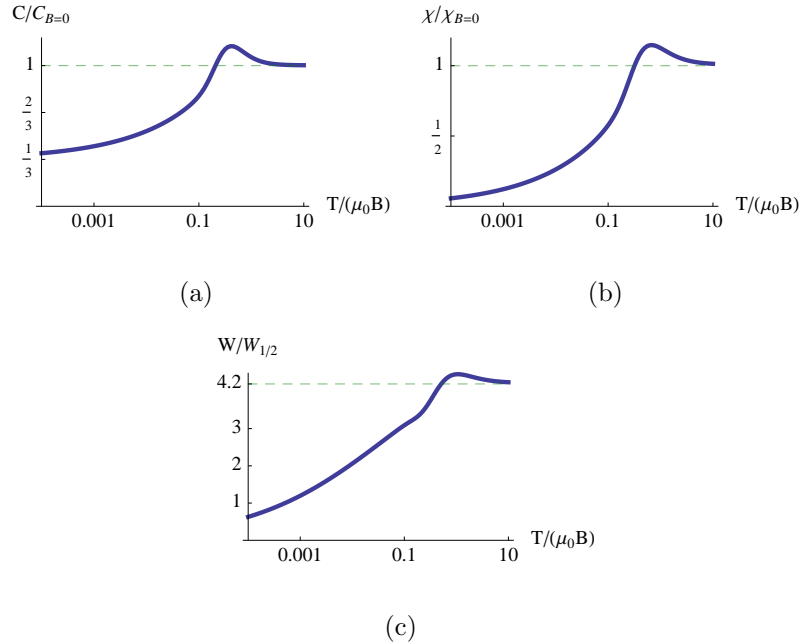


Figure 7.6: The suppression of specific heat (a) and the spin susceptibility (b) by a magnetic field that couples via a Zeeman term and gaps out the  $S_z = \pm 1$  excitations with  $z = 3$ . This also leads to the suppression of the Wilson ratio at low temperatures, as shown in (c). At temperatures much higher than the Zeeman energy, these quantities recover their zero field values.

## 7.5 Effects of weak disorder

### 7.5.1 The bond impurity potential

The Majorana bilinear Hamiltonian does not allow the incorporation of the widely-used on-site local impurity model, since  $\gamma^2(\mathbf{x})$  has to be equal to 1. The simplest kind of spin-rotation symmetric local impurity allowed in the spin model is a disrupted bond which has the following mean field form, assuming that the disrupted bond is oriented along the direction  $\boldsymbol{\delta}$ , joining  $\mathbf{r}$  and  $\mathbf{r} + \boldsymbol{\delta}$ :

$$V_{\boldsymbol{\delta}}(\mathbf{r}) = \delta J \langle \mathbf{S}(\mathbf{r}) \cdot \mathbf{S}(\mathbf{r} + \boldsymbol{\delta}) \rangle \simeq iU \sum_{\mathbf{p}, \mathbf{q}} b_{\mathbf{p}}^{\alpha} b_{\mathbf{q}}^{\alpha} e^{i(\mathbf{p} + \mathbf{q}) \cdot \mathbf{r}} (e^{i\mathbf{p} \cdot \boldsymbol{\delta}} - e^{i\mathbf{q} \cdot \boldsymbol{\delta}}) \quad (7.30)$$

Here,  $U \propto g \delta J$  is a real number and we have used the (anti)symmetry of the relevant operators.

### 7.5.2 The disorder-averaged self energy in the Born approximation

The disorder-averaged self energy in the Born approximation is given by (not including averaging over different bond directions)

$$\begin{aligned} \Sigma_{\mathbf{p}}^{\text{ret}}(\omega) &\simeq -n_{\text{imp}} U^2 \int \frac{d^2 q}{4\pi^2} \mathcal{G}_{\mathbf{q}}(\omega + i0+) (e^{i\mathbf{p} \cdot \boldsymbol{\delta}} - e^{-i\mathbf{q} \cdot \boldsymbol{\delta}}) (e^{i\mathbf{q} \cdot \boldsymbol{\delta}} - e^{-i\mathbf{p} \cdot \boldsymbol{\delta}}) \\ &= n_{\text{imp}} U^2 \int \frac{d^2 q}{2\pi^2} \frac{1 - \cos((\mathbf{p} + \mathbf{q}) \cdot \boldsymbol{\delta})}{\omega - E_{\mathbf{q}} + i0+} \\ &= n_{\text{imp}} U^2 \int \frac{d^2 q}{2\pi^2} \frac{1 - \cos \mathbf{p} \cdot \boldsymbol{\delta} \cos \mathbf{q} \cdot \boldsymbol{\delta} + \sin \mathbf{p} \cdot \boldsymbol{\delta} \sin \mathbf{q} \cdot \boldsymbol{\delta}}{\omega - E_{\mathbf{q}} + i0+} \end{aligned} \quad (7.31)$$

At this point, we take into account the fact that these bond disruptions are randomly oriented in space by averaging the above expression over the three values of  $\delta$  related by rotations through  $2\pi/3$ , as shown in Figure 7.2. We perform this average by using the fact that the denominator of the integrand in equation (7.31) is separately invariant under rotations of  $\mathbf{q}$  by  $2\pi/3$  and also using the following expressions for averages over  $2\pi/3$  rotations over the direction of any arbitrary vector  $\mathbf{d}$ :

$$\langle \cos \mathbf{d} \cdot \hat{\mathbf{e}} \rangle_{2n\pi/3} \equiv \varphi_{\hat{\mathbf{e}}}(\mathbf{d}) \stackrel{d \ll 1}{\equiv} 1 - \frac{d^2}{4} + \mathcal{O}(d^4) \quad (7.32a)$$

$$\langle \sin \mathbf{d} \cdot \hat{\mathbf{e}} \rangle_{2n\pi/3} \equiv \chi_{\hat{\mathbf{e}}}(\mathbf{d}) \stackrel{d \ll 1}{\equiv} -\frac{d^3}{24} \cos[3\theta] + \mathcal{O}(d^5) \quad (7.32b)$$

In these equations,  $\theta$  is the angle between  $\mathbf{d}$  and  $\hat{\mathbf{e}}$ . Using these in equation (7.31), we find the rotationally averaged self energy to be<sup>g</sup>

$$\begin{aligned} \Sigma_{\mathbf{p}}^{\text{ret}}(\omega) &\simeq n_{\text{imp}} U^2 \int \frac{d^2 q}{2\pi^2} \frac{1 - \varphi_x(\mathbf{p})\varphi_x(\mathbf{q}) + \chi_x(\mathbf{p})\chi_x(\mathbf{q})}{\omega - E_{\mathbf{q}} + i0+} \\ &\equiv n_{\text{imp}} U^2 (f_0(\omega) + f_1(\omega)\varphi_x(\mathbf{p}) + f_2(\omega)\chi_x(\mathbf{p})) \end{aligned} \quad (7.33)$$

From this expression we see immediately that as  $\omega \rightarrow 0$ , both  $f_{0,1}(\omega) \sim \rho(\omega) \propto \omega^{-1/3}$  diverge as  $\omega \rightarrow 0$  and thus the Born approximation cannot be justified. This leads us to consider the self-consistent Born approximation (SCBA) in the next section.

---

<sup>g</sup>The momenta are in units of  $1/a$ ,  $a$  being the lattice edge length.



### 7.5.3 The disorder-averaged self energy in the self-consistent Born approximation (SCBA)

The SCBA modifies equation (7.33) to the self-consistent equations:

$$\Sigma_{\mathbf{p}}^{\text{ret}}(\omega) \simeq n_{\text{imp}} U^2 \int \frac{d^2 q}{2\pi^2} \frac{1 - \varphi_x(\mathbf{p})\varphi_x(\mathbf{q}) + \chi_x(\mathbf{p})\chi_x(\mathbf{q})}{\omega - E_{\mathbf{q}} - \Sigma_{\mathbf{q}}^{\text{ret}}(\omega) + i0+} \quad (7.34)$$

For small  $\omega$  and  $p$  these equations can be simplified to:

$$\begin{aligned} \Sigma_{\mathbf{p}}^{\text{ret}}(\omega) &\approx \frac{n_{\text{imp}} U^2}{4} \int \frac{d^2 q}{2\pi^2} \frac{p^2 + q^2}{\omega - E_{\mathbf{q}} - \Sigma_{\mathbf{q}}^{\text{ret}}(\omega) + i0+} \\ &\equiv F_0(\omega) + F_1(\omega)p^2 \end{aligned} \quad (7.35)$$

Using this approximate rotational invariance of  $\Sigma_{\mathbf{p}}^{\text{ret}}(\omega)$  for small  $p$  we can simplify these equations to a form that can be easily solved numerically:

$$\Sigma_{\mathbf{p}}^{\text{ret}}(\omega) \approx -i \left( \frac{n_{\text{imp}} U^2}{4\pi} \right) \int_0^{\Lambda \simeq 1} dq q \frac{p^2 + q^2}{\sqrt{q^6 - (\omega - \Sigma_{\mathbf{q}}^{\text{ret}}(\omega))^2}} \quad (7.36)$$

At  $\omega = 0$ , these equations can also be analytically solved to the leading order in the disorder strength  $n_{\text{imp}} U^2 \rightarrow 0$  and they yield a purely imaginary value for  $\Sigma_{\mathbf{p}}^{\text{ret}}(0)$ .

We first deal with  $F_0(0)$  which depends directly on the momentum cutoff  $\Lambda$ :

$$F_0(0) = -i \left( \frac{n_{\text{imp}} U^2}{4\pi} \right) \int_0^{\Lambda} dq q \frac{q^2}{q^3} = -i \frac{\Lambda}{4\pi} (n_{\text{imp}} U^2) \quad (7.37)$$

The value of  $F_1(0)$  is given by (relabeling  $F_0(0)$  by  $-i\Gamma_0$  below, with  $\Gamma_0 > 0$ )

$$F_1(0) \approx -i \left( \frac{n_{\text{imp}} U^2}{4\pi} \right) \int_0^{\Lambda} dq \frac{q}{\sqrt{q^6 + \Gamma_0^2}} \stackrel{n_{\text{imp}} U^2 \ll \Lambda^2}{\simeq} -i 0.26 \frac{(n_{\text{imp}} U^2)^{2/3}}{\Lambda^{1/3}} \quad (7.38)$$

Numerical solutions to the SCBA equation (7.35) agree with these analytic results (setting  $\Lambda \approx 1$ ). The variation of the imaginary parts of the self energy with frequency and impurity strength are shown in Figure 7.7.

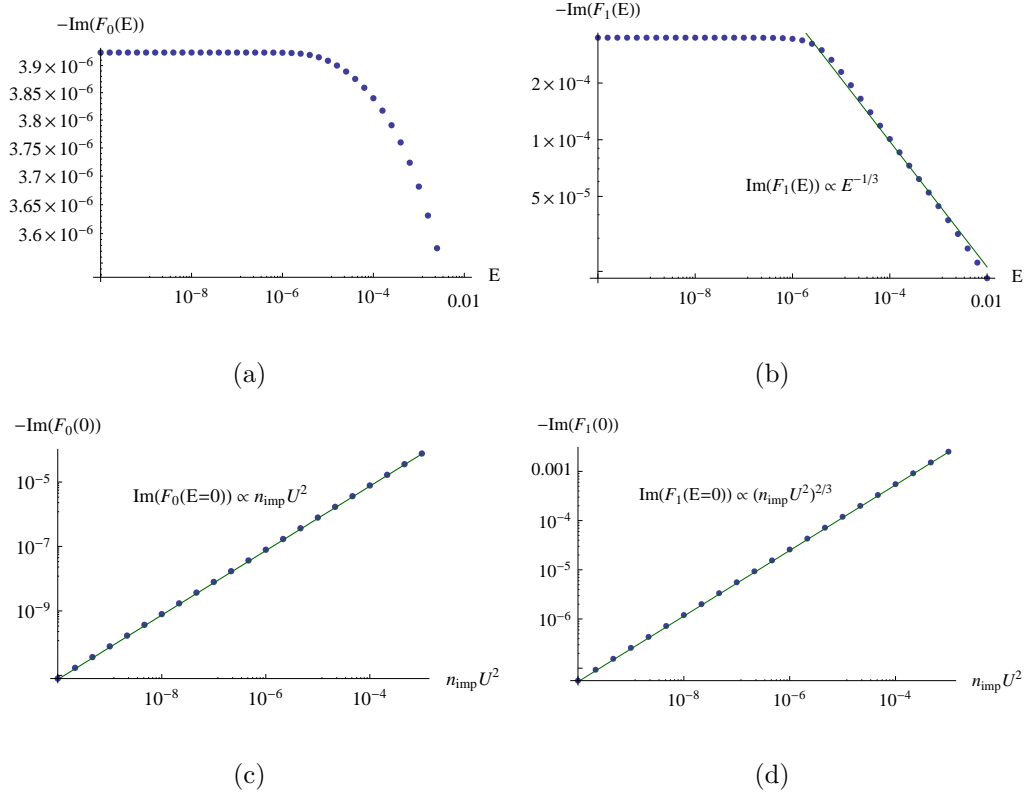


Figure 7.7: Figures showing the variation of the imaginary parts of  $F_{0,1}$ , as defined in equation (7.35) and equation (7.36), with frequency as well as the disorder strength. Wherever possible, power law fits have been made. In (a) and (b), we have used the disorder strength value  $n_{\text{imp}}U^2 = 5 \times 10^{-5}$ .

### 7.5.4 The disorder-averaged single particle density of states

The single particle density of states (DOS) is given by:

$$\begin{aligned}
 \rho(E) &= - \int \frac{d^2p}{4\pi^3} \text{Im} \left( \frac{1}{E - E_{\mathbf{p}} - \Sigma_{\mathbf{p}}^{\text{ret}}(E)} \right) \\
 &= \frac{1}{2\pi^2} \text{Re} \left( \int_0^{\Lambda \simeq 1} dp \frac{p}{\sqrt{p^6 - (\omega - (F_0(\omega) + F_1(\omega)p^2))^2}} \right) \quad (7.39)
 \end{aligned}$$

Since  $\text{Im}(\Sigma_{\mathbf{p}}^{\text{ret}}(E = 0))$  is a finite number, we expect the DOS to become constant at low energies, instead of diverging as  $E^{-1/3}$  like in the clean case (7.22). This quenching of the low energy divergence in the DOS is shown in Figure 7.8(a). The

variation with disorder strength of the low energy saturation value of the DOS is also plotted in 7.8(b).

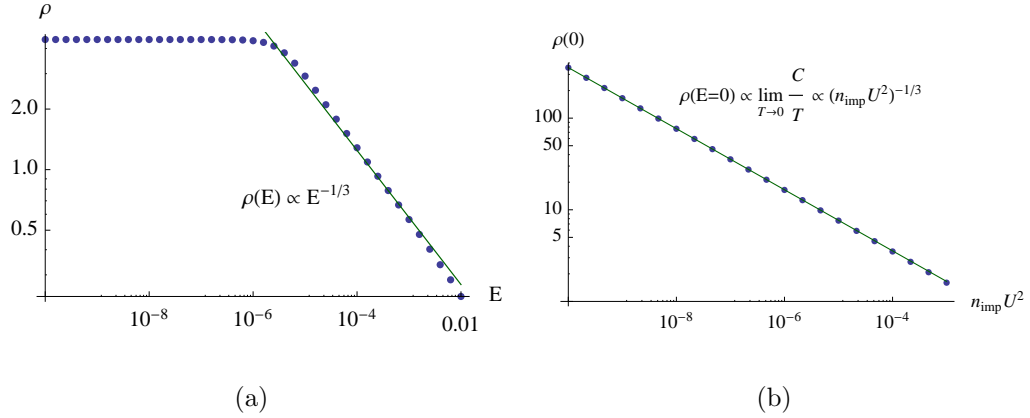


Figure 7.8: Figures showing the variation of the DOS equation (7.39) with energy in (a) in the presence of disorder with strength  $n_{\text{imp}}U^2 = 5 \times 10^{-5}$ , as well as the variation of the low energy saturation value with the disorder strength in (b).

### 7.5.5 The specific heat in the presence of impurities

Using the SCBA analysis result that the low energy DOS  $\rho(0)$  is finite, the low temperature specific heat is found to be

$$C = \int_0^{\Lambda \simeq 1} dE E \left( \frac{\partial n_F(E)}{\partial T} \right) \rho(E) \stackrel{T \rightarrow 0}{\approx} \left( \frac{\pi^2 \rho(0)}{6} \right) T \quad (7.40)$$

Thus, at very low temperatures, the specific heat is *linear* in temperature and the coefficient of this linear variation is proportional to  $\rho(0)$  and hence to  $(n_{\text{imp}}U^2)^{-1/3}$  (see Figure 7.8(b)). The variation of  $C/T$  with temperature is shown in Figure 7.9(a) where the transition, at higher temperatures, to the behavior (7.23) in the clean limit can be seen.

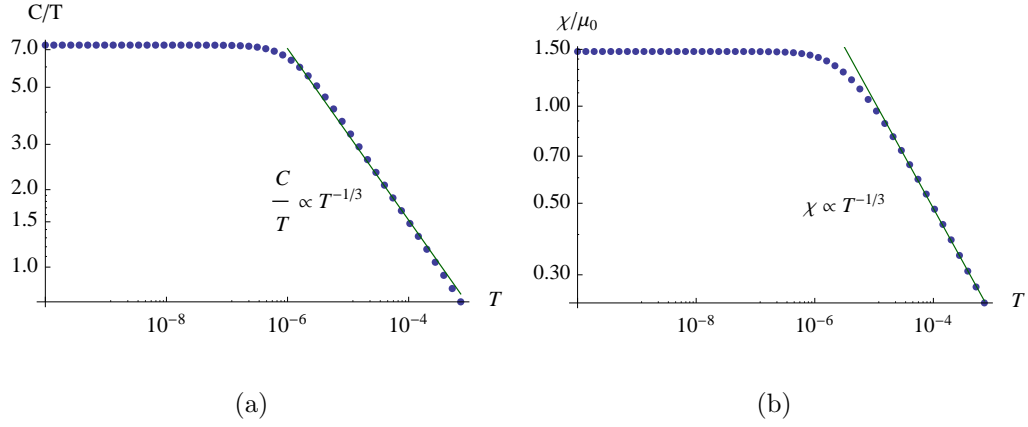


Figure 7.9: Figures showing the temperature variations of the specific heat divided by temperature  $C/T$  in (a) as well as the static spin susceptibility  $\chi$  in (b). At temperatures larger than a value set by the disorder strength  $n_{\text{imp}}U^2 = 5 \times 10^{-5}$ , the quantities regain their behaviors equation (7.23) and equation (7.24) in the clean limit.

### 7.5.6 The spin susceptibility in the presence of impurities

The spin susceptibility is found to be

$$\begin{aligned} \chi_{zz} &= 2\mu_0 \int_0^\infty dE \frac{\rho(E)}{3} \left( -\frac{\partial n_F(E)}{\partial E} \right) \\ &\stackrel{T \rightarrow 0}{\simeq} \frac{2\mu_0\rho(0)}{3} \int_0^\infty dE \left( -\frac{\partial n_F(E)}{\partial E} \right) = \frac{\mu_0\rho(0)}{3} \end{aligned} \quad (7.41)$$

The variation of the spin susceptibility with temperature is shown in Figure 7.9(b) where we can again see the transition to the behavior (7.24) in the clean limit at higher temperatures.

### 7.5.7 The Wilson ratio in the presence of impurities – comparison with a 2DEG

As  $T \rightarrow 0$ , the Wilson ratio for our model is the same as that of a 2DEG of spin 1 fermions<sup>h</sup> because of the finite DOS at low energies:

$$\frac{W}{W_{1/2}} \stackrel{T \rightarrow 0}{=} \frac{\frac{\mu_0 \rho(0)}{3}}{\frac{\pi^2 \rho(0)}{6}} \times \frac{\frac{\pi^2}{3} \rho_{2\text{DEG}} T}{\frac{\rho_{2\text{DEG}}}{4}} = \frac{8}{3} \equiv \frac{W_1}{W_{1/2}} \quad (7.42)$$

where  $W_{1/2}$  is the Wilson ratio of the free spin 1/2 electron gas. We have, as before, assumed that the effective magnetic moment of the spins  $\mu_0 = \mu_B$ , the Bohr magneton.

Figure 7.10 shows the variation of this ratio as a function of temperature, showing the transition to the clean limit value in equation (7.26) at higher temperatures.

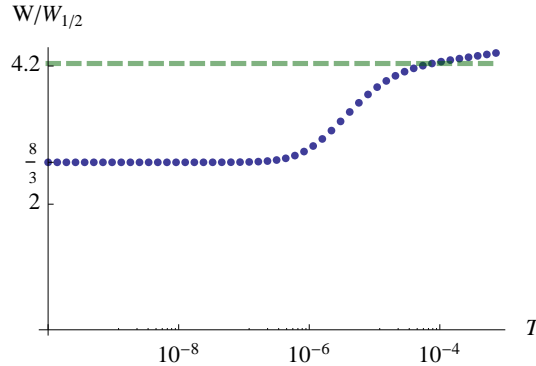


Figure 7.10: The Wilson ratio  $W = T\chi/C$  as a multiple of that of the spin 1/2 2DEG  $W_{1/2}$ , calculated as a function of temperature, in the presence of disorder with strength  $n_{\text{imp}}U^2 = 5 \times 10^{-5}$ . As  $T \rightarrow 0$ , the value becomes that of a spin 1 2DEG while at larger temperatures it increases to the value derived in equation (7.26) for the clean system.

<sup>h</sup>The Wilson ratio  $W_S$  of a spin  $S$  2DEG can be shown to be proportional to  $S(S+1)$ .

### 7.5.8 The thermal conductivity

The thermal current is[71]

$$\hat{\mathbf{J}}(\mathbf{q} \rightarrow \mathbf{0}, \Omega \rightarrow 0) = \sum_{\mathbf{k} \in BZ', \omega} \mathbf{v}_{\mathbf{k}} \left( \omega + \frac{\Omega}{2} \right) b_{-\mathbf{k}, -\omega}^{\alpha} b_{\mathbf{k}, \omega + \Omega}^{\alpha} \quad (7.43)$$

The thermal conductivity tensor is given by[31]

$$\frac{\kappa}{T} = - \lim_{\Omega \rightarrow 0} \lim_{\mathbf{q} \rightarrow \mathbf{0}} \frac{\text{Im } \Pi_{\text{ret}}(\mathbf{q}, \Omega)}{\Omega T^2} \quad (7.44)$$

where  $\Pi$  is a tensor whose components are the correlation functions of the thermal current components.  $\Pi$  is diagonal because averaging over three fold rotations makes the off-diagonal component  $J_x J_y \propto v_x v_y$  vanish.

For the following calculation, it will be useful to mention these formulæ for the quasiparticle velocities, assuming a low energy long wavelength energy dispersion

$$E_{\mathbf{q}} = t q^3 \cos(3\theta_{\mathbf{q}} + \phi):$$

$$\begin{aligned} v_x &= \left( \cos \theta_{\mathbf{q}} \partial_q - \frac{\sin \theta_{\mathbf{q}}}{q} \partial_{\theta} \right) E_{\mathbf{q}} = 3q^2 t \cos(2\theta_{\mathbf{q}} + \phi) \\ v_y &= \left( \sin \theta_{\mathbf{q}} \partial_q + \frac{\cos \theta_{\mathbf{q}}}{q} \partial_{\theta} \right) E_{\mathbf{q}} = -3q^2 t \sin(2\theta_{\mathbf{q}} + \phi) \end{aligned} \quad (7.45)$$

Thus  $v_{\mathbf{q}}^2 \simeq 9q^4$ , using units in which  $t = 1$ .

The bare thermal polarization bubble (using the renormalized propagators, though) yields, after a three-fold rotational averaging that converts  $v_{x,y}^2 \rightarrow v^2/2$ ,

$$\begin{aligned} \frac{\kappa}{T} &= 3 \sum_{\mathbf{p} \in BZ'} \frac{v_{\mathbf{p}}^2}{2\pi} \int_{-\infty}^{\infty} d\omega \left( \frac{\omega}{T} \right)^2 \left( -\frac{\partial n(\omega)}{\partial \omega} \right) (\text{Im } G_{\text{ret}}(\mathbf{p}, \omega))^2 \\ &\approx \frac{27}{32\pi^3} \int_{BZ'} d^2 p p^4 \int_0^{\infty} d\omega \left( \frac{\omega}{T} \right)^2 \left( -\frac{\partial n(\omega)}{\partial \omega} \right) [(\text{Im } G_{\text{ret}}(\mathbf{p}, \omega))^2 + (\text{Im } G_{\text{ret}}(-\mathbf{p}, \omega))^2] \\ &\stackrel{T \rightarrow 0}{\approx} \frac{9}{32\pi} \int d^2 p p^4 (\text{Im } G_{\text{ret}}(\mathbf{p}, \omega = 0))^2 \end{aligned} \quad (7.46)$$

Thus, at low temperatures the thermal conductivity is also *linear* in temperature (shown in Figure 7.11(b)). The coefficient of this linear variation is plotted vs the disorder strength in Figure 7.11(a). We find that the low temperature value of  $\kappa/T$  varies as  $(n_{\text{imp}}U^2)^{-2/3}$  with the disorder strength.

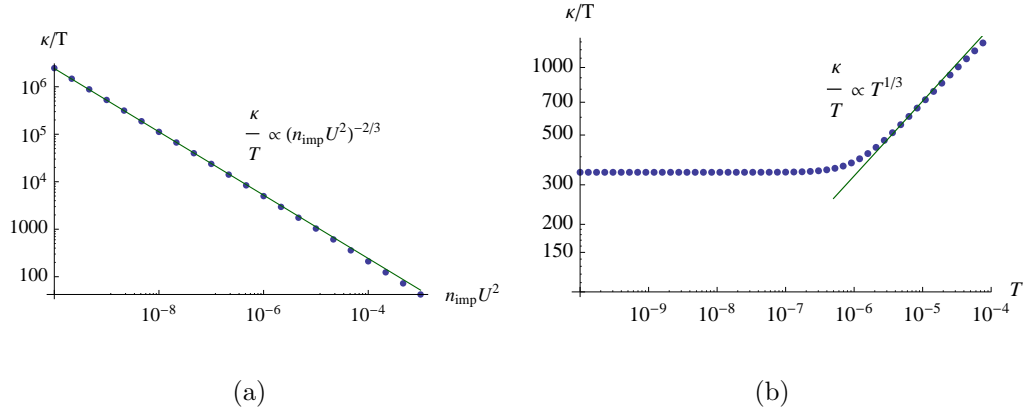


Figure 7.11: The  $T = 0$  thermal coefficient of the thermal conductivity equation (7.46)  $\kappa$  is plotted against the disorder strength in (a). (b) shows the variation of this thermal coefficient with temperature.

The value of  $\kappa/T$  in the dmit-131 compound was found to be 0.2 in SI units[168], which is equivalent to about 332 per triangular spin lattice sheet in units of  $k_B^2/\hbar$ , using the provided value of 3nm as the interlayer distance. From Figure 7.11(a) we find that we require the disorder strength to be  $n_{\text{imp}}U^2 \approx 5 \times 10^{-5}$  to reproduce this value.

The vertex corrections to the thermal current can be achieved by replacing[71] the quasiparticle energy function  $E_{\mathbf{k}}$  in the calculation of the quasiparticle velocities by  $E_{\mathbf{k}} + \text{Re}\Sigma_{\mathbf{k}}(\omega)$ . However,  $\text{Re}\Sigma_{\mathbf{k}}(\omega)$  is negligible with respect to  $E_{\mathbf{k}}$  and so the vertex corrections are negligible at low disorder strengths[31].

## 7.6 Conclusions

Let us summarize the characteristic properties of the Majorana spin liquid state on the triangular lattice.

- There are low energy spin excitations near  $\mathbf{q} = 0$  which disperse as  $\omega \sim q^3$ . In addition there are six Fermi lines which intersect at  $\mathbf{q} = 0$ , with linear dispersion across the Fermi lines.
- The spin susceptibility,  $\chi$ , and the specific heat,  $C$  are dominated by the  $z = 3$  excitations near  $\mathbf{q} = 0$ ; hence  $\chi \sim C/T \sim T^{-1/3}$ , and the Wilson ratio is found to be  $W \simeq 4.2$ .
- In the presence of weak disorder, these divergencies saturate at low enough  $T$ . Hence  $\chi \sim C/T \sim T^0$ , and the Wilson ratio  $W = 8/3$ , as expected for a Fermi surface of  $S = 1$  fermions.
- The longitudinal thermal conductivity  $\kappa \sim T$  as  $T \rightarrow 0$  with non-zero disorder scattering. The thermal current is carried mostly by the excitations on the Fermi lines.
- In the presence of an applied magnetic field, there is no orbital coupling to transverse thermal current, and so no thermal Hall effect.
- Two-thirds of the  $\omega \sim q^3$  excitations are gapped out by an applied magnetic field by the Zeeman coupling. Consequently, the specific heat and the spin susceptibility are suppressed by the applied field. On the other hand, the thermal



conductivity is insensitive to the field because it is dominated by the Fermi line excitations, and these survive the Zeeman coupling.

We emphasize that the qualitative aspects of the above results rely only on the assumption of a spin liquid ground state on the triangular lattice with SU(2) spin rotation invariance and spin-ful Majorana excitations obeying a trivial PSG.

Many of these properties make our Majorana state an attractive candidate for EtMe<sub>3</sub>Sb[Pd(dmit)<sub>2</sub>]<sub>2</sub>: the behavior  $\chi \sim C/T \sim \kappa/T \sim T^0$ , and the absence of a thermal Hall effect. An interesting distinguishing feature of our theory is that  $\chi$  and  $C$  are suppressed by an applied magnetic field, while  $\kappa/T$  is not. It would be interesting to test this in future experiments.

# Bibliography

- [1] *Mathematica 7.0*. Wolfram Research, Inc., Champagne, IL, 2008.
- [2] E. Abrahams, P. W. Anderson, D. C. Licciardello, and T. V. Ramakrishnan. Scaling theory of localization: Absence of quantum diffusion in two dimensions. *Phys. Rev. Lett.*, 42(10):673–676, Mar 1979.
- [3] Shaffique Adam, E. H. Hwang, V. M. Galitski, and S. Das Sarma. A self-consistent theory for graphene transport. *Proceedings of the National Academy of Sciences*, 104(47):18392–18397, May 2007.
- [4] Ian Affleck, Z. Zou, T. Hsu, and P. W. Anderson.  $Su(2)$  gauge symmetry of the large- $u$  limit of the hubbard model. *Phys. Rev. B*, 38(1):745–747, Jul 1988.
- [5] Zhanybek Alpichshev, J. G. Analytis, J.-H. Chu, I. R. Fisher, Y. L. Chen, Z. X. Shen, A. Fang, and A. Kapitulnik. Stm imaging of electronic waves on the surface of  $bi_2se_3$ : Topologically protected surface states and hexagonal warping effects. *Phys. Rev. Lett.*, 104(1):016401, Jan 2010.
- [6] P. W. Anderson. The resonating valence bond state in  $la_2cuo_4$  and superconductivity. *Science*, 235(4793):1196–1198, Mar 1987.
- [7] A. V. Balatsky, I. Vekhter, and Jian-Xin Zhu. Impurity-induced states in conventional and unconventional superconductors. *Rev. Mod. Phys.*, 78(2):373, May 2006.
- [8] G. Baskaran, Saptarshi Mandal, and R. Shankar. Exact results for spin dynamics and fractionalization in the kitaev model. *Phys. Rev. Lett.*, 98(24):247201, Jun 2007.
- [9] G. Baskaran, G. Santhosh, and R. Shankar. Exact quantum spin liquids with fermi surfaces in spin-half models. *arXiv:0908.1614*, Aug 2009.
- [10] C. W. J. Beenakker. Colloquium: Andreev reflection and klein tunneling in graphene. *Reviews of Modern Physics*, 80(4):1337, Oct 2008.

- 
- [11] Cristina Bena. Effect of a single localized impurity on the local density of states in monolayer and bilayer graphene. *Phys. Rev. Lett.*, 100(7):076601, Feb 2008.
- [12] Cristina Bena. The local density of states in the presence of impurity scattering in graphene at high magnetic field. Jun 2009.
- [13] Cristina Bena and Steven A. Kivelson. Quasiparticle scattering and local density of states in graphite. *Phys. Rev. B*, 72(12):125432, Sep 2005.
- [14] B. Andrei Bernevig, Taylor L. Hughes, and Shou-Cheng Zhang. Quantum spin hall effect and topological phase transition in hgte quantum wells. *Science*, 314(5806):1757–1761, Dec 2006.
- [15] B. Bernu, P. Lecheminant, C. Lhuillier, and L. Pierre. Exact spectra, spin susceptibilities, and order parameter of the quantum heisenberg antiferromagnet on the triangular lattice. *Phys. Rev. B*, 50(14):10048–10062, Oct 1994.
- [16] Rudro R. Biswas and Alexander V. Balatsky. Impurity-induced states on the surface of 3d topological insulators. *arXiv:0910.4604*, Oct 2009.
- [17] Rudro R. Biswas and Alexander V. Balatsky. Power laws in surface state Idos oscillations near a step edge. *arXiv:1005.4780*, May 2010.
- [18] J. Bobroff, H. Alloul, W. A. MacFarlane, P. Mendels, N. Blanchard, G. Collin, and J.-F. Marucco. Persistence of li induced kondo moments in the superconducting state of cuprates. *Phys. Rev. Lett.*, 86(18):4116–4119, Apr 2001.
- [19] Henrik Bruus and Karsten Flensberg. *Many-body Quantum Theory in Condensed Matter Physics: An Introduction*. Oxford University Press, 2004.
- [20] Han-Dong Chen and Jiangping Hu. Exact mapping between classical and topological orders in two-dimensional spin systems. *Phys. Rev. B*, 76(19):193101, Nov 2007.
- [21] Y. L. Chen, J. G. Analytis, J. H. Chu, Z. K. Liu, S. K. Mo, X. L. Qi, H. J. Zhang, D. H. Lu, X. Dai, Z. Fang, S. C. Zhang, I. R. Fisher, Z. Hussain, and Z. X. Shen. Experimental realization of a three-dimensional topological insulator,  $\text{Bi}_2\text{Te}_3$ . *Science*, 325(5937):178–181, Jul 2009.
- [22] Gia-Wei Chern. Three-dimensional topological phases in a layered honeycomb spin-orbital model. *Phys. Rev. B*, 81(12):125134, Mar 2010.
- [23] Victor Chua, Hong Yao, and Gregory A. Fiete. Exact chiral spin liquid with stable spin fermi surface on the kagome lattice. *arXiv:1010.1035*, Oct 2010.

- 
- [24] P. Coleman, E. Miranda, and A. Tsvelik. Odd-frequency pairing in the kondo lattice. *Phys. Rev. B*, 49(13):8955–8982, Apr 1994.
- [25] M. F. Crommie, C. P. Lutz, and D. M. Elgler. Imaging standing waves in a two-dimensional electron gas. *Nature*, 363:524, Jun 1993.
- [26] L. C. Davis, M. P. Everson, R. C. Jaklevic, and Weidian Shen. Theory of the local density of surface states on a metal: Comparison with scanning tunneling spectroscopy of a au(111) surface. *Phys. Rev. B*, 43(5):3821, Feb 1991.
- [27] Jacques des Cloizeaux and J. J. Pearson. Spin-wave spectrum of the antiferromagnetic linear chain. *Phys. Rev.*, 128(5):2131–2135, Dec 1962.
- [28] Kusum Dhochak, R. Shankar, and V. Tripathi. Magnetic impurities in the honeycomb kitaev model. *Phys. Rev. Lett.*, 105(11):117201, Sep 2010.
- [29] P. A. M. Dirac. The quantum theory of the electron. *Proceedings of the Royal Society of London. Series A*, 117(778):610–624, Feb 1928.
- [30] D. P. DiVincenzo and E. J. Mele. Self-consistent effective-mass theory for intralayer screening in graphite intercalation compounds. *Phys. Rev. B*, 29(4):1685–1694, Feb 1984.
- [31] Adam C. Durst and Patrick A. Lee. Impurity-induced quasiparticle transport and universal-limit wiedemann-franz violation in d-wave superconductors. *Phys. Rev. B*, 62(2):1270–1290, Jul 2000.
- [32] Sebastian Eggert and Ian Affleck. Magnetic impurities in half-integer-spin heisenberg antiferromagnetic chains. *Phys. Rev. B*, 46(17):10866–10883, Nov 1992.
- [33] Sebastian Eggert and Ian Affleck. Impurities in  $s = 1/2$  heisenberg antiferromagnetic chains: Consequences for neutron scattering and knight shift. *Phys. Rev. Lett.*, 75(5):934–937, Jul 1995.
- [34] Xiao-Yong Feng, Guang-Ming Zhang, and Tao Xiang. Topological characterization of quantum phase transitions in a spin-1/2 model. *Phys. Rev. Lett.*, 98(8):087204, Feb 2007.
- [35] Serge Florens, Lars Fritz, and Matthias Vojta. Kondo effect in bosonic spin liquids. *Phys. Rev. Lett.*, 96(3):036601, Jan 2006.
- [36] Eduardo Fradkin. Critical behavior of disordered degenerate semiconductors. i. models, symmetries, and formalism. *Phys. Rev. B*, 33(5):3257, Mar 1986.

- 
- [37] J. Friedel. The distribution of electrons round impurities in monovalent metals. *Phil. Mag*, 43:153, Feb 1952.
- [38] Lars Fritz and Matthias Vojta. Phase transitions in the pseudogap anderson and kondo models: Critical dimensions, renormalization group, and local-moment criticality. *Phys. Rev. B*, 70(21):214427, Dec 2004.
- [39] Liang Fu. Hexagonal warping effects in the surface states of the topological insulator  $bi_2te_3$ . *Phys. Rev. Lett.*, 103(26):266801, Dec 2009.
- [40] Liang Fu and C. L. Kane. Topological insulators with inversion symmetry. *Physical Review B (Condensed Matter and Materials Physics)*, 76(4):045302, Jul 2007.
- [41] Liang Fu and C. L. Kane. Superconducting proximity effect and majorana fermions at the surface of a topological insulator. *Phys. Rev. Lett.*, 100(9):096407, Mar 2008.
- [42] Liang Fu, C. L. Kane, and E. J. Mele. Topological insulators in three dimensions. *Physical Review Letters*, 98(10):106803, Mar 2007.
- [43] Kenjiro K. Gomes, Wonhee Ko, Warren Mar, Yulin Chen, Zhi-Xun Shen, and Hari C. Manoharan. Quantum imaging of topologically unpaired spin-polarized dirac fermions. *arXiv:0909.0921*, Sep 2009.
- [44] J. Gonzalez, F. Guinea, and M. A. H. Vozmediano. Non-fermi liquid behavior of electrons in the half-filled honeycomb lattice (a renormalization group approach). *Nuclear Physics B*, 424(3):595–618, Apr 1994.
- [45] J. Gonzalez, F. Guinea, and M. A. H. Vozmediano. Marginal-fermi-liquid behavior from two-dimensional coulomb interaction. *Phys. Rev. B*, 59(4):R2474–R2477, Jan 1999.
- [46] L.P. Gor'kov and P.A. Kalugin. Defects and an unusual superconductivity. *JETP Lett.*, 41(5):253, 1985.
- [47] Tarun Grover, N. Trivedi, T. Senthil, and Patrick A. Lee. Weak mott insulators on the triangular lattice: Possibility of a gapless nematic quantum spin liquid. *Phys. Rev. B*, 81(24):245121, Jun 2010.
- [48] F. D. M. Haldane.  $O(3)$  nonlinear  $\sigma$  model and the topological distinction between integer- and half-integer-spin antiferromagnets in two dimensions. *Phys. Rev. Lett.*, 61(8):1029–1032, Aug 1988.
- [49] Michael Hermele, T. Senthil, and Matthew P. A. Fisher. Algebraic spin liquid

- as the mother of many competing orders. *Phys. Rev. B*, 72(10):104404, Sep 2005.
- [50] Michael Hermele, T. Senthil, Matthew P. A. Fisher, Patrick A. Lee, Naoto Nagaosa, and Xiao-Gang Wen. Stability of  $u(1)$  spin liquids in two dimensions. *Phys. Rev. B*, 70(21):214437, Dec 2004.
- [51] A. C Hewson. *The Kondo problem to heavy fermions*. Cambridge University Press, Cambridge, 1st pbk. ed. with corrections edition, 1997.
- [52] Kaj H. Höglund and Anders W. Sandvik. Impurity effects at finite temperature in the two-dimensional  $s = 1/2$  heisenberg antiferromagnet. *Phys. Rev. B*, 70(2):024406, Jul 2004.
- [53] D. Hsieh, D. Qian, L. Wray, Y. Xia, Y. S. Hor, R. J. Cava, and M. Z. Hasan. A topological dirac insulator in a quantum spin hall phase. *Nature*, 452(7190):970–974, Apr 2008.
- [54] D. Hsieh, Y. Xia, D. Qian, L. Wray, J. H. Dil, F. Meier, J. Osterwalder, L. Patthey, J. G. Checkelsky, N. P. Ong, A. V. Fedorov, H. Lin, A. Bansil, D. Grauer, Y. S. Hor, R. J. Cava, and M. Z. Hasan. A tunable topological insulator in the spin helical dirac transport regime. *Nature*, 460:1101–1105, Jul 2009.
- [55] E. W. Hudson, K. M. Lang, V. Madhavan, S. H. Pan, H. Eisaki, S. Uchida, and J. C. Davis. Interplay of magnetism and high- $T_c$  superconductivity at individual ni impurity atoms in  $\text{Bi}_2\text{Sr}_2\text{CaCu}_2\text{O}_{8+\delta}$ . *Nature*, 411(6840):920–924, Jun 2001.
- [56] David A. Huse and Veit Elser. Simple variational wave functions for two-dimensional heisenberg spin-1/2 antiferromagnets. *Phys. Rev. Lett.*, 60(24):2531–2534, Jun 1988.
- [57] T. Itou, A. Oyamada, S. Maegawa, and R. Kato. Instability of a quantum spin liquid in an organic triangular-lattice antiferromagnet. *Nat Phys*, 6(9):673–676, Sep 2010.
- [58] T. Itou, A. Oyamada, S. Maegawa, M. Tamura, and R. Kato. Quantum spin liquid in the spin- 1/2 triangular antiferromagnet  $\text{EtMe}_3\text{Sb}[\text{Pd}(\text{dmit})_2]_2$ . *Phys. Rev. B*, 77(10):104413, Mar 2008.
- [59] Claude Itzykson and Jean Bernard Zuber. *Quantum field theory*. Dover Publications, Mineola, N.Y., dover ed edition, 2005.

- 
- [60] B. A. Jones, C. M. Varma, and J. W. Wilkins. Low-temperature properties of the two-impurity kondo hamiltonian. *Phys. Rev. Lett.*, 61(1):125–128, Jul 1988.
- [61] William Jones and Norman H March. *Theoretical solid state physics*, volume 1. Dover Publications, New York, 1973.
- [62] C. L. Kane and Matthew P. A. Fisher. Transport in a one-channel luttinger liquid. *Phys. Rev. Lett.*, 68(8):1220–1223, Feb 1992.
- [63] C. L. Kane and E. J. Mele. Quantum spin hall effect in graphene. *Phys. Rev. Lett.*, 95(22):226801, Nov 2005.
- [64] C. L. Kane and E. J. Mele.  $z_2$  topological order and the quantum spin hall effect. *Phys. Rev. Lett.*, 95(14):146802, Sep 2005.
- [65] M. I. Katsnelson, K. S. Novoselov, and A. K. Geim. Chiral tunneling and the klein paradox in graphene. *Nat. Phys.*, 2(9):620–625, Sep 2006.
- [66] Hosho Katsura, Naoto Nagaosa, and Patrick A. Lee. Theory of the thermal hall effect in quantum magnets. *Phys. Rev. Lett.*, 104(6):066403, Feb 2010.
- [67] G. Khaliullin, R. Kilian, S. Krivenko, and P. Fulde. Impurity-induced moments in underdoped cuprates. *Phys. Rev. B*, 56(18):11882–11888, Nov 1997.
- [68] Alexei Kitaev. Anyons in an exactly solved model and beyond. *Annals of Physics*, 321(1):2–111, Jan 2006.
- [69] Alexei Kolezhuk, Subir Sachdev, Rudro R. Biswas, and Peiqiu Chen. Theory of quantum impurities in spin liquids. *Phys. Rev. B*, 74(16):165114, Oct 2006.
- [70] Markus König, Steffen Wiedmann, Christoph Brüne, Andreas Roth, Hartmut Buhmann, Laurens W. Molenkamp, Xiao-Liang Qi, and Shou-Cheng Zhang. Quantum spin hall insulator state in hgte quantum wells. *Science*, 318(5851):766–770, 11 2007.
- [71] Hiroshi Kontani. General formula for the thermoelectric transport phenomena based on fermi liquid theory: Thermoelectric power, nernst coefficient, and thermal conductivity. *Phys. Rev. B*, 67(1):014408, Jan 2003.
- [72] H. Kramers. *Proc. Acad. Sci. Amsterdam*, 33:959, 1930.
- [73] S. A. Krivenko and G. G. Khaliullin. Formation of a local moment near a vacancy in a spin liquid. *JETP Lett.*, 62(9):723, Nov 1995.
- [74] Hsin-Hua Lai and Olexei I. Motrunich. Power-law behavior of bond energy

- correlators in a kitaev-type model with a stable parton fermi surface. *Phys. Rev. B*, 83(15):155104, Apr 2011.
- [75] Dung-Hai Lee, Guang-Ming Zhang, and Tao Xiang. Edge solitons of topological insulators and fractionalized quasiparticles in two dimensions. *Phys. Rev. Lett.*, 99(19):196805, Nov 2007.
- [76] Sung-Sik Lee and Patrick A. Lee. U(1) gauge theory of the hubbard model: Spin liquid states and possible application to  $\kappa - (bedt - ttf)_2cu_2(cn)_3$ . *Phys. Rev. Lett.*, 95(3):036403, Jul 2005.
- [77] Rundong Li, Jing Wang, Xiao-Liang Qi, and Shou-Cheng Zhang. Dynamical axion field in topological magnetic insulators. *Nat Phys*, 6(4):284–288, Mar 2010.
- [78] Qin Liu, Chao-Xing Liu, Cenke Xu, Xiao-Liang Qi, and Shou-Cheng Zhang. Magnetic impurities on the surface of a topological insulator. *Phys. Rev. Lett.*, 102(15):156603, Apr 2009.
- [79] Adina Luican, Guohong Li, and Eva Y. Andrei. Quantized landau level spectrum and its density dependence in graphene. *Phys. Rev. B*, 83(4):041405, Jan 2011.
- [80] E. Majorana. A symmetric theory of electrons and positrons. *Il Nuovo Cimento*, 14:171–184, 1937.
- [81] S. Mandal, Subhro Bhattacharjee, K.Sengupta, R. Shankar, and G. Baskaran. Spin correlations and phase diagram of the perturbed kitaev model. *arXiv:1101.1388*, Jan 2011.
- [82] Saptarshi Mandal and Naveen Surendran. Exactly solvable kitaev model in three dimensions. *Phys. Rev. B*, 79(2):024426, Jan 2009.
- [83] J. L. Manes. Symmetry-based approach to electron-phonon interactions in graphene. *Phys. Rev. B*, 76(4):045430, Jul 2007.
- [84] J. Martin, N. Akerman, G. Ulbricht, T. Lohmann, J. H. Smet, K. von Klitzing, and A. Yacoby. Observation of electron-hole puddles in graphene using a scanning single-electron transistor. *Nat Phys*, 4(2):144–148, Nov 2007.
- [85] J. L. Martin. Generalized classical dynamics, and the 'classical analogue' of a fermi oscillator. *Proceedings of the Royal Society of London. Series A, Mathematical and Physical Sciences*, 251(1267):536–542, Jun 1959.



- [86] J. W. McClure. Diamagnetism of graphite. *Phys. Rev.*, 104(3):666–671, Nov 1956.
- [87] N. D. Mermin and H. Wagner. Absence of ferromagnetism or antiferromagnetism in one- or two-dimensional isotropic heisenberg models. *Phys. Rev. Lett.*, 17(22):1133–1136, Nov 1966.
- [88] David L. Miller, Kevin D. Kubista, Gregory M. Rutter, Ming Ruan, Walt A. de Heer, Phillip N. First, and Joseph A. Stroscio. Observing the quantization of zero mass carriers in graphene. *Science*, 324(5929):924–927, May 2009.
- [89] J. E. Moore and L. Balents. Topological invariants of time-reversal-invariant band structures. *Physical Review B (Condensed Matter and Materials Physics)*, 75(12):121306, Mar 2007.
- [90] Olexei I. Motrunich. Variational study of triangular lattice spin-1/2 model with ring exchanges and spin liquid state in  $\kappa - (et)_2cu_2(cn)_3$ . *Phys. Rev. B*, 72(4):045105, Jul 2005.
- [91] Shuichi Murakami, Naoto Nagaosa, and Shou-Cheng Zhang. Spin-hall insulator. *Phys. Rev. Lett.*, 93(15):156804, Oct 2004.
- [92] Naoto Nagaosa and Patrick A. Lee. Kondo effect in high-  $t_c$  cuprates. *Phys. Rev. Lett.*, 79(19):3755–3758, Nov 1997.
- [93] Naoto Nagaosa and Tai-Kai Ng. Nonmagnetic impurity in the spin-gap state. *Phys. Rev. B*, 51(21):15588–15591, Jun 1995.
- [94] A. A. Nersesyan, A. M. Tsvelik, and F. Wenger. Disorder effects in two-dimensional d-wave superconductors. *Phys. Rev. Lett.*, 72(16):2628–2631, Apr 1994.
- [95] A. H. Castro Neto, F. Guinea, N. M. R. Peres, K. S. Novoselov, and A. K. Geim. The electronic properties of graphene. *Rev. Mod. Phys.*, 81(1):109, Jan 2009.
- [96] Flavio S. Nogueira and Hagen Kleinert. Quantum electrodynamics in 2 + 1 dimensions, confinement, and the stability of  $u(1)$  spin liquids. *Phys. Rev. Lett.*, 95(17):176406, Oct 2005.
- [97] D. S. Novikov. Elastic scattering theory and transport in graphene. *Phys. Rev. B*, 76(24):245435, Dec 2007.
- [98] K S Novoselov, A K Geim, S V Morozov, D Jiang, M I Katsnelson, I V Grig-

- orieva, S V Dubonos, and A A Firsov. Two-dimensional gas of massless dirac fermions in graphene. *Nature*, 438(7065):197–200, Nov 2005.
- [99] K S Novoselov, A K Geim, S V Morozov, D Jiang, Y Zhang, S V Dubonos, I V Grigorieva, and A A Firsov. Electric field effect in atomically thin carbon films. *Science*, 306(5696):666–669, Oct 2004.
- [100] P. Nozieres and A. Blandin. Kondo effect in real metals. *J. Phys. France*, 41(3):193–211, Mar 1980.
- [101] Zohar Nussinov and Gerardo Ortiz. Bond algebras and exact solvability of hamiltonians: Spin  $s = \frac{1}{2}$  multilayer systems. *Phys. Rev. B*, 79(21):214440, Jun 2009.
- [102] Taisuke Ohta, Aaron Bostwick, J. L. McChesney, Thomas Seyller, Karsten Horn, and Eli Rotenberg. Interlayer interaction and electronic screening in multilayer graphene investigated with angle-resolved photoemission spectroscopy. *Phys. Rev. Lett.*, 98(20):206802, May 2007.
- [103] P. M. Ostrovsky, I. V. Gornyi, and A. D. Mirlin. Electron transport in disordered graphene. *Phys. Rev. B*, 74(23):235443, Dec 2006.
- [104] S. Ouazi, J. Bobroff, H. Alloul, M. Le Tacon, N. Blanchard, G. Collin, M. H. Julien, M. Horvatić, and C. Berthier. Impurity-induced local magnetism and density of states in the superconducting state of  $yba_2cu_3o_7$ . *Phys. Rev. Lett.*, 96(12):127005, Mar 2006.
- [105] S. H. Pan, E. W. Hudson, K. M. Lang, H. Eisaki, S. Uchida, and J. C. Davis. Imaging the effects of individual zinc impurity atoms on superconductivity in  $bi_2sr_2cacu_2o_8 + [\delta]$ . *Nature*, 403(6771):746–750, Feb 2000.
- [106] Catherine Pépin and Patrick A. Lee. Order from disorder: Nonmagnetic impurities in the spin-gap phase of the cuprates. *Phys. Rev. Lett.*, 81(13):2779–2782, Sep 1998.
- [107] Catherine Pépin and Patrick A. Lee. Density of states of a d-wave superconductor in the presence of strong impurity scatterers: A nonperturbative result. *Phys. Rev. B*, 63(5):054502, Jan 2001.
- [108] Vitor M. Pereira, Johan Nilsson, and A. H. Castro Neto. Coulomb impurity problem in graphene. *Phys. Rev. Lett.*, 99(16):166802, Oct 2007.
- [109] F. L. Pratt, P. J. Baker, S. J. Blundell, T. Lancaster, S. Ohira-Kawamura, C. Baines, Y. Shimizu, K. Kanoda, I. Watanabe, and G. Saito. Magnetic and

- non-magnetic phases of a quantum spin liquid. *Nature*, 471(7340):612–616, Mar 2011.
- [110] Yang Qi, Cenke Xu, and Subir Sachdev. Dynamics and transport of the  $z_2$  spin liquid: Application to  $\kappa - (et)_2cu_2(cn)_3$ . *Phys. Rev. Lett.*, 102(17):176401, Apr 2009.
- [111] Walter Rantner and Xiao-Gang Wen. Electron spectral function and algebraic spin liquid for the normal state of underdoped high  $t_c$  superconductors. *Phys. Rev. Lett.*, 86(17):3871–3874, Apr 2001.
- [112] Walter Rantner and Xiao-Gang Wen. Spin correlations in the algebraic spin liquid: Implications for high- $t_c$  superconductors. *Phys. Rev. B*, 66(14):144501, Oct 2002.
- [113] N. Read and Subir Sachdev. Large- $n$  expansion for frustrated quantum antiferromagnets. *Phys. Rev. Lett.*, 66(13):1773–1776, Apr 1991.
- [114] Pedram Roushan, Jungpil Seo, Colin V. Parker, Y. S. Hor, D. Hsieh, Dong Qian, Anthony Richardella, M. Z. Hasan, R. J. Cava, and Ali Yazdani. Topological surface states protected from backscattering by chiral spin texture. *Nature*, 460(7259):1106–1109, Aug 2009.
- [115] Pedram Roushan, Jungpil Seo, Colin V. Parker, Y. S. Hor, D. Hsieh, Dong Qian, Anthony Richardella, M. Z. Hasan, R. J. Cava, and Ali Yazdani. Topological surface states protected from backscattering by chiral spin texture. *Nature*, 460, Aug 2009.
- [116] Rahul Roy. Topological phases and the quantum spin hall effect in three dimensions. *Physical Review B (Condensed Matter and Materials Physics)*, 79(19):195322, May 2009.
- [117] Shinsei Ryu, Christopher Mudry, Hideaki Obuse, and Akira Furusaki.  $z_2$  topological term, the global anomaly, and the two-dimensional symplectic symmetry class of anderson localization. *Phys. Rev. Lett.*, 99(11):116601, Sep 2007.
- [118] Subir Sachdev. Static hole in a critical antiferromagnet: field-theoretic renormalization group. *Physica C: Superconductivity*, 357-360(Part 1):78–81, Sep 2001.
- [119] Subir Sachdev. Quantum phases and phase transitions of mott insulators. In Ulrich Schollwöck, Johannes Richter, Damian Farnell, and Raymod Bishop, editors, *Quantum Magnetism*, volume 645 of *Lecture Notes in Physics*, pages 381–432. 2004.

- 
- [120] Subir Sachdev, Chiranjeeb Buragohain, and Matthias Vojta. Quantum impurity in a nearly critical two-dimensional antiferromagnet. *Science*, 286(5449):2479–2482, Dec 1999.
- [121] Subir Sachdev, Matthias Troyer, and Matthias Vojta. Spin orthogonality catastrophe in two-dimensional antiferromagnets and superconductors. *Phys. Rev. Lett.*, 86(12):2617–2620, Mar 2001.
- [122] Subir Sachdev and Matthias Vojta. Quantum impurity in an antiferromagnet: Nonlinear sigma model theory. *Phys. Rev. B*, 68(6):064419, Aug 2003.
- [123] Saeed Saremi. Rkky in half-filled bipartite lattices: Graphene as an example. *Phys. Rev. B*, 76(18):184430, Nov 2007.
- [124] Andreas P. Schnyder, Shinsei Ryu, Akira Furusaki, and Andreas W. W. Ludwig. Classification of topological insulators and superconductors in three spatial dimensions. *Phys. Rev. B*, 78(19):195125, Nov 2008.
- [125] E. Schrodinger. An undulatory theory of the mechanics of atoms and molecules. *Phys. Rev.*, 28(6):1049–1070, Dec 1926.
- [126] Diptiman Sen and B Sriram Shastry. A majorana fermion t - j model in one dimension. *Journal of Physics: Condensed Matter*, 9(38):7963, Sep 1997.
- [127] Anirvan M. Sengupta. Spin in a fluctuating field: The bose(+fermi) kondo models. *Phys. Rev. B*, 61(6):4041–4043, Feb 2000.
- [128] T. Senthil, Leon Balents, Subir Sachdev, Ashvin Vishwanath, and Matthew P. A. Fisher. Quantum criticality beyond the landau-ginzburg-wilson paradigm. *Phys. Rev. B*, 70(14):144407, Oct 2004.
- [129] T. Senthil and Matthew P. A. Fisher.  $z_2$  gauge theory of electron fractionalization in strongly correlated systems. *Phys. Rev. B*, 62(12):7850–7881, Sep 2000.
- [130] T. Senthil, Ashvin Vishwanath, Leon Balents, Subir Sachdev, and Matthew P. A. Fisher. Deconfined quantum critical points. *Science*, 303(5663):1490–1494, Mar 2004.
- [131] Todadri Senthil, Leon Balents, Subir Sachdev, Ashvin Vishwanath, and Matthew P. A. Fisher. Deconfined criticality critically defined. *Journal of the Physical Society of Japan*, 74S(Supplement):1–9, 2005.
- [132] Jungpil Seo, Pedram Roushan, Haim Beidenkopf, Y. S. Hor, R. J. Cava, and

- Ali Yazdani. Transmission of topological surface states through surface barriers. (*accepted by Nature*), 2010.
- [133] B. Sriram Shastry and Diptiman Sen. Majorana fermion representation for an antiferromagnetic spin- chain. *Phys. Rev. B*, 55(5):2988–2994, Feb 1997.
- [134] Y. Shimizu, K. Miyagawa, K. Kanoda, M. Maesato, and G. Saito. Spin liquid state in an organic mott insulator with a triangular lattice. *Phys. Rev. Lett.*, 91(10):107001, Sep 2003.
- [135] Y. Shimizu, K. Miyagawa, K. Kanoda, M. Maesato, and G. Saito. Emergence of inhomogeneous moments from spin liquid in the triangular-lattice mott insulator  $\kappa - (et)_2cu_2(cn)_3$ . *Phys. Rev. B*, 73(14):140407, Apr 2006.
- [136] A. V. Shytov, M. I. Katsnelson, and L. S. Levitov. Vacuum polarization and screening of supercritical impurities in graphene. *Phys. Rev. Lett.*, 99(23):236801, Dec 2007.
- [137] Andrei V. Shytov, Dmitry A. Abanin, and Leonid S. Levitov. Long-range interaction between adatoms in graphene. *Phys. Rev. Lett.*, 103(1):016806, Jul 2009.
- [138] Qimiao Si, Silvio Rabello, Kevin Ingersent, and J. Llewellyn Smith. Locally critical quantum phase transitions in strongly correlated metals. *Nature*, 413(6858):804–808, 10 2001.
- [139] D. T. Son. Quantum critical point in graphene approached in the limit of infinitely strong coulomb interaction. *Phys. Rev. B*, 75(23):235423, Jun 2007.
- [140] P. T. Sprunger, L. Petersen, E. W. Plummer, E. Lagsgaard, and F. Besenbacher. Giant friedel oscillations on the beryllium(0001) surface. *Science*, 275(5307):1764–1767, Mar 1997.
- [141] Elena Stolyarova, Kwang Taeg Rim, Sunmin Ryu, Janina Maultzsch, Philip Kim, Louis E. Brus, Tony F. Heinz, Mark S. Hybertsen, and George W. Flynn. High-resolution scanning tunneling microscopy imaging of mesoscopic graphene sheets on an insulating surface. *PNAS*, 104(22):9209–9212, May 2007.
- [142] Ivan S. Terekhov, Alexander I. Milstein, Valeri N. Kotov, and Oleg P. Sushkov. Screening of coulomb impurities in graphene. *Phys. Rev. Lett.*, 100(7):076803, Feb 2008.
- [143] K. S. Tikhonov and M. V. Feigel'man. Quantum spin metal state on a decorated honeycomb lattice. *Phys. Rev. Lett.*, 105(6):067207, Aug 2010.

- 
- [144] Kostantin S. Tikhonov, Mikhail V. Feigel'man, and Alexei Yu. Kitaev. Power-law spin correlations in a perturbed honeycomb spin model. *arXiv:1008.4106*, Aug 2010.
- [145] Matthias Troyer. Static and dynamic holes in a quantum critical antiferromagnet. *Prog. Theor. Phys. Suppl.*, 145:326–331, 2002.
- [146] A. M. Tsvelik. New fermionic description of quantum spin liquid state. *Phys. Rev. Lett.*, 69(14):2142–2144, Oct 1992.
- [147] Julien Vidal, Kai Phillip Schmidt, and Sébastien Dusuel. Perturbative approach to an exactly solved problem: Kitaev honeycomb model. *Phys. Rev. B*, 78(24):245121, Dec 2008.
- [148] Matthias Vojtá, Chiranjeeb Buragohain, and Subir Sachdev. Quantum impurity dynamics in two-dimensional antiferromagnets and superconductors. *Phys. Rev. B*, 61(22):15152–15184, Jun 2000.
- [149] Matthias Vojtá and Lars Fritz. Upper critical dimension in a quantum impurity model: critical theory of the asymmetric pseudogap kondo problem. *Phys. Rev. B*, 70(9):094502, Sep 2004.
- [150] G. E. Volovik. *The universe in a helium droplet*, volume 117 of *International series of monographs on physics*. Clarendon Press, Oxford, 2003.
- [151] P. R. Wallace. The band theory of graphite. *Phys. Rev.*, 71(9):622–634, May 1947.
- [152] Fa Wang. Realization of the exactly solvable kitaev honeycomb lattice model in a spin-rotation-invariant system. *Phys. Rev. B*, 81(18):184416, May 2010.
- [153] Fa Wang and Ashvin Vishwanath.  $z_2$  spin-orbital liquid state in the square lattice kugel-khomskii model. *Phys. Rev. B*, 80(6):064413, Aug 2009.
- [154] Ziqiang Wang and Patrick A. Lee. Local moment formation in the superconducting state of a doped mott insulator. *Phys. Rev. Lett.*, 89(21):217002, Nov 2002.
- [155] T. O. Wehling, A. V. Balatsky, M. I. Katsnelson, A. I. Lichtenstein, K. Scharnberg, and R. Wiesendanger. Local electronic signatures of impurity states in graphene. *Phys. Rev. B*, 75(12):125425, Mar 2007.
- [156] X. G. Wen. Mean-field theory of spin-liquid states with finite energy gap and topological orders. *Phys. Rev. B*, 44(6):2664–2672, Aug 1991.

- 
- [157] Xiao-Gang Wen. Quantum orders and symmetric spin liquids. *Phys. Rev. B*, 65(16):165113, Apr 2002.
- [158] Xiao-Gang Wen. Quantum order from string-net condensations and the origin of light and massless fermions. *Phys. Rev. D*, 68(6):065003, Sep 2003.
- [159] Xiao-Gang Wen and Patrick A. Lee. Theory of underdoped cuprates. *Phys. Rev. Lett.*, 76(3):503–506, Jan 1996.
- [160] Eugene P. Wigner. Normal form of antiunitary operators. *Journal of Mathematical Physics*, 1(5):409–413, Sep 1960.
- [161] Frank Wilczek. Majorana returns. *Nat Phys*, 5(9):614–618, Sep 2009.
- [162] A. J. Willans, J. T. Chalker, and R. Moessner. Disorder in a quantum spin liquid: Flux binding and local moment formation. *Phys. Rev. Lett.*, 104(23):237203, Jun 2010.
- [163] Mark Wilson. Electrons in atomically thin carbon sheets behave like massless particles. *Physics Today*, 59(1):21–23, Jan 2006.
- [164] L. Andrew Wray, Su-Yang Xu, Yuqi Xia, David Hsieh, Alexei V. Fedorov, Yew San Hor, Robert J. Cava, Arun Bansil, Hsin Lin, and M. Zahid Hasan. A topological insulator surface under strong coulomb, magnetic and disorder perturbations. *Nat Phys*, 7(1):32–37, Jan 2011.
- [165] Congjun Wu, Daniel Arovas, and Hsiang-Hsuan Hung.  $\gamma$ -matrix generalization of the kitaev model. *Phys. Rev. B*, 79(13):134427, Apr 2009.
- [166] Y. Xia, D. Qian, D. Hsieh, L. Wray, A. Pal, H. Lin, A. Bansil, D. Grauer, Y. S. Hor, R. J. Cava, and M. Z. Hasan. Observation of a large-gap topological-insulator class with a single dirac cone on the surface. *Nat Phys*, 5(6):398–402, Jun 2009.
- [167] Minoru Yamashita, Norihito Nakata, Yuichi Kasahara, Takahiko Sasaki, Naoki Yoneyama, Norio Kobayashi, Satoshi Fujimoto, Takasada Shibauchi, and Yuji Matsuda. Thermal-transport measurements in a quantum spin-liquid state of the frustrated triangular magnet  $\kappa$ -(bedt-ttf)<sub>2</sub>cu<sub>2</sub>(cn)<sub>3</sub>. *Nat Phys*, 5(1):44–47, Jan 2008.
- [168] Minoru Yamashita, Norihito Nakata, Yoshinori Senshu, Masaki Nagata, Hiroshi M. Yamamoto, Reizo Kato, Takasada Shibauchi, and Yuji Matsuda. Highly mobile gapless excitations in a two-dimensional candidate quantum spin liquid. *Science*, 328(5983):1246–1248, Jun 2010.

- 
- [169] Satoshi Yamashita, Yasuhiro Nakazawa, Masaharu Oguni, Yugo Oshima, Hiroyuki Nojiri, Yasuhiro Shimizu, Kazuya Miyagawa, and Kazushi Kanoda. Thermodynamic properties of a spin-1/2 spin-liquid state in a  $\kappa$ -type organic salt. *Nat Phys*, 4(6):459–462, 06 2008.
- [170] Hong Yao and Steven A. Kivelson. Exact chiral spin liquid with non-abelian anyons. *Phys. Rev. Lett.*, 99(24):247203, Dec 2007.
- [171] Hong Yao and Dung-Hai Lee. Fermionic magnons, non-abelian spinons, and spin quantum hall effect from an exactly solvable kitaev hamiltonian with  $su(2)$  symmetry. *arXiv:1010.3724*, Oct 2010.
- [172] Hong Yao, Shou-Cheng Zhang, and Steven A. Kivelson. Algebraic spin liquid in an exactly solvable spin model. *Phys. Rev. Lett.*, 102(21):217202, May 2009.
- [173] Ali Yazdani, B. A. Jones, C. P. Lutz, M. F. Crommie, and D. M. Eigler. Probing the local effects of magnetic impurities on superconductivity. *Science*, 275(5307):1767–1770, Mar 1997.
- [174] Fei Ye, Guo-Hui Ding, Hui Zhai, and Zhao-Bin Su. Spin helix of magnetic impurities in two-dimensional helical metal. *arXiv:1002.0111v1*, Feb 2010.
- [175] Jinwu Ye and Subir Sachdev. Coulomb interactions at quantum hall critical points of systems in a periodic potential. *Phys. Rev. Lett.*, 80(24):5409–5412, Jun 1998.
- [176] Takehito Yokoyama, Alexander V. Balatsky, and Naoto Nagaosa. Gate-controlled one-dimensional channel on the topological surface. *arXiv:1002.0112*, 2010.
- [177] Gergely Zaránd and Eugene Demler. Quantum phase transitions in the bose-fermi kondo model. *Phys. Rev. B*, 66(2):024427, Jul 2002.
- [178] Haijun Zhang, Chao-Xing Liu, Xiao-Liang Qi, Xi Dai, Zhong Fang, and Shou-Cheng Zhang. Topological insulators in  $bi_2se_3$ ,  $bi_2te_3$  and  $sb_2te_3$  with a single dirac cone on the surface. *Nat Phys*, 5(6):438–442, May 2009.
- [179] Tong Zhang, Peng Cheng, Xi Chen, Jin-Feng Jia, Xucun Ma, Ke He, Lili Wang, Haijun Zhang, Xi Dai, Zhong Fang, Xincheng Xie, and Qi-Kun Xue. Experimental demonstration of topological surface states protected by time-reversal symmetry. *Phys. Rev. Lett.*, 103(26):266803, Dec 2009.
- [180] Yuanbo Zhang, Yan-Wen Tan, Horst L. Stormer, and Philip Kim. Experimental observation of the quantum hall effect and berry’s phase in graphene. *Nature*, 438(7065):201–204, Nov 2005.



- 
- [181] Xiaoting Zhou, Chen Fang, Wei-Feng Tsai, and JiangPing Hu. Theory of quasi-particle scattering in a two-dimensional system of helical dirac fermions: Surface band structure of a three-dimensional topological insulator. *Phys. Rev. B*, 80(24):245317, Dec 2009.
- [182] Lijun Zhu and Qimiao Si. Critical local-moment fluctuations in the bose-fermi kondo model. *Phys. Rev. B*, 66(2):024426, Jul 2002.

# Appendix A

## The relation between the Majorana and spin 1/2 Hilbert spaces

There are three Majorana operators  $\gamma^{x,y,z}$  per spin. If we consider a collection of an *even* number  $N$  of spins, this will lead to a Hilbert space of dimension  $2^{3N/2}$ . We will review here how this is equivalent to  $2^{N/2}$  copies of the  $2^N$ -dimensional spin half Hilbert space.

We assume that the Majorana Hilbert space is composed by randomly picking up pairs of Majoranas and representing them by a two-state complex fermion Hilbert space. We can show that this space is independent of which scheme of pairing is used.

Let us now define the following site and bond operators using the Majorana fermion

operators:

$$\mathcal{O}(\mathbf{r}) = i\gamma^x(\mathbf{r})\gamma^y(\mathbf{r})\gamma^z(\mathbf{r}) \quad (\text{A.1a})$$

$$\mathcal{T}(\mathbf{r}_1, \mathbf{r}_2) = \mathcal{O}(\mathbf{r}_1)\mathcal{O}(\mathbf{r}_2) \quad (\text{for } \mathbf{r}_1 \neq \mathbf{r}_2 \text{ only}) \quad (\text{A.1b})$$

These commute with the spin operators

$$[\mathcal{O}(\mathbf{r}_1), S^a(\mathbf{r}_2)] = 0 \quad (\text{A.2a})$$

$$\mathcal{O}(\mathbf{r}) = 2\gamma^a(\mathbf{r})S^a(\mathbf{r}) = 2S^a(\mathbf{r})\gamma^a(\mathbf{r}) \quad (\text{A.2b})$$

and also satisfy the following algebraic/(anti)commutation relations (in the following,  $\mathbf{r}_i \neq \mathbf{r}_j$  as long as  $i \neq j$ ):

$$\{\mathcal{O}(\mathbf{r}_i), \mathcal{O}(\mathbf{r}_j)\} = 2\delta_{ij} \quad (\text{A.3})$$

$$[\mathcal{T}(\mathbf{r}_1, \mathbf{r}_2), \mathcal{T}(\mathbf{r}_3, \mathbf{r}_4)] = 0 \quad (\text{A.4})$$

$$\{\mathcal{T}(\mathbf{r}_1, \mathbf{r}), \mathcal{T}(\mathbf{r}_2, \mathbf{r})\} = 0 \quad (\text{A.5})$$

$$\mathcal{T}(\mathbf{r}_1, \mathbf{r}_2) = -\mathcal{T}(\mathbf{r}_2, \mathbf{r}_1); \quad \mathcal{T}^2 = -1 \quad (\text{A.6})$$

$$\mathcal{T}(\mathbf{r}_1, \mathbf{r})\mathcal{T}(\mathbf{r}, \mathbf{r}_2) = \mathcal{T}(\mathbf{r}_1, \mathbf{r}_2) \quad (\text{A.7})$$

$$[\gamma^\alpha(\mathbf{r}_1), \mathcal{T}(\mathbf{r}_2, \mathbf{r}_3)] = \{\gamma^\alpha(\mathbf{r}_1), \mathcal{T}(\mathbf{r}_1, \mathbf{r}_2)\} = 0 \quad (\text{A.8})$$

The consequences of the foregoing relations are as follows. Let us cover the lattice with a pattern of bonds (assuming an even number  $\mathcal{N}$  of sites; there are  $\mathcal{N}!/(2^{\mathcal{N}/2}(\mathcal{N}/2)!)$  such coverings). For such a covering, the  $\mathcal{N}/2$  number of  $\mathcal{T}$  operators on the bonds may be diagonalized simultaneously and each operator assumes one of the values  $\pm i$ . There are  $2^{\mathcal{N}/2}$  such choices. However, for each such choice, the spin operators may be diagonalized simultaneously within each subspace – any spin Hamiltonian

is thus not going to mix equivalent subspaces. Since there were  $2^{3\mathcal{N}/2}$  states in the original Majorana Hilbert space, each subspace contains  $2^{3\mathcal{N}/2}/2^{\mathcal{N}/2} = 2^{\mathcal{N}}$  states which matches the number of states we require for the  $\mathcal{N}$  spin 1/2's.

We can explicitly build up such a subspace from the Majorana Hilbert space and demonstrate the one-to-one correspondence with the spin states. Let us choose a particular bond structure. Now, within every bond, let us label the two sites as  $m$  and  $n$ . Then, we can form the fermion operator

$$c_{mn}^\alpha = \frac{\gamma_m^\alpha + i\gamma_n^\alpha}{2} \quad (\text{A.9})$$

which satisfies the usual complex fermion anti-commutation rule (no sum over  $\alpha$ )

$$[c_{mn}^\alpha, (c_{mn}^\alpha)^\dagger] = 1 \quad (\text{A.10})$$

and allows us to define a minimal Hilbert space defined by eigenstates of the number operator  $n_{mn}^\alpha \equiv (c_{mn}^\alpha)^\dagger c_{mn}^\alpha = (1 + i\gamma_m^\alpha \gamma_n^\alpha)/2$ . In the following, we shall often drop the sub/superscripts when there is no ambiguity.

The bond operator is proportional to the fermion parity operator specific to that bond

$$\begin{aligned} \mathcal{T}_{mn} &= \mathcal{O}_m \mathcal{O}_n = i(i\gamma_m^x \gamma_n^x)(i\gamma_m^y \gamma_n^y)(i\gamma_m^z \gamma_n^z) \\ &= i(2n^x - 1)(2n^y - 1)(2n^z - 1) = -i(-1)^{n^x + n^y + n^z} \end{aligned} \quad (\text{A.11})$$

Using the notation  $|n^x n^y n^z\rangle \equiv ((c^x)^\dagger)^{n^x} ((c^y)^\dagger)^{n^y} ((c^z)^\dagger)^{n^z} |000\rangle$ , we see that the  $\mathcal{T} = +i$  subspace consists of the states  $|100\rangle, |010\rangle, |001\rangle$  and  $|111\rangle$  having odd number of fermions. The other case of  $\mathcal{T} = -i$  involves states with an even number of fermions.

In this basis the  $S^z$  operators can be expressed as:

$$S_m^z = \frac{1}{2} \begin{pmatrix} \sigma_y & 0 \\ 0 & \sigma_y \end{pmatrix} \quad (\text{A.12})$$

$$S_n^z = \frac{1}{2} \begin{pmatrix} \sigma_y & 0 \\ 0 & -\sigma_y \end{pmatrix} \quad (\text{A.13})$$

which tells us that the spin 1/2 states are related to the Majorana states in the  $\mathcal{T} = +i$  subspace as follows:

$$|S_m^z = \pm 1/2, S_m^z = \pm 1/2\rangle = \frac{|100\rangle \pm i |010\rangle}{\sqrt{2}} \quad (\text{A.14a})$$

$$|S_m^z = \mp 1/2, S_m^z = \pm 1/2\rangle = \frac{|001\rangle \pm i |111\rangle}{\sqrt{2}} \quad (\text{A.14b})$$

We can proceed similarly and build up a correspondence between the spin 1/2 states and a specified subspace, bond-by-bond through the entire collection of spins. We note here that the singlet state on a bond is given by the three fermion state  $|111\rangle$ .

We can now comment about the relation between the  $Z_2$  gauge equivalence apparent in equation (7.1) and the explicit construction of equivalent subspaces above. Such a gauge transformation flips the sign of the  $\mathcal{T}$  operator on the associated bond and thus exchanges the subspaces related by flipping that sign.